nagra
National Cooperative for
the Disposal of Radioactive Waste

TECHNICAL REPORT 90-07

GRIMSEL TEST SITE

GEOPHYSICAL METHODS FOR THE DETECTION OF DISCONTINUITIES AHEAD OF A TUNNEL FACE

P. BLÜMLING [1)]
C. COSMA [2)]
M. KORN [3)]
C. GELBKE [4)]
B. CASSELL [5)]

FEBRUARY 1992

[1)] Nagra, Wettingen
[2)] Vibrometric, Helsinki
[3)] University of Frankfurt
[4)] Deutsche Montan Technologie, Bochum
[5)] Schlumberger, Hannover

GRIMSEL TEST SITE/SWITZERLAND
A JOINT RESEARCH PROGRAM BY

- NAGRA – National Cooperative for the Disposal of Radioactive Waste, Wettingen, Switzerland
- BGR – Federal Institute for Geoscience and Natural Reseources, Hannover, Federal Republic of Germany
- GSF – Research Centre for Environmental Sciences, Munich, Federal Republic of Germany

Hardstrasse 73, CH-5430 Wettingen/Switzerland, Telephone + 41-56-37 11 11

nagra National Cooperative for the Disposal of Radioactive Waste

TECHNICAL REPORT 90-07

GRIMSEL TEST SITE

GEOPHYSICAL METHODS FOR THE DETECTION OF DISCONTINUITIES AHEAD OF A TUNNEL FACE

P. BLÜMLING [1)]
C. COSMA [2)]
M. KORN [3)]
C. GELBKE [4)]
B. CASSELL [5)]

FEBRUARY 1992

[1)] Nagra, Wettingen
[2)] Vibrometric, Helsinki
[3)] University of Frankfurt
[4)] Deutsche Montan Technologie, Bochum
[5)] Schlumberger, Hannover

GRIMSEL TEST SITE/SWITZERLAND
A JOINT RESEARCH PROGRAM BY

- NAGRA – National Cooperative for the Disposal of Radioactive Waste, Wettingen, Switzerland
- BGR – Federal Institute for Geoscience and Natural Reseources, Hannover, Federal Republic of Germany
- GSF – Research Centre for Environmental Sciences, Munich, Federal Republic of Germany

Hardstrasse 73, CH-5430 Wettingen/Switzerland, Telephone + 41-56-37 11 11

FOREWORD

Concepts for the disposal of radioactive waste in geological formations place a significant emphasis on acquiring extensive knowledge of the proposed host rock and the surrounding strata. For this reason, Nagra has, since May 1984, been operating the **Grimsel Test Site (GTS)** which is located at a depth of 450 m in the crystalline rock of the Aare Massif of the Central Swiss Alps. The general objectives of the research being carried out in this underground laboratory include

- the build-up of know-how in planning, performing and interpreting field experiments in various scientific and technical disciplines and

- the acquisition of practical experience in the development of investigation methodologies, measuring techniques and test equipment which will be of use during actual repository site explorations.

The GTS is operated by Nagra and, on the basis of a German-Swiss co-operative agreement, various experiments are carried out by Nagra, the "Bundesanstalt für Geowissenschaften und Rohstoffe, Hannover" (BGR) and the "Forschungszentrum für Umwelt und Gesundheit, München" (GSF). The Grimsel projects of both GSF and BGR are supported by the German Federal Ministry for Research and Technology (BMFT). NTB 85-46 (German version NTB 85-47) provide an overview of the German-Swiss investigation programme. In a special issue of the Nagra Bulletin 1988 (German version "Nagra Informiert 1+2/1988") the status of the programme up to 1988 is described.

This report, issued simultaneously as Nagra NTB and PSI Report #117, was produced in accordance with the cooperation agreements mentioned above. The authors have presented their own opinions and conclusions which do not necessarily coincide with those of Nagra or its participating partners.

VORWORT

Bei Konzepten, welche die Endlagerung radioaktiver Abfälle in geologischen Formationen vorsehen, ist die Kenntnis des Wirtgesteins und der angrenzenden Gesteinsschichten von grundlegender Bedeutung. Die Nagra betreibt deshalb seit Mai 1984 das **Felslabor Grimsel (FLG)** in 450 m Tiefe im Kristallin des Aarmassivs. Die generelle Zielsetzung für die Arbeiten in diesem System von Versuchsstollen umfasst

- den Aufbau von Know-how in der Planung, Ausführung und Interpretation von Untergrundversuchen in verschiedenen wissenschaftlichen und technischen Fachgebieten, und

- den Erwerb praktischer Erfahrung in der Entwicklung und der Anwendung von Untersuchungsmethoden, Messverfahren und Messgeräten, die für die Erkundung von potentiellen Endlagerstandorten in Frage kommen.

Im Felslabor der Nagra werden, auf der Basis eines deutsch-schweizerischen Zusammenarbeitsvertrages, verschiedene Versuche von den beiden deutschen Partnern Bundesanstalt für Geowissenschaften und Rohstoffe, Hannover (BGR) und Forschungszentrum für Umwelt und Gesundheit GmbH, München (GSF) durchgeführt. Das Deutsche Bundesministerium für Forschung und Technologie (BMFT) fördert die Arbeiten der BGR und der GSF im FLG. Der NTB 85-47 (englische Version NTB 85-46) enhält eine Uebersicht des FLG und die Zusammenfassung der Untersuchungsprogramme mit Status August 1985. In der Ausgabe 1+2/1988 des Heftes "Nagra informiert" bzw. der englischen Spezialausgabe "Nagra Bulletin '1988" ist der Stand der Arbeiten anfangs 1988 beschrieben.

Der vorliegende Bericht erscheint gleichzeitig als Nagra NTB und als PSI Bericht Nr. 117 und wurde im Rahmen der erwähnten Zusammenarbeitsverträge erstellt. Die Autoren haben ihre eigenen Ansichten und Schlussfolgerungen dargelegt. Diese müssen nicht unbedingt mit denjenigen der Nagra oder der beteiligten Partner übereinstimmen.

AVANT - PROPOS

Lors d'études de concepts de stockage de déchets radioactifs dans des formations géologiques, on attache une grande importance à l'acquisition d'informations étendues sur la roche d'accueil et les formations rocheuses environnantes. C'est pour cette raison que la Cédra exploite depuis mai 1984 son **laboratoire souterrain du Grimsel (LSG)** situé à 450 m de profondeur dans le cristallin du massif de l'Aar, situé au milieu des Alpes centrales. Les principaux objectifs des recherches effectuées dans ce réseau de galeries comprennent:

- l'acquisition de savoir-faire dans diverses disciplines techniques et scientifiques en ce qui concerne la conception, la réalisation et l'interprétation d'expériences in situ, ainsi que

- l'accumulation d'expériences pratiques dans la mise au point et l'application de méthodes d'investigation, de techniques et d'appareillages de mesure, qui pourraient être utilisés lors de l'exploration de sites potentiels de dépôts finals.

Le LSG est exploité par la Cédra et diverses expériences y sont réalisées par celle-ci et deux institutions allemandes: la "Bundesanstalt für Geowissenschaften und Rohstoffe, Hannover" (BGR) et le "Forschungszentrum für Umwelt und Gesundheit GmbH, München" (GSF) dans le cadre d'un traité de collaboration germano-suisse. Les projets poursuivis au Grimsel par la BGR et le GSF sont financés par le Ministère fédéral allemand de la recherche et de la technologie (BMFT). Les rapports NTB 85-46 (version anglaise) et NTB 85-47 (version allemande) présentent un aperçu du laboratoire souterrain et un résumé des programmes de recherches avec état au mois d'août 1985. L'état d'avancement de ce programme en 1988 est présenté dans la publication "Cédra informe 1+2/1988" (version française) et "Nagra informiert 1+2/1988" (version allemande), ainsi que dans une édition spéciale en anglais (Nagra Bulletin 1988).

Le présent rapport, publié simultanément en tant que rapport technique Cédra (NTB) et rapport IPS Nº 117, a été élaboré dans le cadre des accords de collaboration mentionnés. Les auteurs ont présenté leurs vues et conclusions personnelles. Celles-ci ne doivent pas forcément correspondre à celles de la Cédra ou à celles de ses partenaires participants.

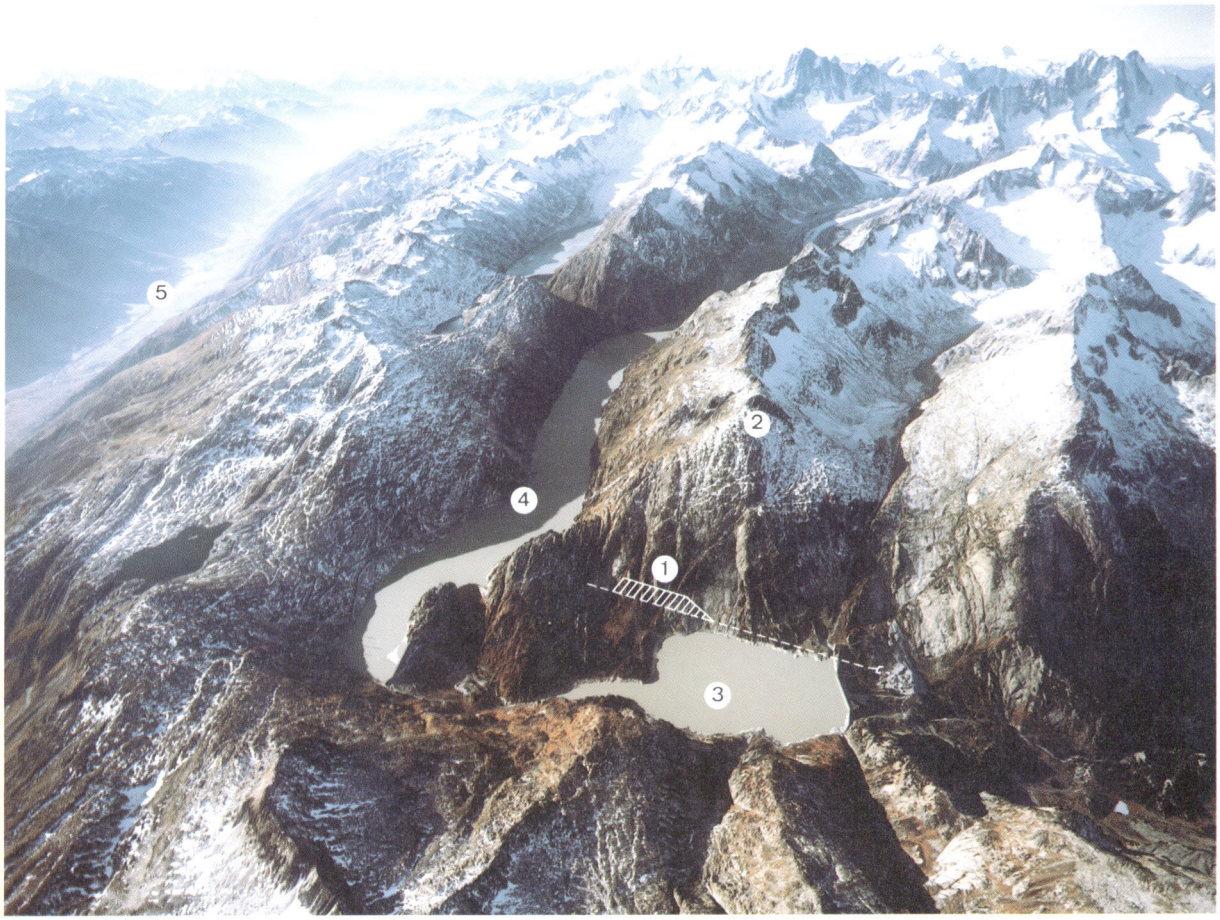

GRIMSEL-GEBIET

Blick nach Westen

1 Felslabor
2 Juchlistock
3 Räterichsbodensee
4 Grimselsee
5 Rhonetal

GRIMSEL AREA

View looking West

1 Test Site
2 Juchlistock
3 Lake Raeterichsboden
4 Lake Grimsel
5 Rhone Valley

FLG FELSLABOR GRIMSEL
GTS *GRIMSEL TEST SITE*

Situation

0 100 m

- Zugangsstollen / *Access tunnel*
- Fräsvortrieb / *by tunnel boring machine*
- Sprengvortrieb / *excavated by blasting*
- Zentraler Aaregranit ZAGR / *Central Aaregranite CAGR*
- Biotitreicher ZAGR / *CAGR with high content of biotite*
- Grimsel-Granodiorit / *Grimsel-Granodiorite*
- Scherzone / *Shear zone*
- Lamprophyr / *Lamprophyre*
- Wasserzutritt / *Water inflow*
- SB — Sondierbohrung / *Exploratory borehole*
- US — US Bohrung / *US borehole*

ZB	Zentraler Bereich / *Central facilities*
AU	Auflockerung / *Excavation effects*
BK	Bohrlochkranz / *Fracture system flow*
EM	El.magn. HF-Messungen / *-measurements*
FRI	Kluftzone / *Fracture zone investigation*
GS	Gebirgsspannungen / *Rock stresses*
HPA	Hydr. Parameter / *Hydr. parameters*
MI	Migration / *Migration*
MOD	Hydrodyn. Modellierung / *H. modeling*
NM	Neigungsmesser / *Tiltmeters*
UR	Untertageradar / *Underground radar*
US	Seismik / *Underground seismic testing*
VE	Ventilationstest / *Ventilation test*
WT	Wärmeversuch / *Heat test*

A — A Schnitt / *Section*

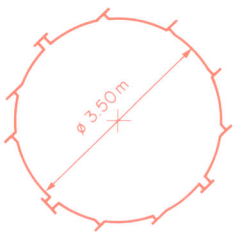

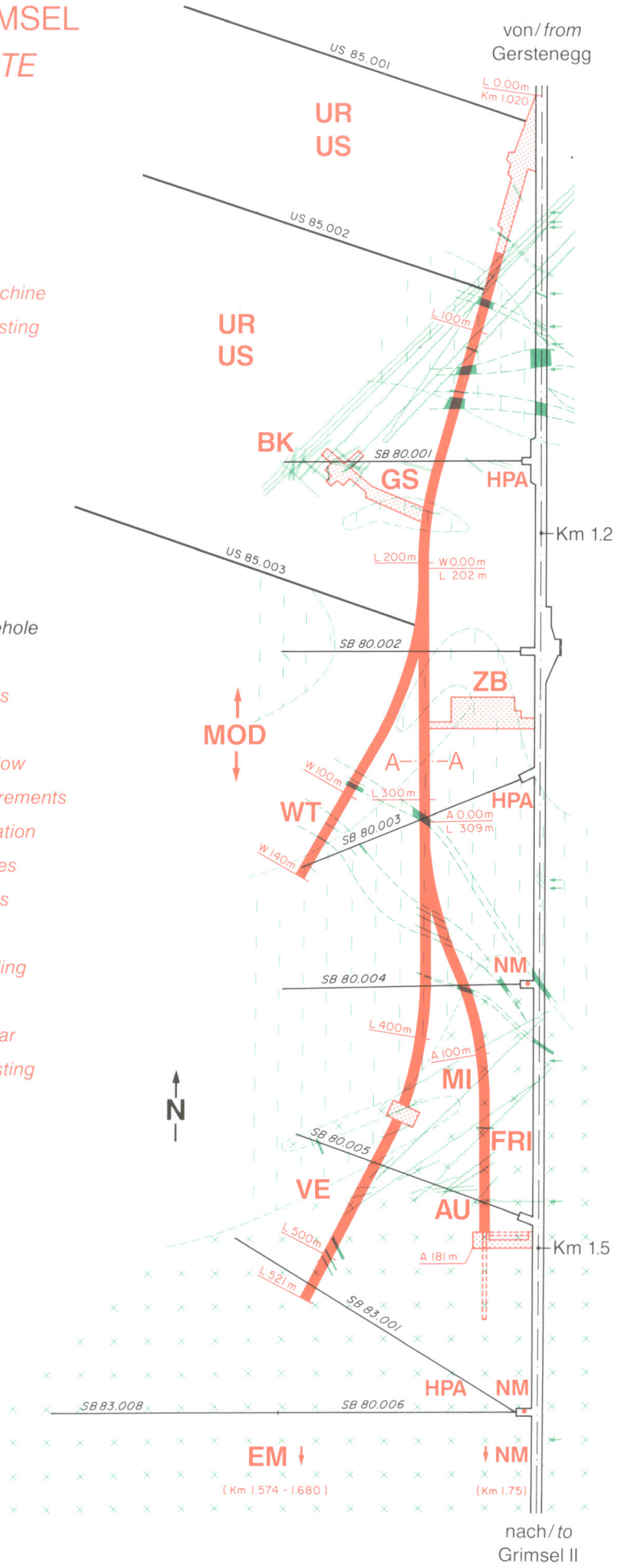

6/88

Summary

In 1988 NAGRA started a research and development program at Grimsel Test Site (GTS) to investigate the potential of geophysical remote sensing methods (radar and seismics) to predict discontinuities ahead of the tunnel face.

This task was initiated as an attempt to provide a more complete knowledge of the rockmass for a safe construction of a tunnel. If we can tell in advance where the main fracture zones are to be encountered during excavations, the safety risks as well as the costs of tunneling will be greatly reduced.

A number of practical goals were set to guide the studies and experiments during the project:

- The measurements should be performed during the breaks of the normal construction operation. No additional stand-by times should result for the construction work.

- The investigation depth should be in the order of at least 100 m to allow enough time for data processing and interpretation before the tunnel arrives at the located discontinuities.

- The preparation for the measurements should not interrupt or interfere with the construction work.

- The method should be applicable for conventional drill and blast techniques as well as for full face drilling operations

The first investigations were done using a subset from an existing data base, obtained from both radar and seismic experiments, originally recorded for a tomography project at GTS. Although the data recording, station spacing etc. were optimized for the tomographic application and far from ideal for a reflection survey, it was possible to reach some meaningful results. Reflection events were identified which could be attributed to known fracture zones and lamprophyre dykes.

Radar measurements give good results in rocks with high electrical resistance (e.g. granite, rock salt) but have a very limited investigation depth in materials with lower resistance (e.g. marls, clays). NAGRA's near future interests being focused on measurements in sediments and considering the results of the first tests, we decided to concentrate our efforts on seismics rather than radar.

After discussions with several experts, it was agreed that in this case the most adequate approach for the seismic measurements is a modified "Vertical Seismic Profiling (VSP)" technique which is well known in borehole geophysics. A more suggestive name could have been, for example, "Horizontal Tunnel Profiling" but as we liberally refer to routines developed initially for boreholes, we prefer to conserve the generic name of VSP. For a more objective evaluation of the results, conventional seismic measurements along the tunnel were also recommended.

Theoretical calculations (FD-modeling) were done to determine the optimal test layout. This study showed that, ideally, the source and the receivers should be placed at a certain distance (several meters) away from the tunnel wall. In practice this is hardly possible as it would require many boreholes to be drilled radially from the tunnel. The best compromise between theoretical and operational aspects is to place the source into a side wall drillhole at a minimum distance of about 4 m from the tunnel wall and to attach the receivers directly to the tunnel wall. In this case we expect to reduce the tunnel wave and still achieve a realistic operational time. However, as the measurements at GTS were primarily a scientific experiment, we decided not to measure only the most promising layout according to the theory, but to proceed with different test configurations to prove the validity of the theoretical results optimize the operational routine.

The following VSP configurations were tested:

1. Receiver chain with 7 receivers in a radial borehole and a sledge hammer as the source. The shot points were placed along the tunnel with a spacing of 0.7 m.

2. Receiver chain with 7 receivers in a radial borehole and small explosives as the source. The shot points were placed along the tunnel with a spacing of 0.7 m. The shots were fired in small holes (l=400 mm, Φ=14 mm).

3. Explosives in the radial borehole and receivers along the tunnel. The receiver spacing was 0.7 m.

Additionally to the VSP-type measurements we measured a conventional reflection seismic profile along the tunnel by shooting through the array. Shotpoint and receiver spacings were 0.7 m with an offset between shot and receiver of 0.35 m, leading to a CDP (Common Depth Point) spacing of 0.35 m.

The raw sections of all records showed only very weak reflections. This was caused by the very low reflectivity of the fracture zones at GTS, if compared with surveys conducted in layered sediments. Accordingly, the processing consisted of a relatively large number of steps which are not discussed in this paper in detail. In general, the direct P- and S-waves as well as the reflected S-waves were suppressed by using a median filter while the remaining P- reflections were enhanced by Image Point filtering, a method based on the generalized Radon transform developed by C. Cosma and his collaborators at Vibrometric.

A large effort has been put for the completion of this project in the development of routines for translating the geophysical results into a reliable and unambiguous geological picture. Due to the many experiments carried out previously at Grimsel Test Site (GTS), we had the possibility to compare in different phases the geophysical predictions expressed in terms of geological structure with the exhaustive information available. The agreement between predicted and real location was excellent. We were able to detect discontinuities up to distances of about 150 m.

The conventional reflection section was processed using standard seismic processing routines. Due to the weak source (sledge hammer) the investigation depth was in the order of about 40 m. Within this area a number of reflectors (mainly lamprophyre dykes) were detected. Additionally we got good reflections from a nearby tunnel. Although this test was successful we consider the VSP configuration as the better layout for the prediction measurements.

As a trial of the method in a realistic environment, VSP measurements were conducted in August 1990 in the Leissigen tunnel (a road tunnel in the canton of Bern), which was under construction at the time of the test. The processing sequences tested in earlier experiments were used. Although the circumstances were more complicated and the field conditions more difficult than in GTS, the predictions coincided well with the geological structures known or supposed to exist at the tunnel site.

ZUSAMMENFASSUNG

Im Jahr 1988 startete die NAGRA ein Forschungs- und Entwicklungsprogramm im Felslabor Grimsel (FLG), um zu klären, in wie weit geophysikalische Fernerkundungsmethoden zur Vorhersage von Störungen im Vor- und Umfeld eines Tunnels eingesetzt werden können.

Dieses Projekt wurde angeregt, um eine Möglichkeit zu schaffen, umfassendere Informationen über das Gebirge im Bereich eines Tunnels zu erhalten und so die Sicherheit beim Vortrieb des Tunnels zu erhöhen. Eine frühe Kenntnis über Hauptstörungszonen im Umfeld des Tunnels können sowohl zur Reduktion des Sicherheitsrisikos und auch der Kosten führen.

Folgende praktische Ziele wurden als Leitfaden für die Studie und Experimente aufgestellt:

- Die Messungen sollten während der Pausen des normalen Vortriebs durchgeführt werden können. Es sollten keine zusätzlichen Wartezeiten entstehen.

- Die minimale Reichweite bei den Untersuchungen sollte 100 m betragen, um genügend Zeit für die Datenbearbeitung und Interpretation zu gewährleisten, bevor der Ausbruch die lokalisierte Störung erreicht.

- Die Vorbereitungen für die Arbeiten sollten den Vortrieb weder behindern noch verzögern.

- Die Methode sollte sowohl bei konventionellem Sprengvortrieb als auch beim Einsatz von Vollschnitt-Tunnelbohrmaschinen möglich sein.

Erste Untersuchungen wurden mit Hilfe eines Teils von existierenden Datensätzen aus Radar- und Seismikprojekten durchgeführt, die für Tomographieprojekte im FLG erhoben worden waren. Obwohl die Erfassung dieser Daten (Stationsabstände etc) für die Tomographieanwendung optimiert und nicht ideal für Reflexionsauswertungen war, konnten gute Resultate erreicht werden. In den prozessierten Daten konnten Reflektoren identifiziert und bekannten Störungen und Lamprophyren zugeordent werden.

Radarmessungen führen zu guten Resultaten in Gesteinen mit hohem elektrischen Widerstand (z.B. Granit, Steinsalz) aber in Gesteinen mit geringen elektrischen Widerständen (z.B. Mergel, Ton) lassen sich nur sehr begrenzte Reichweiten realisieren. Da die NAGRA in der näheren Zukunft ihre Feldarbeiten auf Sedimentgestein fokussiert und wegen der Resultate der ersten Radartests, beschlossen wir, die Radarmethode zugunsten der Seismik zurückzustellen.

Die Diskussion mit verschiedenen Experten ergab, dass die für die gegebene Fragestellung am besten angepasste seismischen Untersuchungsmethode eine modifizierte Version der "Vertical Seismic Profiling (VSP)"-Methode ist. Diese Methode ist bekannt und erprobt in der Bohrlochgeophysik. Obwohl für diese Anwendung der besser angepasste Namen z.B. "Horizontal Tunnel Profiling" gewesen wäre, beschlossen wir den Namen VSP zu behalten.. Um eine objektive Wertung der VSP-Resultate zu ermöglichen, wurden empfohlen, die Ergebnisse mit Standard-Reflexionsseismikresultaten zu vergleichen.

Theoretische Rechnungen (FD-Modellierung) wurden durchgeführt, um das optimale Layout zu ermitteln. Diese Studie zeigte, dass idealerweise die Quelle und die Empfänger in einer gewissen Entfernung von der Tunnelwand (einige Meter) plaziert werden sollten, um Tunnelwellen zu vermeiden. In der praktischen Anwendung ist dies wegen der grossen Anzahl der benötigten radialen Bohrungen nicht möglich. Der beste Kompromiss zwischen theoretischer Anforderung und praktischer Machbarkeit ist, die Quelle in einer Radialbohrung in einem minimalen Abstand von 4 m zur Tunnelwand zu plazieren und die Empfänger direkt an der Tunnelwand zu befestigen. In diesen Fall kann eine Reduktion der Tunnelwellenamplitude erreicht werden, ohne unrealistische Vorbereitungszeiten in Kauf nehmen zu müssen. Da es sich im FLG in erster Linie um ein wissenschaftliches Experiment handelte, wurde beschlossen, nicht nur das Messlayout mit den besten Erfolgschancen, sondern auch andere Möglichkeiten zu testen, um die theoretische Ergebnisse überprüfen und die Feldarbeiten optimieren zu können.

Folgende VSP-Konfigurationen wurden untersucht:

1. Empfängerkette mit 7 Aufnehmern in einer Bohrung radial zur Stollenachse und einer Handhammerquelle. Die Schusspunkte befanden sich im Stollen in einem Abstand von 0.7 m.

2. Empfängerkette mit 7 Aufnehmern in einer Bohrung radial zur Stollenachse. Als Quelle wurden Schüsse in kleinen Bohrlöchern (l= 400 mm, Φ=14 mm) verwendet. Der Schusspunktabstand betrug 0.7 m.

3. Schüsse in den Bohrungen radial zur Stollenachse. Die Aufnehmer befanden sich in einem Abstand von je 0.7 m im Stollen.

Zusätzlich zu den VSP-Messungen wurde eine konventionelles seismisches Reflexionsprofil entlang des Stollens gemessen. Die Schuss- und Aufnehmerpunkte hatten einen Abstand von jeweils 0.7 m, wobei die Schusspunkt in der Mitte zwischen den Aufnehmerpunkten

lagen. Dadurch ergab sich ein "Common Depth Point (CDP) - Abstand von 0.35 m.

Die Rohdaten aller Sektionen zeigen, bedingt durch die geringen Reflexionskoeffizienten der Störungszonen im FLG, nur sehr schwache Refexionen. Daher war im Vergleich zu anderen Daten (z.B. reflexionsseismische Daten in Sedimenten) ein sehr umfangreiches Processing notwendig, das hier nicht in allen Einzelheiten erklärt wird. Generell wurden die direkten P- und S-Wellen sowie die reflektierten S-Wellen durch Medianfilter unterdrückt und die reflektierten P-Wellen mit Hilfe der Bildpunkt-Verarbeitung (Image Point Filtering) hervorgehoben. Diese Methode basiert auf der generalisierten Radon Transformation und wurde von C. Cosma und seinen Mitarbeitern entwikkelt.

Es wurden auch grosse Anstrengungen unternommen, um Programme zu entwickeln, die es erlauben, die geophysikalischen Ergebnisse in ein zuverlässliches geologisches Bild umzusetzen. Aufgrund der guten Kenntnis des FLG's aus anderen Projekten war es möglich, die gewonnenen geophysikalischen Vorhersagen in den verscheidenen Phasen der Auswertung direkt mit den bekannten geologischen Strukturen zu vergleichen. Die Uebereinstimmung von vorhergesagter und wahrer Lokation der erkannten Strukturen war sehr gut. Es konnten Störungen bis in 150 m Entfernung lokalisiert werden.

Die konventionellen Reflexionsdaten wurden mit Standard-Processingroutinen bearbeitet. Wegen der geringen Energie der verwendeten Quelle (Handhammer) betrug die Eindringtiefe nur ca 40 m. Innerhalb dieses Bereichs konnten mehrere Reflektoren erkannt werden (hauptsächlich Lamprophyre). Ausserdem waren Reflexionen vom benachbarten Labortunnel zu erkennen. Obwohl dieser Test recht gute Resultate ergab, zeigte es sich, dass die VSP-Methode für die Vorhersage besser geeignet ist.

Der abschliessende Test der Methode unter realistischen Bedingungen erfolgte im August 1990 im Tunnel bei Leissigen, einem Strassentunnel im Kanton Bern. Dieser Tunnel war zur Zeit der Messungen im Bau. Obwohl die Messsituation in diesem Fall komplizierter war als im FLG, stimmten die Vorhersagen recht gut mit den später angetroffenen Verhältnissen überein.

RÉSUMÉ

En 1988, la Cédra a entamé au Site d'Éssai du Grimsel (GTS) un programme de recherche et de développement sur les possibilités de prédiction de discontinuités, au-delà du front d'un tunnel, par des méthodes géophysiques (techniques radar et sismiques).

Ce programme a pour objectif d'accroître les connaissances préalables de la masse rocheuse, pour garantir une sécurité suffisante lors de la construction d'un tunnel. En effet, les risques encourrus aussi bien que les coûts consentis seront grandement réduits s'il est possible de détecter à l'avance les principales zones de failles que le tunnel va recouper.

Les études et les essais ont été définis en fonction d'un certain nombre de buts pratiques:

- les mesures doivent pouvoir s'insérer pendant les interruptions du cours normal des opérations. Elles ne devraient pas occasionner une augmentation des temps morts lors des travaux de construction.
- la profondeur de pénétration des investigations devrait être d'au moins 100 m environ, afin que le traitement des données et leur interprétation puisse se faire avant que le tunnel ne recoupe les discontinuités identifiées.
- la préparation des mesures ne devrait pas interrompre ou gêner les travaux de construction.
- la méthode doit être applicable aussi bien aux techniques d'avancement conventionnelles qu'à celles mettant en oeuvre un tunnelier de pleine section.

Les premières investigations se basent sur la banque de données existante du GTS, elles utilisent à la fois des données d'essais radar et des données sismiques récoltées lors d'un projet de tomographie. Bien que le dispositif et le mode d'acquisition des données aient alors été dimensionnés pour une application tomographique et que les données soient loin d'être idéales pour une étude de sismique réflection, il a été possible d'obtenir quelques résultats significatifs. On a pu attribuer certains des réflecteurs identifiés à des zones de failles et des filons de lamprophyres connus.

Les mesures radar ont donné de bons résultats dans les roches à haute résistivité électrique comme le granite ou le sel gemme, mais possèdent une profondeur de pénétration trop faible dans les roches électriquement conductrices comme les marnes et argiles. Les travaux de la Cédra portant principalement sur les roches sédimentaires au cours des prochaines années, nous

avons décidé, au vu des premiers résultats, de concentrer nos efforts sur les méthodes sismiques plutôt que sur les méthodes radar.

A la suite de discussions avec plusieurs experts, il est ressorti que l'approche la plus appropriée, dans notre cas, serait un "Profil Sismique Vertical" (VSP) modifié, une technique bien connue dans la géophysique de forage. Dans notre cas, il aurait été plus suggestif d'appeler cette méthode "Profil Horizontal de Tunnel", mais puisque nous nous référons à des méthodes développées pour des forages, nous conserverons le nom de VSP. Pour une évaluation plus objective des résultats, on recommande d'effectuer également des mesures sismiques conventionnelles le long du tunnel.

L'optimisation du dispositif de test a été faite par des calculs théoriques (modèle à différences finies). Elle montre que dans un cas idéal la source et les récepteurs devraient être placés à une certaine distance des parois du tunnel. En pratique, ce n'est guère possible, car cela nécessiterait plusieurs forages disposés radialement par rapport à l'axe du tunnel. Le meilleur compromis entre l'optimisation théorique et les contraintes pratiques consiste à placer la source dans un forage radial à une distance d'au moins 4 m de la paroi du tunnel, et de placer les récepteurs directement sur cette dernière. Avec un tel dispositif, on pense réduire l'onde de surface du tunnel tout en maintenant une durée de mesures raisonnable. Toutefois, comme les mesures au GTS consistaient à expérimenter une méthodologie, on ne s'est pas contenté de tester le dispositif le plus prometteur en théorie. On a également testé d'autres configurations, pour confirmer la validité des résultats théoriques et optimiser le procédé opérationnel.

On a testé les configurations VSP suivantes:

1. Chaîne de 7 récepteurs dans un forage radial et marteau manuel comme source. Les points de tir ont été placés le long du tunnel et espacés de 0.7 m.
2. Chaîne de 7 récepteurs dans un forage radial et petits explosifs comme source. Les points de tir ont été placés le long du tunnel et espacés de 0.7 m. Les charges explosives étaient placées dans de petits trous (l = 400 mm, Φ= 14 mm).
3. Explosifs comme source dans le forage radial et récepteurs le long du tunnel, espacés de 0.7 m.

En plus des mesures de type VSP, on a effectué un profil sismique conventionnel le long du tunnel, avec tirs sur la ligne de mesures (array). Les points de tir et les récepteurs étaient disposés avec un

espacement respectif de 0.7 m, avec un décalage (offset) de 0.35 m entre le point de tir et le récepteur, correspondant à une distance entre des positions miroir ("Common Depth Point") de 0.35 m.

Les sections brutes de tous les enregistrements n'ont révélé que de faibles réflections. Ceci est dû à la réflectibilité très faible des zones de failles au GTS, comparée à celle de sédiments stratifiés. En conséquence, le traitement a nécessité un grand nombre de paliers qui ne sont pas discutés en détail dans cet article. En général, les ondes directes P et S ainsi que les ondes S réfléchies ont été supprimées en utilisant un filtre bidimensionnel (median filter), tandis que les réflections P restantes ont été réhaussées par un filtrage spécial (Image Point Filtering), une méthode basée sur les transformations généralisées de Radon et développée par C. Cosma et ses collaborateurs à la société Vibrometric.

Pour clore ce projet, on a investi un grand effort dans le développement de techniques de transformation des résultats géophysiques en une image géologique non ambiguë et fiable. Les nombreuses études effectuées préalablement au GTS nous ont permis de comparer, au cours des différentes étapes du travail, nos prédictions géophysiques formulées en termes de structures avec l'information exhaustive disponible. On a constaté un excellent accord entre la localisation des structures prédites et celle des structures réelles. Nous avons pu identifier les discontinuités jusqu'à des distances d'environ 150 m.

La section de réflection conventionnelle a été établie en utilisant les procédures de traitement sismique standard. La profondeur d'investigation se situait aux alentours de 40 m seulement, à cause de la faible intensité du signal source (marteau manuel). Dans cet espace toutefois nous avons pu détecter un certain nombre de réflecteurs, principalement des filons de lamprophyre. De plus, nous avons obtenu de bonnes réflections d'une galerie proche. Bien que cet essai ait été couronné de succès, nous pensons que la configuration VSP représente un meilleur dispositif de mesure pour la prédiction.

Afin de tester la méthode dans un cas réel, nous avons effectué des mesures VSP dans le tunnel de Leissigen en août 1990, un tunnel routier alors en construction dans le canton de Berne. Nous avons utilisé les mêmes séquences de traitement que pour les essais antérieurs. Bien que la situation géologique et les conditions de travail aient été plus compliquées qu'au GTS, les prédictions obtenues ont bien reproduit les structures géologiques connues ou supposées sur le site du tunnel.

CONTENTS PAGE

LIST OF FIGURES

LIST OF TABLES

1 INTRODUCTION

In 1988 Nagra - the National Cooperative for the Storage of Radioactive Waste - decided to start a new research and development program to use geophysical remote sensing techniques to look ahead of the tunnel face while the tunnel is under construction. This task was initiated as an attempt to provide a more complete knowledge of the rockmass for a safe construction of a tunnel. If we can tell in advance where the main fracture zones are to be encountered during excavations, the safety risks as well as the costs of tunneling will be greatly reduced.

Geophysical methods are used in many different applications. They can be conducted on surface, in underground mines or in boreholes. Their advantage over direct probing, e.g. drilling, is that they can provide information on a large volume with relatively modest requirements for setting up the measurements. An often quoted drawback is that the results consist of distributions of physical parameters rather than of a geological model. A large effort has been put for the completion of this project in the development of routines for translating the geophysical results into a reliable and unambiguous geological picture. Due to the many experiments carried out previously at Grimsel Test Site (GTS), we had the possibility to compare in different phases the geophysical predictions expressed in terms of geological structure with the exhaustive information available. The agreement has been remarkable.

The task described in this report was to evaluate geophysical methods which are capable of investigating the area in front and around the tunnel. The discussion at the beginning of the program led to the assumption that only the wave field method has the potential to detect inhomogeneities with the accuracy desired for this project. Other methods (e.g. potential field methods) were rated as less adequate to the problem (less resolution, non-unique solutions).

During two workshops with foreign experts at the Nagra office it was recommended that seismic and radar reflection measurements be tried to evaluate their potential to fulfill the specific requirements related to tunneling works. Not only the general merits of the measurement techniques were deemed important; additionally the possible layouts of the measurement lines were discussed in detail. A number of practical arguments had to be taken into account:

- The measurements should be performed during the breaks of the normal construction operation. No additional stand-by times should result for the construction work.

- The investigation depth should be in the order of at least 100 m to allow enough time for data processing and interpretation before the tunnel arrives at the located discontinuities.

- The preparation for the measurements should not interrupt or interfere with the construction work.

- The method should be applicable for conventional drill and blast techniques as well as for full face drilling operations

The axial symmetry of the tunnel leads logically to the most convenient layout for reflection profiling. The situation is in principle identical to a particular borehole seismic technique - the vertical seismic profiling (VSP) /Hardage, 1983/. Here the receivers (or in case of a reversed VSP the shot points) are distributed along the borehole (or tunnel) while the source (the receiver respectively) stays at a fixed position at the end of the array. This kind of array technique is normally used in the exploration industry for reflectors lying nearly perpendicular to the array and more or less standard methods exist for this case. In a tunnel it is required to get information from reflectors with any other orientations. Hence the need to experiment also with new methods. Other important differences with respect to borehole measurements are the larger diameter and the fact that the tunnel is filled with air. These circumstances lead to the conversion of part of the energy to tunnel waves (surface waves) which can mask the reflections of the body waves and therefore disturb the whole measurement. Therefore, it was considered necessary to perform a theoretical study for choosing among the many possible variations of the method the one which would lead to the most efficient elimination of tunnel waves.

It was decided that a pilot program be conducted first using existing data which could be sorted from data sets collected earlier for a radar and respectively a seismic tomographic project at Grimsel Test Site /Gelbke, 1988; Niva et al, 1988/.

The geometrical boundary conditions were far from ideal as the layout of the existing measurements had been optimized for tomographic investigations and therefore the station spacing was too large for reflection processing, e.g. for avoiding spatial aliasing. However, the results were so good that a new program has been started immediately, including

new seismic field measurements at GTS followed by laborious processing and interpretation work. Further investigations on the radar method were dropped from the program for the following reasons:

- The attenuation of radar waves is dependant on the electrical properties of the medium (electrical resistivity, dielectric constant) penetrated by the wave. These values (especially the resistivity) vary in the order of magnitudes for different rocks. The method would be applicable only in highly resistive rocks.

- Site characterization work at Nagra will be focused in the near future to sediments with low electrical resistivity (e.g. marl, clay). Penetration depth in this material is expected not to exceed 10-30 m.

Nevertheless, the methods and especially the data processing techniques developed for seismic measurements, can be used for radar application as well. In case of radar measurements in granite, salt or limestone one can directly use the same field layouts and processing procedures as described in this report for seismics.

After completing the GTS experiment and evaluating the results, a real life test at a site of unknown geology was conducted in Leissigen in 1990.

The structure of this report reflects the logic of the experimental approach followed by the project. Chapter 1, which is this introduction, outlines the basic justification of the project itself. The previous measurements at GTS showed that tunnel waves will cause problems in data by masking weak reflections. To find the best acquisition methods for seismic experiments, numerical studies on the behavior of the tunnel waves were done and they are described in chapter 2. The basics of the VSP method are explained in chapter 3. The seismic results obtained with the pilot project using tomographic data from GTS are discussed in chapter 4 and the corresponding results from radar data in chapter 5. In chapter 6 we concentrate on the new seismic measurements at GTS. In chapter 7 the test in Leissigen is analyzed. This experiment is meant to prove the relevance of the results obtained in the controlled environment of Grimsel for a real life survey, where little previous information is available and the experimental conditions are those of a construction site rather than those of a very carefully kept rock laboratory.

2 NUMERICAL STUDIES ON SEISMIC TUNNEL WAVES

The first tests at GTS using part of the tomography data indicated that one has to expect serious problems with tunnel waves and their reflections propagating along the tunnel.

These waves add a ringing in the seismograms which can physically be explained as free oscillations of the tunnel. They are less attenuated than the body waves and therefore they mask the reflections. The velocity of the tunnel waves is approximately equal or a little less than the S-wave velocity. Therefore their suppression is not trivial and one of the purposes of this study was to find efficient ways to eliminate these disturbances directly by optimizing the recording geometry.

Theoretical seismograms were calculated for a two-dimensional case but a three-dimensional analysis was performed to calculate attenuation, dispersion and kinematic aspects of the tunnel wave.

2.1 Two-Dimensional Modeling

For the numerical modeling, a finite difference (FD) algorithm was used which was capable of solving numerically the two-dimensional elasto-dynamic wave equation. The model used for this study had a dimension of 23.6 m x 19.6 m (Figure 2.1) and was parameterized in 0.1 m steps. Absorbing boundary conditions were used to suppress reflections from the boundary of the model. The input parameters of the model are:

V_p = 5300 m/s
V_s = 3060 m/s
ρ = 2500 kg/m^3
Φ = 3.5 m

Where V_p is the P- wave velocity, V_s the S- wave velocity, ρ the density and Φ the tunnel diameter.

The tunnel in the model was realized by reducing the velocity within a circular area to 1 % of the seismic velocity of the surrounding rock. Additionally, the model was set up in such a way that an excavation zone of circular or elliptical shape could be introduced. In several model calculations the excavation zone around the tunnel was realized as a low velocity zone with a velocity reduction of 5 % .

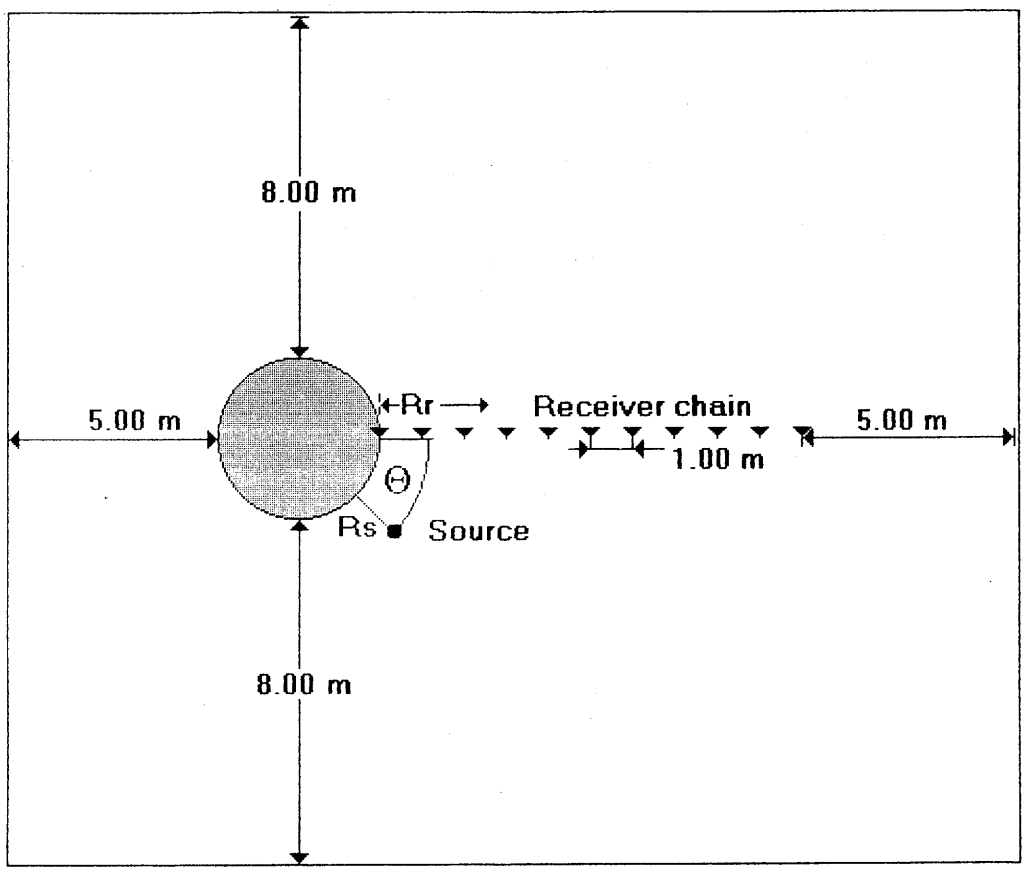

Figure 2.1 Finite difference model used for the calculation of the theoretical seismogram. The shaded circle represents the tunnel which is numerically realized by changing the seismic velocity in the tunnel area to 1 % of the seismic velocity of the surrounding rock.

The position of the source is determined by the distance along the radius from the source to the tunnel wall and the polar angle taking as origin the direction of the receiver array (Figure 2.1). The source was realized as a single force, radial or tangential to the tunnel wall. The wavelet used for the calculations of the synthetic seismograms was a pulse of 1 ms duration, its frequency ranging from 800 to 3000 Hz.

One of the objectives of the theoretical calculations has been to find relations between source / receiver positions and the energy of the tunnel waves. The first theoretical seismogram section was calculated to try the behavior of the model in an undisturbed space, i.e. in absence of the tunnel. As expected, this section (Figure 2.2 b) showed nothing but the direct P- and S-waves and therefore verified both the code and the boundary conditions used in the modeling. The introduction of the tunnel lead to more complicated seismograms. Ringing and additional phases due to surface waves appeared (Figure 2.2 a). Especially the receiver positions close to the tunnel wall displayed a lot of energy past the direct arrival times.

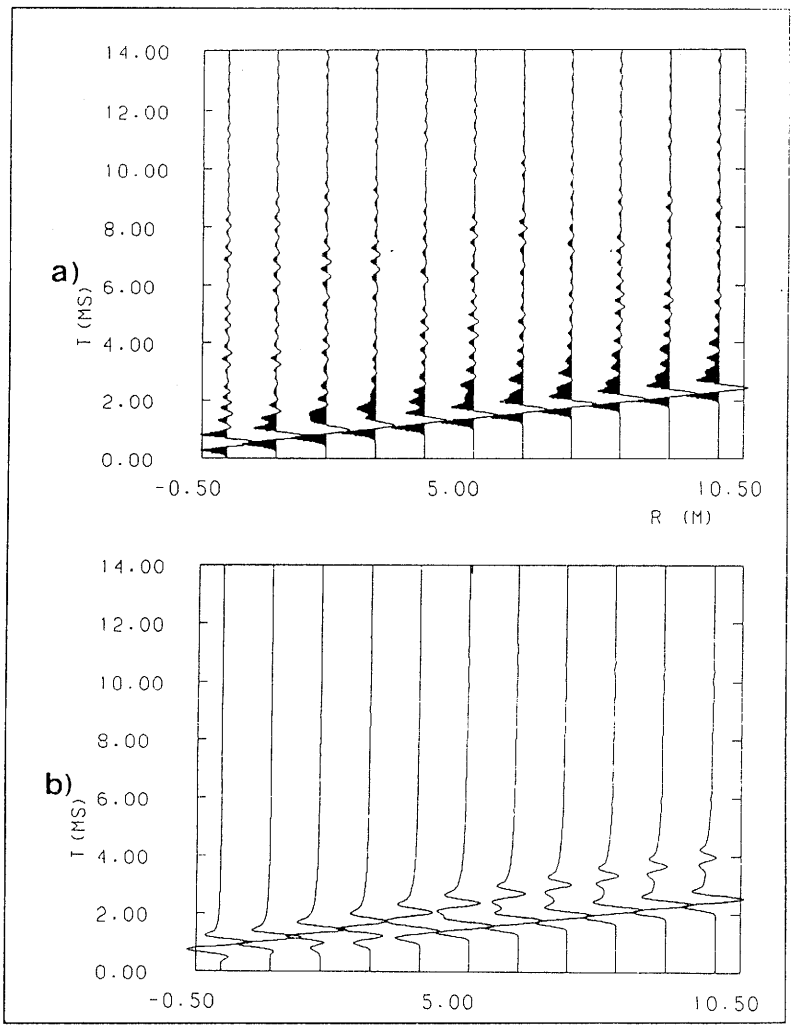

Figure 2.2 Theoretical seismograms calculated by finite difference method using the model described in Figure 2.1.

a) Synthetic seismograms obtained with Rs = 0, θ = 0 and $V_{tunnel} = 0,01 \times V_{rock}$

b) Synthetic seismograms obtained by the same setup, but setting $V_{tunnel} = V_{rock}$

This first example shows seismograms calculated for a radial source acting directly on the tunnel wall, the angle (θ in Figure 2.1) between source and receiver chain being 0° .

For this case, only the X component (radial direction) exists while the Z component (perpendicular to X) vanishes due to reasons of symmetry. The theoretical seismograms show that in this situation the location of the receiver with respect to the tunnel wall has no significant influence on the ringing of the signal (Figure 2.2 a).

Two facts can be observed by changing the position of the source with respect to the receiver chain by varying the angle θ. The Z component does not vanish any more. On the X axis the amplitude of the ringing increases, especially for the receiver at the tunnel wall level (Figure 2.3). The influence of the angle θ is partly due to the shadow zone of the tunnel. In the real three-dimensional space one can decrease this effect by moving the source along the tunnel.

The following numerical simulation investigated the influence of the source position with constant θ but changing distance from the tunnel wall. In reality this can be achieved by using radial drillholes for the source. Figure 2.4 displays the results for source distances of 0 - 7 m to the tunnel wall with $\theta = 90°$. A significant reduction of the ringing can be observed. Additionally a decay of the tunnel wave as a function of the receiver position can be observed for source positions with $R_s > 2m$. In the case of $R_s = 4$ m the most significant decay of the tunnel wave is observed at receiver positions between 1 and 2 m radial distance from the tunnel wall.

Finally, we investigated the influence of a disturbed excavation zone on the tunnel waves and on the ringing in the theoretical seismograms. Calculations were carried out using a low velocity zone 1 m thick around the tunnel. The seismic velocity was 5 % less in the excavation zone than in the undisturbed rock. The results were nearly identical with the case without disturbed zone. In conclusion, the excavation zone does not seem to affect the seismic tests.

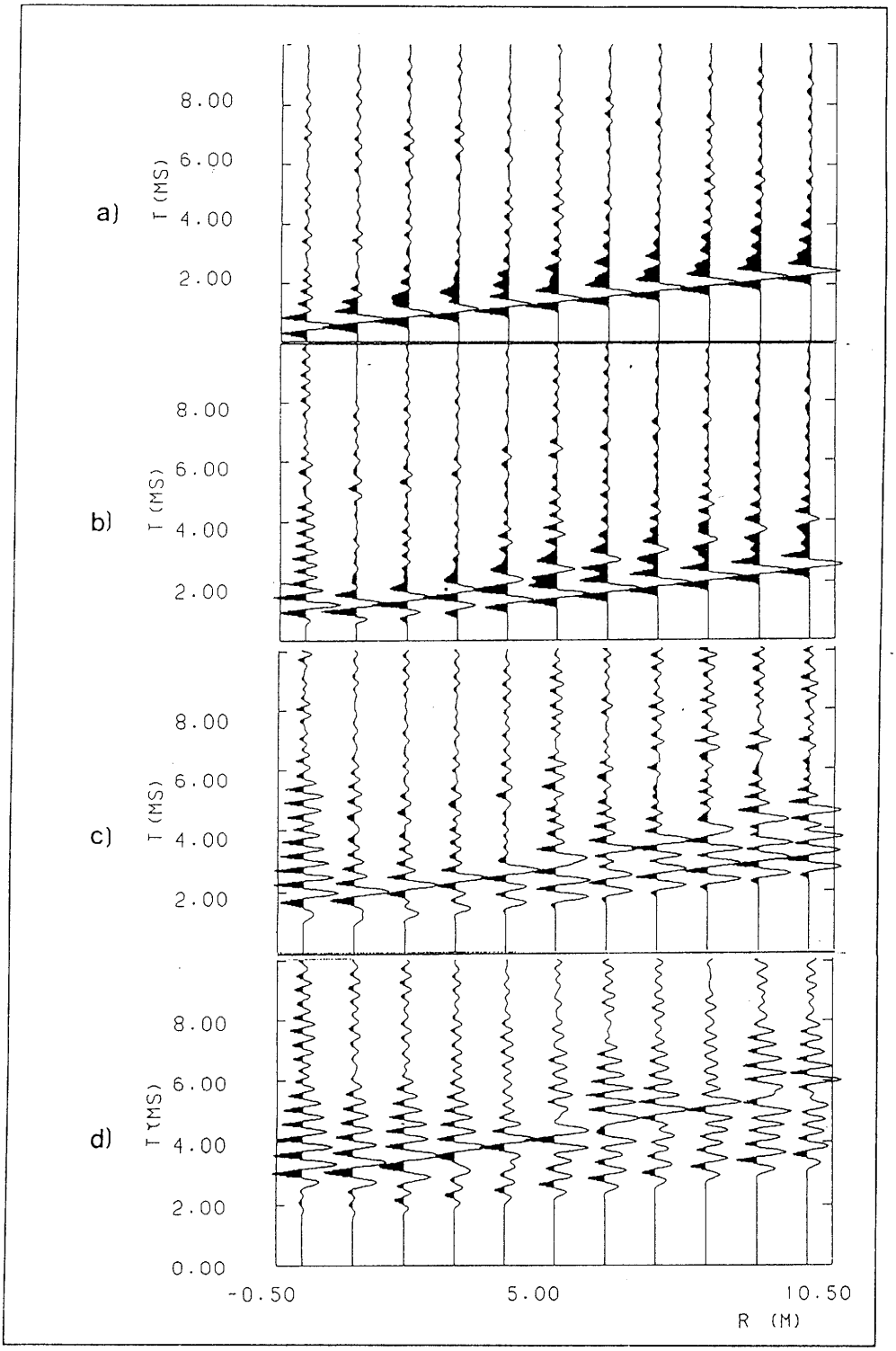

Figure 2.3 Theoretical seismograms (x-components) calculated for Rs = 0 and:

a) $\theta = 0^\circ$
b) $\theta = 45^\circ$
c) $\theta = 90^\circ$
d) $\theta = 180^\circ$

Rs, Rr and θ are defined in Figure 2.1

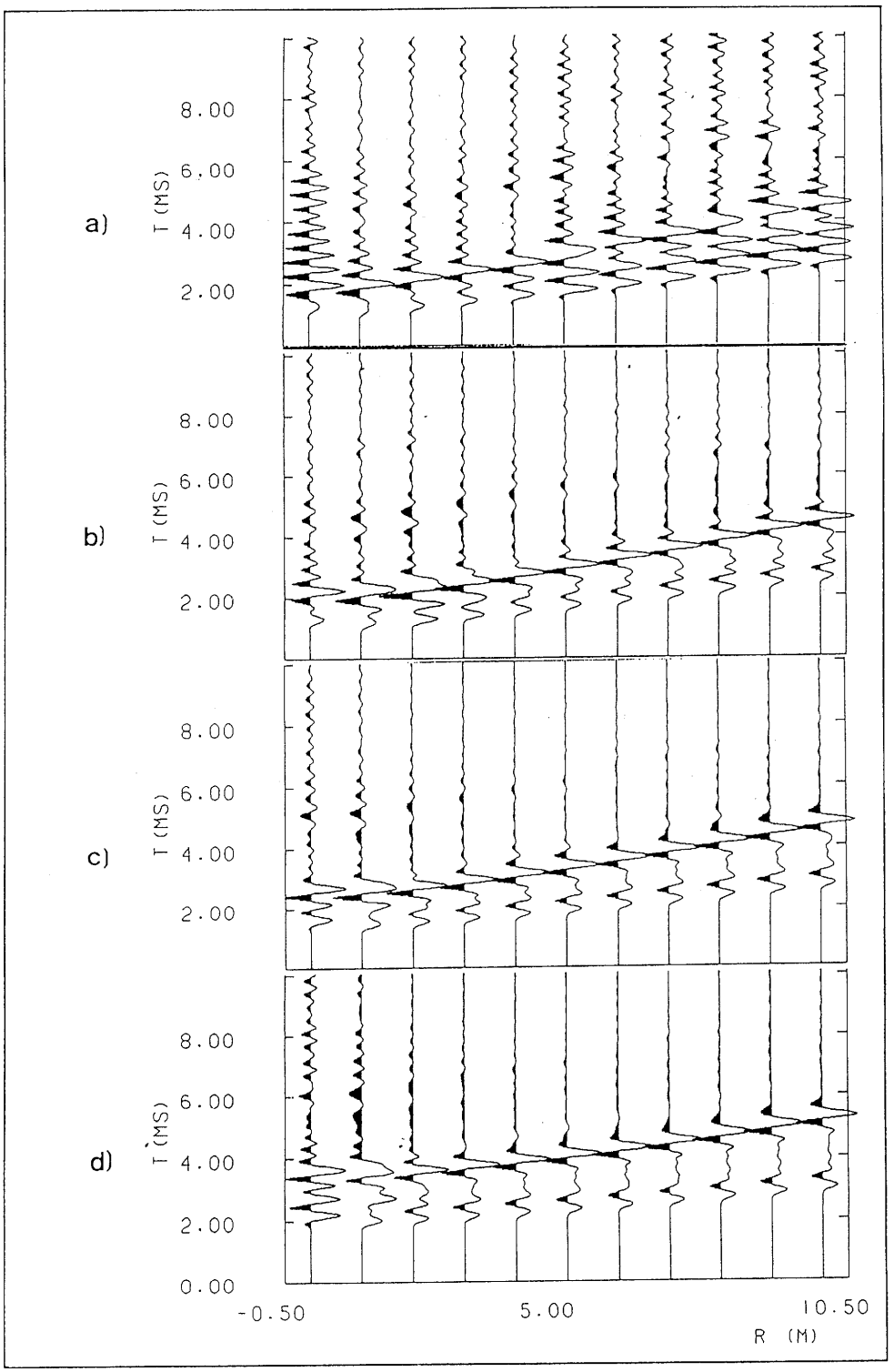

Figure 2.4 Theoretical seismograms (x-components) for $\theta=90^0$ and
a) Rs = 0 m
b) Rs = 2 m
c) Rs = 4 m
d) Rs = 7 m
Rs, Rr and θ are defined in Figure 2.1

2.2 Three-dimensional Modeling

The tunnel wave problem in three dimensions was approached analytically. A cylindrical coordinate system (r, θ , x) was used (Figure 2.5) to evaluate dispersion and amplitude decay. It was assumed that the tunnel wave is independent on θ and therefore, only Rayleigh waves are considered in this study. The displacement vector $\vec{u}$ can be expressed by the rotational displacement potential $\vec{\Psi}$ and the dilatational displacement potential Φ. For the special case of cylindrical symmetry, as $\vec{u}$ = grad Φ + rot $\vec{\Psi}$, one gets:

$$u_r = \delta\Phi/\delta r - \delta\Psi/\delta x$$

$$u_\varphi = 0$$

$$u_x = \delta\Phi/\delta x + \delta\Psi/\delta r + \Psi/r$$

By solving the wave equations :

$$\delta^2\Phi/\delta r^2+1/r\cdot\delta\Phi/\delta r+\delta^2\Phi/\delta x^2=1/\alpha^2\cdot\delta^2\Phi/\delta t^2$$

$$\delta^2\Psi/\delta r^2+1/r\cdot\delta\Psi/\delta r+\delta^2\Psi/\delta x^2-\Psi/r^2=1/\beta^2\cdot\delta^2\Psi/\delta t^2$$

and satisfying the dispersion equation, one obtains the following displacements assuming that the radial compressional and the shear stresses vanish at the tunnel wall:

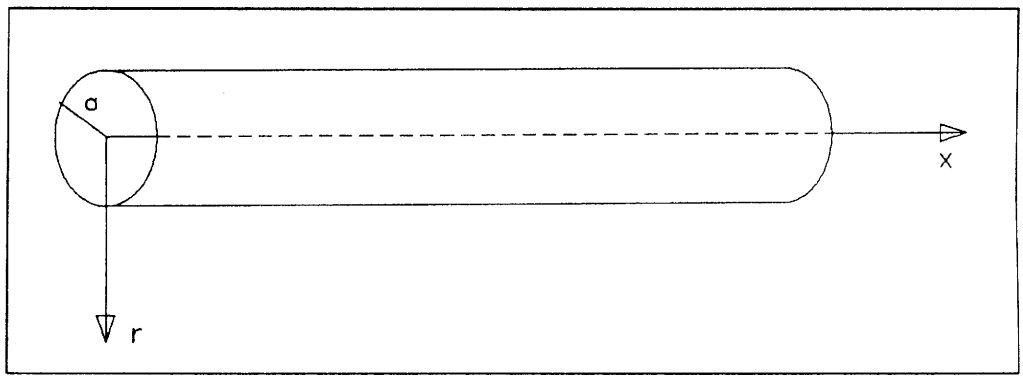

Figure 2.5 The 3-dimensional model of the tunnel (a=diameter of the tunnel, r = radial component, x= axial component)

$$u_r \approx -l\left(\frac{k_1(l\,r)}{k_1(l\,a)} - \frac{1}{1-c^2/\,2\beta^2}\cdot\frac{k_1(l'r)}{k_1(l'a)}\right)\cos(\omega t-kx)$$

$$u_x \approx k\left(\frac{k_0(l\,r)}{k_1(l\,a)} - \frac{(1-c^2/\beta^2)^{1/2}\;(1-c^2/\alpha^2)^{1/2}}{1-c^2/\,2\beta^2}\cdot\frac{k_1(l'r)}{k_1(l'a)}\right)\sin(\omega t-kx)$$

where:

α = P-wave velocity
β = S-wave velocity
ω = angular frequency
k = wave number in x-direction
c = phase velocity
l = P-wave number in r-direction
l′ = S-wave number in r-direction
$k_{0,1}$ = modified Bessel function of the order 0, resp. 1

This is the expression of a wave with an elliptical polarization. For high frequencies the dispersion equation and the displacements described above become similar to the results for a Rayleigh wave in a homogeneous half space.

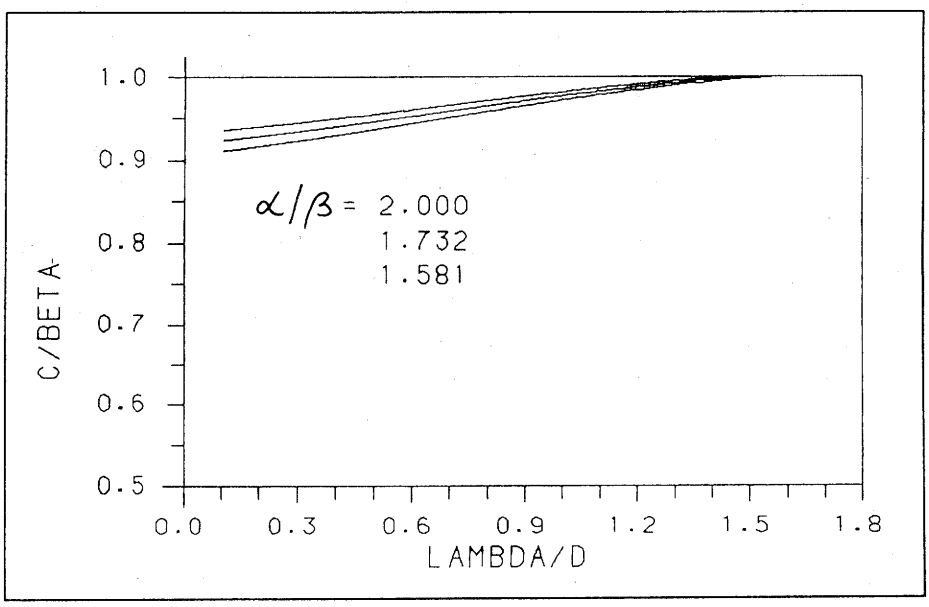

Figure 2.6 Relation of the ratio between the tunnel wave (C) and shear wave velocity (β) and the ratio of wave length (λ) and tunnel diameter (D). α/β is the the ratio of the compressional / shear wave velocity for each of the three curves.

The relation between the phase velocity c and wavelength is expressed in Figure 2.6. It is demonstrated that only very weak dispersion can be expected. In the case of the tunnel at GTS one can conclude that the velocity of the tunnel wave is equal to the S-wave velocity for all frequencies below 600 Hz.

The comparison of displacements generated by tunnel waves and Rayleigh waves at a free surface (Figure 2.7) shows a significant difference in amplitude characteristics below 1000 Hz. The radial displacement u_r produced by a tunnel wave decays much slower in the frequency range 300 to 1000 Hz. For the axial displacement u_x one observes the opposite phenomenon: the displacement of the tunnel wave decays much faster and reaches zero at a radial distance from the tunnel wall of appr. 2 to 3 tunnel diameters. This behavior of the tunnel wave is more characteristic for a shear wave rather than for a surface wave.

The kinematics of a non-axial tunnel wave was studied in order to explain resonances or constructive interferences. In the case that we are dealing with, i.e. a high frequency wavelet, the solution of the problem is quite straight forward. It is possible to investigate only rays travelling along the tunnel on different paths from the source to a given receiver. Figure 2.8 illustrates the possible ray paths. The points P_j are actually the same receiver and the subscript only indicates how many times the wave had travelled around the tunnel before it arrived at the receiver point. The value j = 0 indicates the direct wave while all positive subscripts denote waves traveling counterclockwise around the tunnel. Consequently, all negative subscripts denote all rays travelling in clockwise direction. The travel times for these rays can be expressed in a simple way:

$$t_j = 1/\beta \, (x^2 + (q + ju)^2 \,)^{1/2}$$

where

x = source - receiver distance along tunnel axis

$q = a \, \Delta\varphi$ ($\Delta\varphi$ = angle between source and receiver)

$u = 2\pi \, a$ (a = radius of the tunnel)

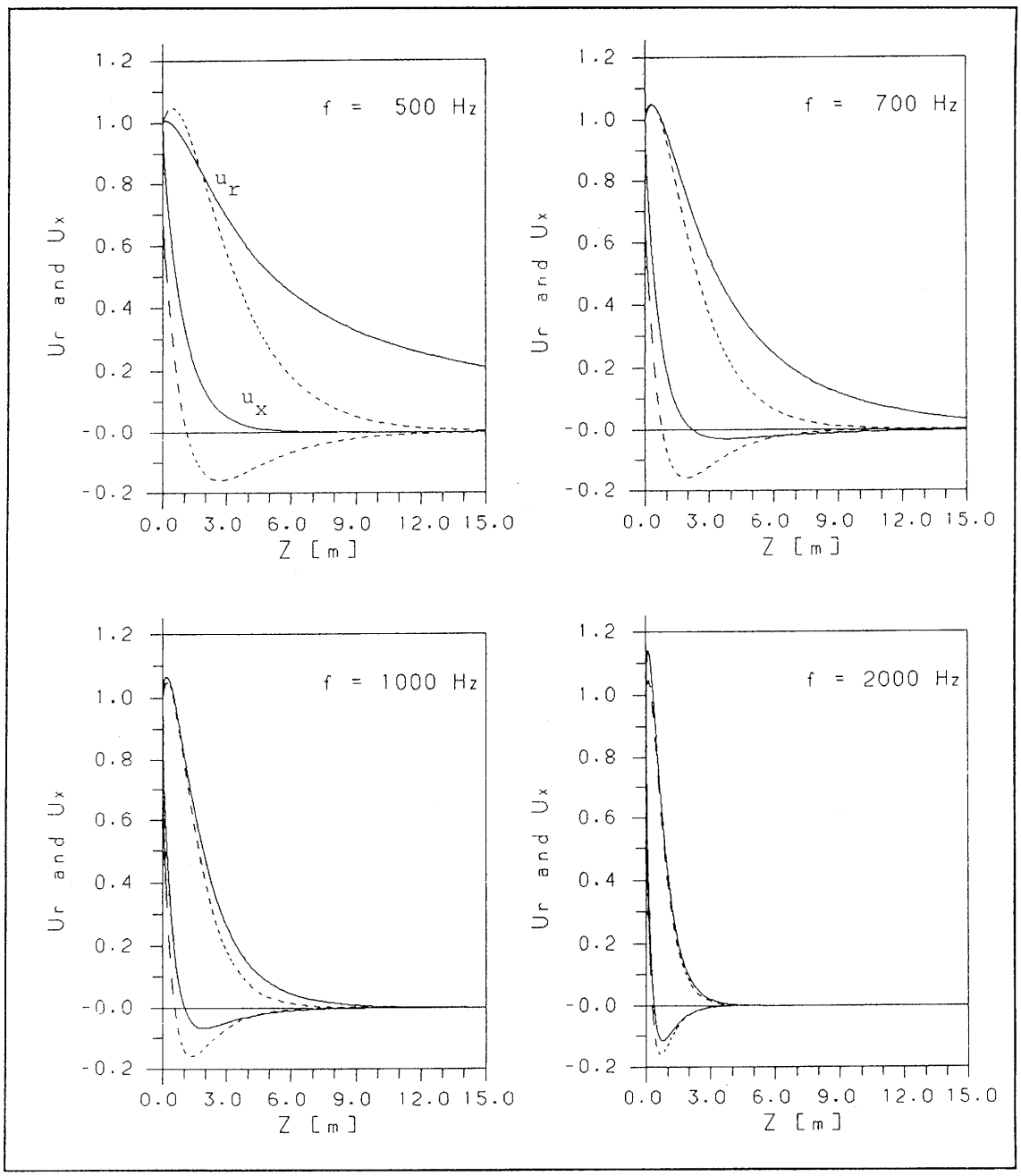

Figure 2.7 Amplitudes of displacements U_x and U_r of the tunnel wave as a function of distance to the tunnel wall.
- Solid line - tunnel of 3,5 m diameter
- Dashed line - half space (infinite diameter)

The ratio between P-velocity and S-velocity is 1.732

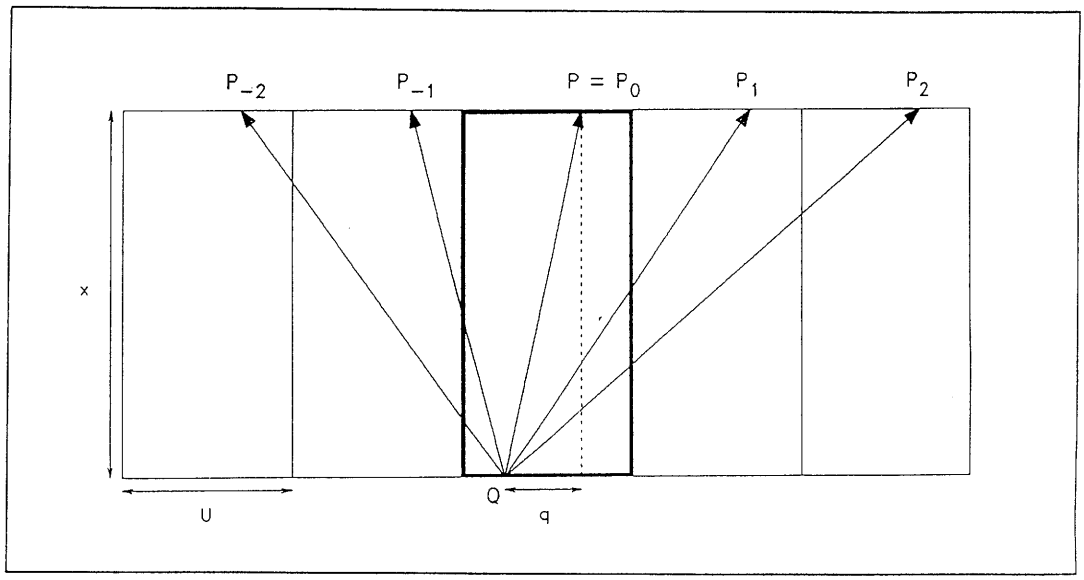

Figure 2.8 Unfolded tunnel (thick box :0 - 2π, thin boxes : multiples of 2π representing waves going around the tunnel several times before reaching the receiver P.
Q = source
P = receiver
→ = ray

A travel time plot (Figure 2.9) can be calculated using this formula. It can be seen that except for the direct wave the apparent velocities are higher than the S-wave velocity and seem to be more or less constant for larger values of j.

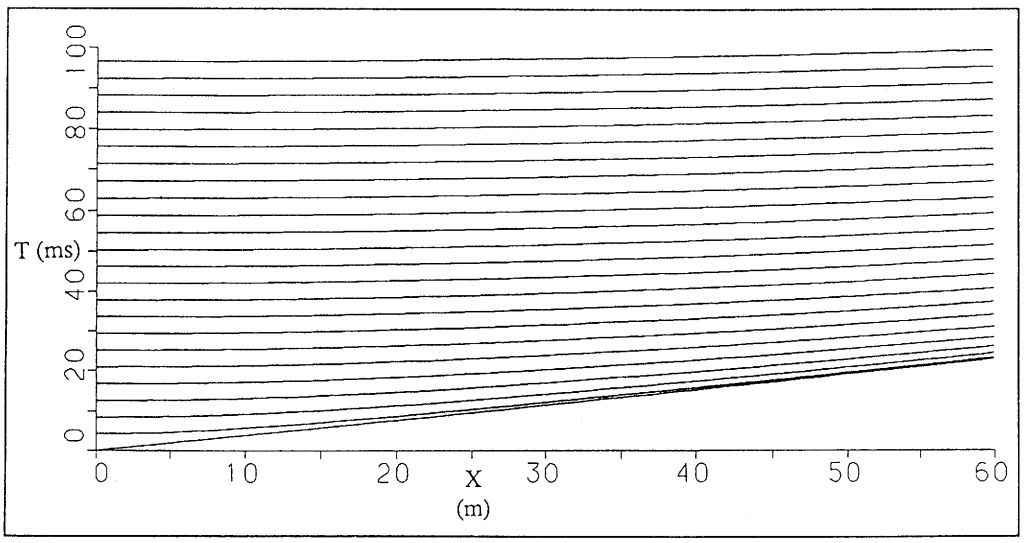

Figure 2.9 Travel time plot for different phases as depicted in Figure 2.8

2.3 Conclusions from Numerical Modeling

The numerical modeling showed that we get the best results by positioning the source and the receivers at several meters away from the tunnel wall. In practice this would require a large number of small boreholes drilled radially from the tunnel. A realistic setup is to put the source in a lateral drillhole at a minimum distance of about 4 m from the tunnel wall and to attach the receivers directly to the tunnel wall. In this case we expect to reduce the tunnel wave and still retain a configuration requiring a comparatively short operational time.

The numerical modeling gave solutions for decreasing the tunnel waves. However, by comparing the synthetic seismograms and the actual signals recorded at Grimsel, it became apparent that tunnel waves account for only a small part of the ringing. Coupling effects are responsible for the rest.

3 THE VERTICAL SEISMIC PROFILING (VSP) METHOD

The VSP technique was developed for borehole seismic measurements. A VSP profile is normally displayed as a group of seismograms (traces) arranged in increasing order of depth of the stations forming the measuring array. All traces have a common time reference. As the other axis is the time history, a VSP section is a two-dimensional space with the axes representing depth and time. Therefore, the tangent of a direction in this space can be treated as a velocity. This apparent velocity is not identical to the physical velocity of a given wave field but, with some conditions imposed on the survey layout, it can be close enough to help in the discrimination of different wave types. More advanced processing techniques /Cosma, Heikkinen and Pekonen, 1991/ use the actual propagation velocity for the same purpose. The most important feature of this data acquisition technique is the fact that two-dimensional filters can be applied to reduce incoherent noise and separate coherent events by their phase velocity.

3.1 Data Acquisition Geometry

The simplest VSP configuration - zero offset - is presented in Figure 3.1. In this case the source and the detector array (geophones, accelerometers, or hydrophones) are collinear, in the same borehole or along the tunnel axis. The direct wave (down going wave) has another apparent velocity than the reflected wave (up going). Actually, in the special case of a zero offset VSP layout and for a planar reflector perpendicular to the detector array, the apparent velocity of the reflected field is equal in modulus to the velocity of the direct wave but with opposite sign. This means that velocity selective operations (e.g. filters) can be used to suppress the direct wave and enhance the reflected energy /Lee and Balch, 1983/. With a more general survey layout and reflector orientation the use of procedures based on the apparent velocity becomes problematic. This is why we have applied in this project also velocity filters taking into account the physical velocity. As a rule, the latter are much more laborious than the former, because they imply the calculation of a geometrical model and ray paths before the real velocity can be introduced. The apparent velocity techniques are still a simple but valuable tool for filtering out waves travelling along the measuring array, like tunnel waves or tube waves.

3.2 Processing Techniques Used to Enhance Reflections in the VSP Data

Several standard and nonstandard processing techniques were used to enhance the reflected signals and to reduce noise in the seismic data. Most of these techniques are designed to enhance certain coherent energy trends in the data and to wipe out non-coherent energy (noise) and correlated energy from phases which are of no use for the work (e.g. direct wave, tube wave). A part of these techniques is especially designed for VSP type data, other routines are modified for our particular needs.

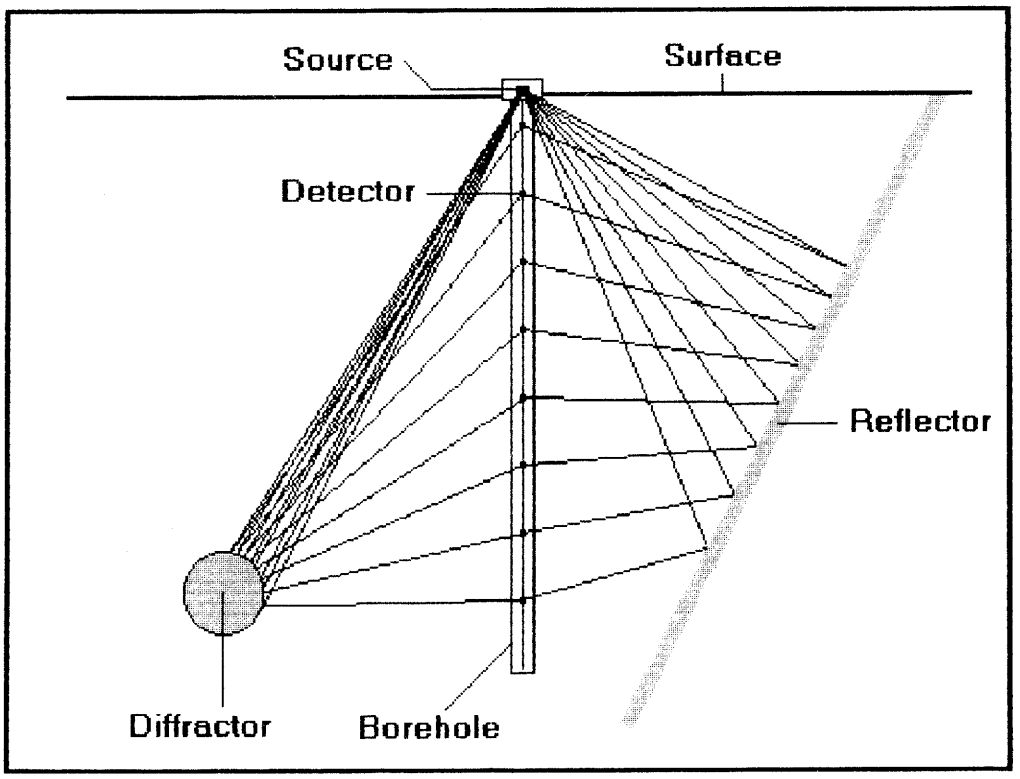

Figure 3.1 Zero offset VSP layout with examples of reflected and diffracted rays.

3.2.1 The Median Filter

With the median filter technique /Hardage, 1983/, the first step is to define in the (z,t) data space the direction associated with a given velocity (here the velocity was estimated from the downgoing wave field). A subset of data points is defined by selecting samples along this direction. This is done over a chosen number of traces on both sides of the reference trace. The median value is obtained in the following way: if N data samples are arranged in ascending order of magnitude, the median value is the sample in the position (N+1)/2 of the sequence. The procedure is repeated for each sample in the profile. The median downgoing wave field thus obtained is then subtracted from the original profile to provide the desired residual field, in our case the reflected (upgoing) wave field.

After suppressing the direct wave, the profile can be further processed by applying the procedure to the upgoing field. This holds if an estimate of velocity for the upgoing field is available. For zero offset VSP and a reflector perpendicular to the measuring array, this amounts to changing the sign of the apparent velocity. The median field consists now mostly of reflected energy while the residual field (obtained by subtraction) represents non-coherent noise and possibly also coherent energy but with other apparent velocities than the one given as parameter.

The median value can be calculated either by taking only one sample from each trace (one- dimensional window), or by taking several time samples per each trace (two-dimensional window). The effect of the two-dimensional window is to reduce high frequency noise and to compensate for differences between the real and the apparent velocities.

The discussion of the median filters concerned so far only approaches based on apparent velocity. It has been assumed implicitly that the offset of the source is negligible with respect to the length of the detector array and that the features of interest are nearly perpendicular to the detector array i.e that the reflection events line up along straight segments. For an accurate treatment of tunnel tests curved events should be also considered. A variant of median filter based on the real propagation velocity has been used by Vibrometric for for this purpose. Another particularity of this filter is that a weighting scheme is applied to eliminate noisy traces from the median estimate /Cosma, Heikkinen and Pekonen, 1991/.

3.2.2 Deconvolution Filter

For a standard VSP configuration, with a fixed source on the surface and the receivers forming the down hole array, we can assume that the down going wave field at a given level illuminates the half space below and is convolved with the earth reflectivity sequence below that level. Therefore the down going wave field for each seismic trace represents a recorded far field signature.

In the reversed VSP configuration, with fixed receiver and array of sources, we can swap source and receivers due to reciprocity. This means that the direct wave field seen at a given surface receiver location is the same as the wave field that would have travelled from the receiver location to the source location. The up going wave fields can be then deconvolved using a deterministic deconvolution operator computed from the down going compressional wave field. The deconvolution operators are first computed and applied to the down going wave field and then the same operators are applied to the up going wave field.

A predictive deconvolution operator can be applied to remove reverberations and multiples. Data adaptive algorithms tuned automatically by the autocorrelation function are efficient and easy to use /Griffiths, Smolka and Trembly, 1977/.

3.2.3 The Tau-P Filtering Method

The Tau-p transform is commonly used in processing seismic reflection data for removing multiples and time dependent dip filtering. This transform and its inverse can also be used as a multichannel filter to enhance the reflected signals /Tatham, 1989/.

In the Tau-p transform the data are stacked (in Data Space) along linear trajectories corresponding to fixed slowness values p (apparent velocity = 1/p). The output for one p-value is a trace where time is replaced by the intercept time τ :

$$G(\tau,p) = \sum_{z} F(z, t=\tau+pz)$$

The inverse transform is calculated in a similar way by stacking in Tau-p space. To preserve the signal shape a further Hilbert transform $\mathcal{H}$ and derivation with respect to time is required :

$$F(z,t) = \frac{d}{dt} \mathcal{H} \left(\sum_{p} G(\tau=t-pz, p) \right)$$

In a variation of this technique / Cosma, Heikkinen and Pekonen, 1991/, the change of the apparent slowness along curved events is accounted for by applying variable slowness limits. The general idea is that, after the two-way transform, each point in the Data Space receives only those τ- and p-contributions which may correspond to real reflections. One can further limit the allowed reflectors by their dip, depth etc.

The profile is divided in overlapping panels. For each panel the traces are stacked with different incremental moveouts, each moveout corresponding to an apparent slowness. A hyperbolic event (as reflection events are in the general case) which is continuous over several panels will stack at a different slowness value in each panel so that curving events are not distorted in the process. By this stacking procedure the transformed profile $G(\tau,p)$ is built only for slowness values obeying the condition: $P1 < p < P2$.

The lower limit for the slowness P1 corresponds to a straight reflection event, i.e. to an apparent velocity equal to the real seismic velocity ($P1 = -1/Vp$). For a zero offset configuration this is the mark produced by a perpendicular reflector. The upper slowness limit is calculated from the geometry of the survey ($P2 = P2(z,t)$. A weighting operator $H(z,t)$ is calculated and substituted to p in the expression of $G(\tau,p)$, which becomes $G(\tau,H(z,t))$. The definition of the operator H is:

$H(z,t) = p$ if $P1 < p < P2(z,t)$

and

$H(z,t) = 0$ otherwise.

When the inverse transform is performed, only the allowed slowness values will be imaged.

3.2.4 The Kirchhoff Migration

The method used to transform VSP coordinates into CDP offset vs. time is a type of Kirchhoff migration based on the Generalized Radon Transform (GRT) /Miller,Oristaglio and Beylkin, 1987; Winkler and Cassel, 1989/. Conceptually, the method is explained by the Huygens' principle, where reflectors can be thought as a grid of diffraction points. Here the subsurface is assumed to consist of a dense grid of tiny reflectors, each with a range of dip angles around the predominant structural dip defined by the velocity depth model. The central dip of each reflecting element is determined by interpolation between the dips of the geological horizons above and below.

Migration is carried out by collapsing the hyperbolic events in the data set corresponding to each reflection element. The time locations of these hyperbolas are calculated by ray tracing assuming a velocity vs. depth model that approximates the subsurface structure. The ray tracing includes ray bending, thus influencing the shape of the reflection patterns which are not mathematically exact hyperbolas in the general case. However, we will continue to call them so, by convention. Wherever a hyperbola is tangent to a real seismic event amplitudes will be summed constructively, while in other situations the amplitudes will cancel by summing and vanish. Excessive stacking of noise is avoided by stacking only along those portions of the hyperbolas that correspond to the prevailing dip range at a given "reflector" location. This dip range is an input parameter and chosen to include only those dip angles that are geologically probable. The final value of the image at a given "reflector" point is the sum for all dips damped by a function depending on the offset relating to the central dip and the maximum aperture. When possible, the background velocity model is updated iteratively until it correlates with the migrated data.

3.2.5 The Image Point Transform ($\rho\zeta$)

The $\rho\zeta$-processing (or Image Space processing) /Cosma, Heikkinen and Pekonen, 1991/ is a technique which Vibrometric AG has developed for filtering and interpretation of reflection profiles and especially for VSP sections. Like the Kirchhoff migration, it is based on a Radon transform performed along curve integrating paths. In this case the transform is performed from the (z,t) Data Space (the normal VSP profile) into a new domain called $\rho\zeta$-space. This transform and its inverse can be used as a multi-channel filter to enhance the reflected signals and as an interpretation tool to estimate the strength and position of reflectors.

The position of a planar reflector is uniquely determined by the coordinates of the virtual image of the source, i.e. the mirror image of the source point with respect to the reflecting plane. We will call this space, where image sources are defined, $\rho\zeta$-space (Image Space). The position of a point in the $\rho\zeta$-space can be defined by two coordinates: the depth along the borehole ζ and the normal distance to the hole ξ. The latter will be replaced by the variable ρ defined as $\rho^2 = \xi^2 + \zeta^2$. The third coordinate, the rotation angle ϕ of the image point around the borehole, is redundant, as all image points with the same ζ and ρ will give the same travel time function whatever the value of ϕ is (Figure 3.2).

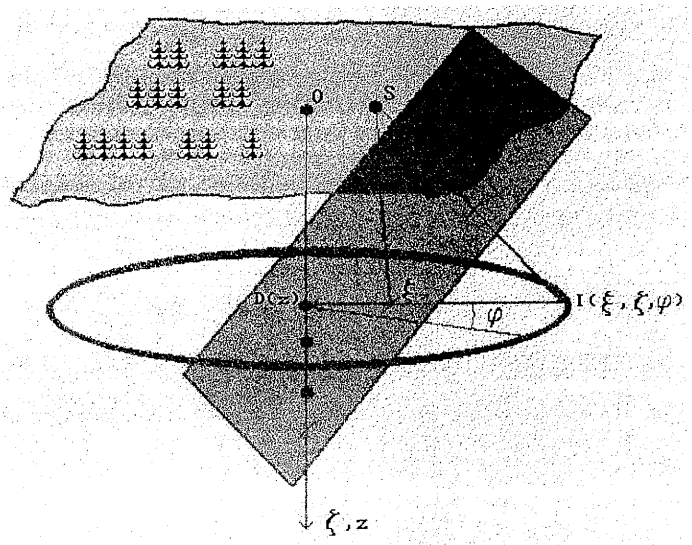

Figure 3.2 Schematic presentation of the way the Image Space is obtained. All virtual images $I(\xi,\zeta,\varphi)$ found on the circle are at the same distance from any given point on the axis of the detector array. Therefore, they correspond to the same hyperbolic pattern in the data space (z,t) and consequently to the same point in Image Space for any value of φ. S is the source position and the detector array is in a borehole along the Oz axis.

The practical way to perform the $\rho\zeta$-transform from Data Space to Image Space is the following : $F(\rho,\zeta)$ is calculated from the Data Space G(z,t) by stacking along the trajectory corresponding to the reflection travel time $t(\rho,\zeta)$. The amplitude of the function F will then depend on the strength of the reflected energy arrived from the reflectors corresponding to the image point of coordinates (ρ,ζ). The travel time $t(\rho,\zeta)$ for the reflection is equal to the distance from the image point to the detector divided by the P-wave velocity c:

$$t^2(\rho,\zeta) = ((z-\zeta)^2+\xi^2)/c = (\rho^2+z^2-2z\zeta)/c$$

If there is a reflector with the coordinates (ρ,ζ), then $F(\rho,\zeta)$ will have high amplitude; if there is no reflector, the amplitude will be low.

By taking the envelope of $F(\rho,\zeta)$, we get a positively defined function, a reflection strength map. Because the amplitude of F is high in those parts of $\rho\zeta$-space, which correspond to existing reflectors, the local maxima of the reflection strength map will tell the positions of the probable reflectors.

It is possible to construct an inverse transform from $\rho\zeta$-space back to Data Space by summing in $\rho\zeta$-space along the path $\rho^2 = (c\ t)^2 - z^2 + 2z\zeta$. In the $\rho\zeta$-inverted section the reflected signals are emphasized, because during transformation only true P-wave reflections stack properly.

After applying the transform, it is better to mute those regions in the $\rho\zeta$-space containing impossible event locations (e.g. $\rho < \zeta$). Theoretically, nothing should be there, but data discretization and numerical truncation errors may create small but still disturbing artifacts. It is also wise to mute the areas corresponding to events seen only in few traces at the top or at the bottom of the original profile. Then the reflection strength maps can be more reliably calculated from the $\rho\zeta$-sections.

We can further reduce the data and simplify the interpretation by using Image Space filters which either reject or pass reflectors depending on the dip angle θ of the image point (ζ,ρ) (θ is defined by $\cos(\theta) = \zeta/\rho$). Before the inverse transform the unwanted regions of the Image Space are blanked by applying a suitable filter function. By this type of filters it is possible to remove much of the interference without destroying the continuity of the reflections.

When the shot point is on the array or its extension θ is the relative dip of the reflector with respect to the array (borehole or tunnel). For the reflectors cutting the borehole (or tunnel) behind the source, θ will have negative sign and for the reflectors cutting the borehole on the detector side the sign will be positive. When the inverse transform is performed after the reflector angles have been limited by filtering, the new section in the Data Space will contain only few strong events, which can quite reliably be interpreted as true reflections.

4 PROCESSING TESTS WITH EXISTING SEISMIC DATA

After a first planning stage it was decided that a processing and interpretation test be conducted using existing data from the GTS underground seismic site (US). An overview on the GTS site is given in Figure 4.1. The data available at that time were the data set used for the seismic and the radar tomography program. To ensure that we would obtain the maximum output and in order to compare different processing and interpretation techniques part of the seismic data set was sent to three different companies for processing.

4.1 Field Geometry

The geometry of the tomography measurements is described in detail in the NTB 88-06 (Gelbke, 1988). The descriptions and labels used in this report are based on the nomenclature introduced by Gelbke (1988). As shown in Figure 4.2 , the seismic data for the tomography project were collected between tunnel and boreholes as well as between boreholes.

The following seismic data subset (Figure 4.3) was chosen in order to get a realistic prediction test.

- Receiver positions in the borehole BOUS 85.001 and 85.003 at shallow depth (2.5 - 10 m). The receiver positions used in this study in borehole BOUS 85.003 are named receiver stations 1-4, the selected positions in BOUS 85.001 are numbered 121-124.

- Source positions along the tunnel with a station spacing of 2.5 m between shot-station 181-240 and 5 m between 241 and 269 for four receiver positions in borehole BOUS 85.003.

- Source positions along the tunnel with a station spacing of 2.5 m between shot-station 269-241 and 5 m between 240 and 181 for four receiver positions in borehole BOUS 85.001.

- A sledge hammer was used as seismic source and Endevco accelerometers as receivers. The acquisition system used at GTS was the Seamex of the Deutsche Montan Technologie (DMT), formerly Westfälische Berggewerkschaftskasse (WBK).

The configuration of one receiver point and an array of source positions is equivalent to reverse VSP (in this case horizontal seismic profiling, i.e. HSP), assuming the tunnel to be a horizontal borehole.

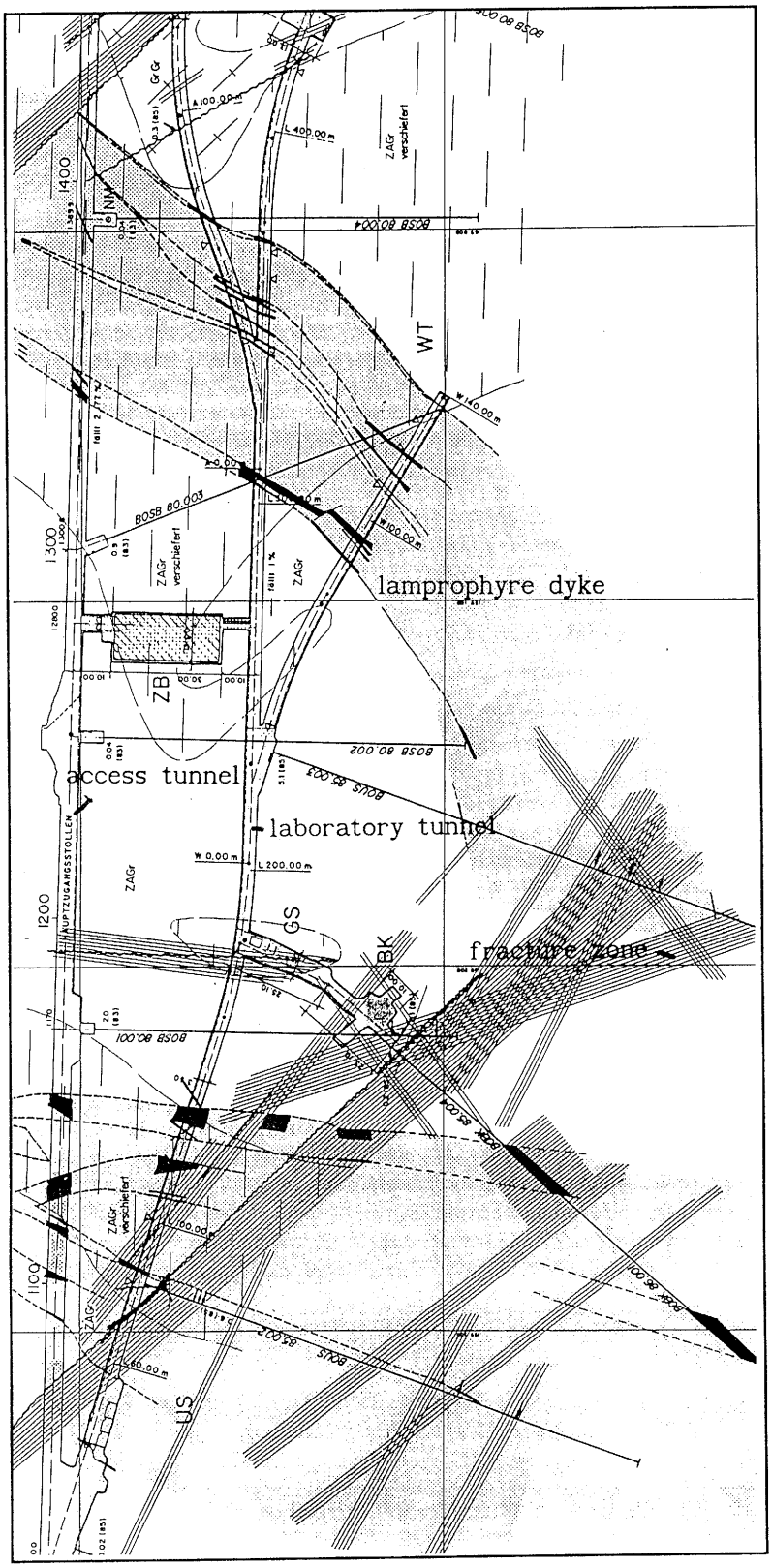

Figure 4.1 Overview of the Grimsel test site.

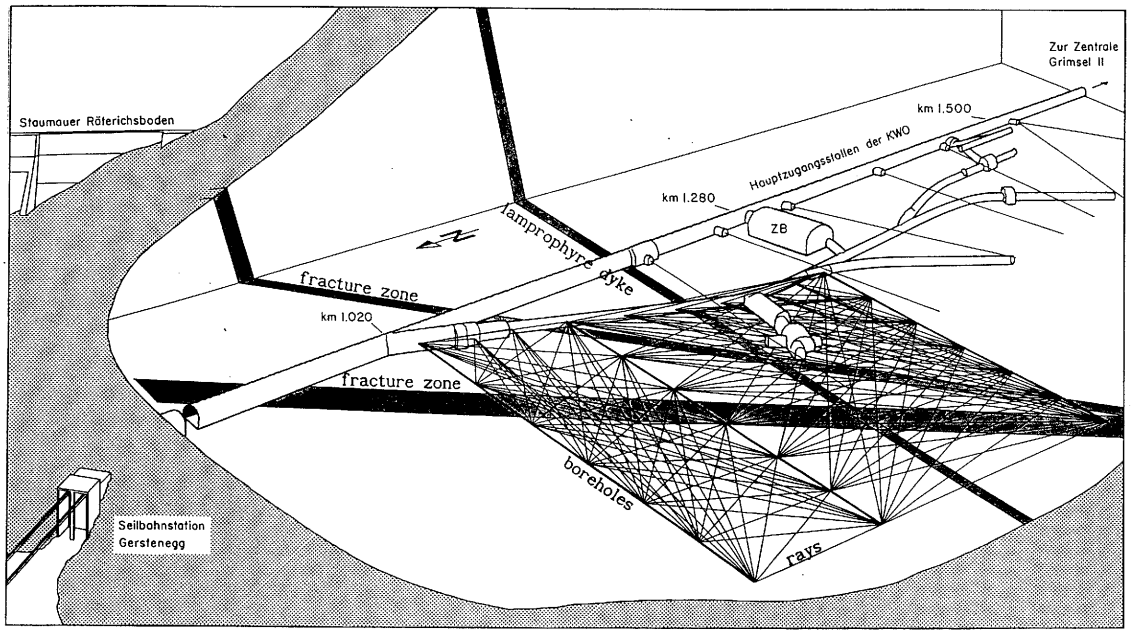

Figure 4.2 Test layout for the tomographic experiment at GTS.

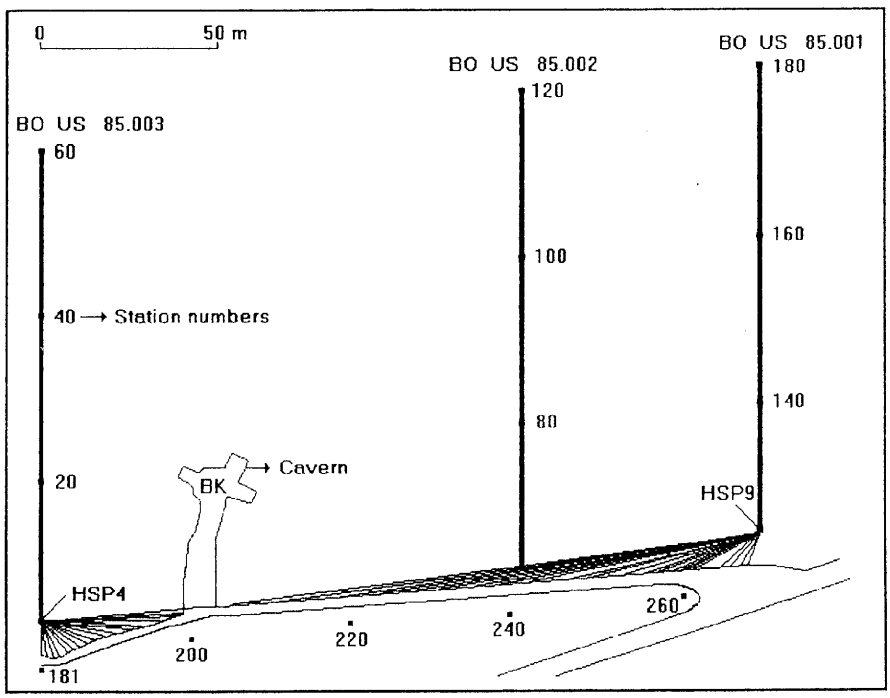

Figure 4.3 The subset of the tomographic experiment data chosen for the test of reflection techniques.

4.2 Data Characteristics

The total data set consists of 8 single receiver reverse VSP data sets and 2 stacked VSP data sets, each of them containing 2 components. One component is perpendicular to the axis of the receiver borehole. Therefore it is expected to contain most of the reflected P-wave energy from reflectors ahead of the array. The other component is parallel to the axis of the receiver hole and therefore preferentially displays the reflected S-waves. All shots are located along the tunnel with shot station spacing of 2.5 resp. 5 m.:

HSP 1-1: receiver in BOUS 85.003 station 1

HSP 1-2: receiver in BOUS 85.003 station 2

HSP 1-3: receiver in BOUS 85.003 station 3

HSP 1-4: receiver in BOUS 85.003 station 4

HSP 1-5: receivers in BOUS 85.003 stack (1-4)

HSP 1-6: receiver in BOUS 85.001 station 121

HSP 1-7: receiver in BOUS 85.001 station 122

HSP 1-8: receiver in BOUS 85.001 station 123

HSP 1-9: receiver in BOUS 85.001 station 124

HSP 1-10: receivers in BOUS 85.001 stack (121-124)

The data were recorded using a digitizing rate of 0.125 ms, as signal frequencies up to 2 KHz had to be digitized. As shown in the wave number-frequency (F-K) plot in Figure 4.4 for section HSP 1-1 most of the energy is present in the frequency band 250 Hz - 1750 Hz. It can be noticed that especially in the frequency range between 1000 and 1250 Hz a lot of noise, probably due to tunnel wave is present for all wave numbers. In general a band pass filter was used to suppress the tunnel wave energy and to avoid spatial aliasing for high frequencies due to large distances between the shot stations. Assuming a seismic P-wave velocity of 4800 - 5200 m/s the high frequency cut-off level for the pass band filter should be in the range of 900 and 1000 Hz for P-wave processing and about 400-500 Hz for S-wave processing. The resulting FK-spectrum of one profile after filtering (200-800 Hz) is shown in Figure 4.5.

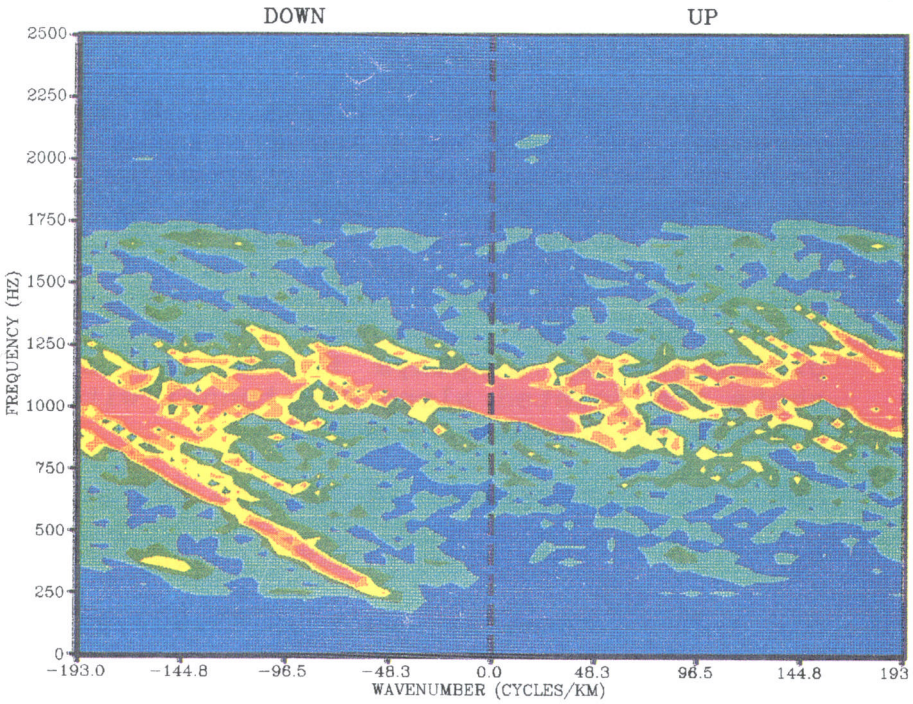

Figure 4.4 F - K transform of the VSP profile 1 - 1. Most of the energy is present in the band 250 Hz - 1750 Hz.

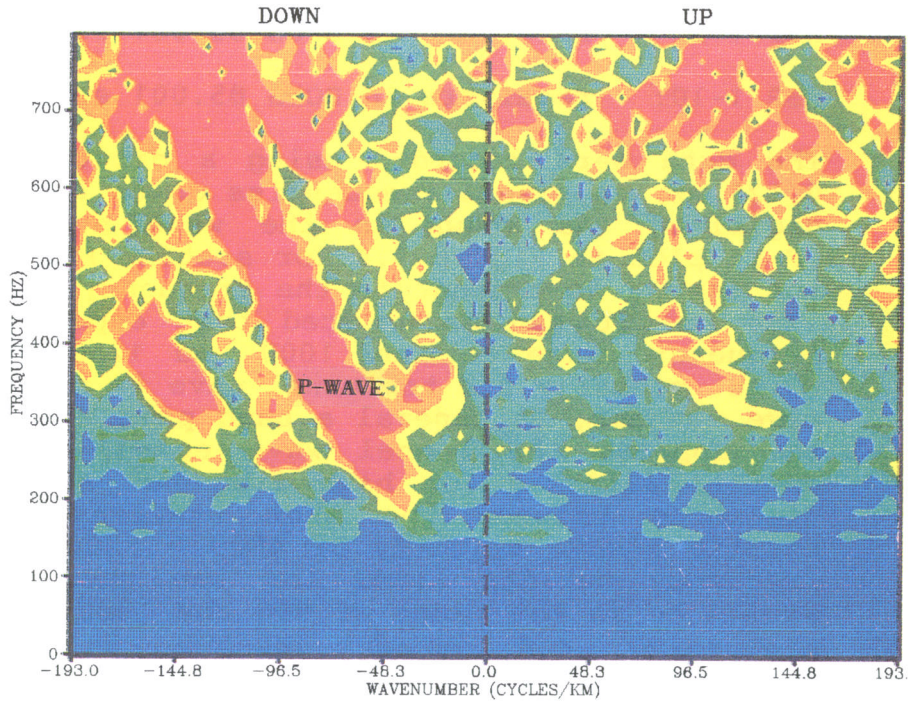

Figure 4.5 F - K transform after band pass filtering from 200 Hz to 800 Hz. The energy associated with the down going P-wave becomes apparent.

Clearly one observes the energy associated with the direct (down going) P-wave and the direct S-wave. The P-wave energy is much higher in this case as the component is the one perpendicular to the direction of BOUS 85.003 (the preferential P-directions are investigated in the example presented in Figures 4.4 and 4.5). Another fact leads to substantial problems: we observe events in the later part of raw data sections which are not directly related to the shot. These events seem to represent acoustic emissions which might be induced by the blast and the seismic wave. The amplitude of those events is quite high and they are present only at a single trace. This can be explained because the section is not recorded at the same time but reconstructed from different shots. Large distortions and artifacts can be expected if these events are not eliminated before processing. Therefore, the sections were despiked before the real processing sequences could be started.

4.3 Processing by Schlumberger

The processing sequence started with a re-picking of the first break times and band pass filtering from 100 Hz to 2500 Hz. Afterwards a time varying gain

$$G_{ain}(t) = t^{1.2}$$

was applied to correct for the effects of spherical spreading of the wave field. This operator is known as True Amplitude Recovery (TAR). In addition, trace normalization was carried out to compensate for amplitude fluctuations due to differences in source power. For this RMS (root mean square) amplitudes were calculated in a 10 ms window after the first breaks.

Three techniques for velocity filtering were tested: Slant Stack (τ-P), Frequency-Wave number (F-K) and Median Filtering (see chapter 3). The first two methods generally suffer from spatial aliasing effects, in this case produced by the under sampling of the tunnel wave (V_t = 2500 m/s). Although it was attempted to alleviate the aliasing problem by band pass filtering of the input data, it was not possible to avoid undesired Rieber mixing /Sheriff, 1973 ; Hardage, 1983/ after the application of selective muting in the FK-domain.

4.3.1 Median Filtering

The median filter value at a particular depth was computed from the values at 5 depth values by taking 3 time samples per depth level (2D window). The

averaging effect of the 2D window reduced the high frequency noise and attenuated the errors due to inaccurate first break times. To eliminate any incoherent noise generated by subsequent deconvolution the median filter on the up going wave field is applied a second time after the deconvolution processes.

4.3.2 Deconvolution

A predictive deconvolution operator was applied to remove reverberations and multiples. The filter length was 60 ms and the prediction gap was 2 ms. The deconvolution operators were computed and applied to the down going wave field, and then the same operators were applied to the up going wave field. As the down going wave field did not contain noticeable reverberation patterns it was found that deconvolution did not improve the data quality and therefore deconvolution was not used in the final processing sequence.

4.3.3 Migration

As a final step, Kirchhoff migration was carried out in an attempt to finally improve the data set and to add the reflected energy at the appropriate spot where the reflector is located. Therefore different apertures were used and the best results were obtained using an aperture of 60°.

4.3.4 Results

Results are shown for the section HSP 1-4 (Figure 4.6) and HSP 1-5 (Figure 4.7). The filtered data which are multiplied by the variable gain function are shown in Figures 4.6 a and 4.7 a. It can be observed that for a single shot there is roughly no energy even in the direct wave past 190 m shot distance due to the weak sledge hammer source. The stacked data sections show more energy in those regions. After applying a wave field separation and an up wave enhancement with the 2D median filter (4.6b), one can see reflected energy from the shear zones and lamprophyre dykes from the vicinity of the tunnel. These reflections are enhanced additionally after the application of an automatic gain control (Figure 4.6 c). The migrated section HSP 1-4 (Figure 4.8) gives some ideas about the location of the reflectors but does not improve the picture significantly.

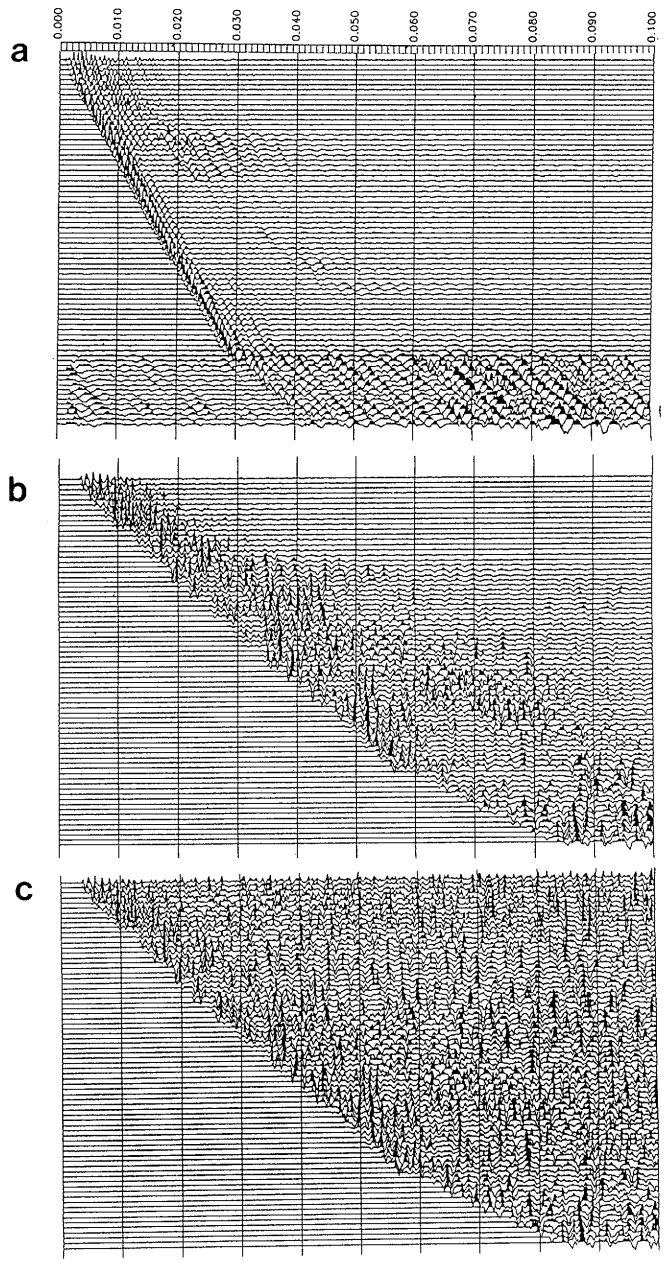

Figure 4.6 Seismic profile HSP 1-4 from GTS with receiver in borehole 85.003 (single receiver) at different processing stages.

a) Application of variable gain operator
b) Application of median filter operator
c) Application of automatic gain control operator

This figure shows the results of the processing from Schlumberger.

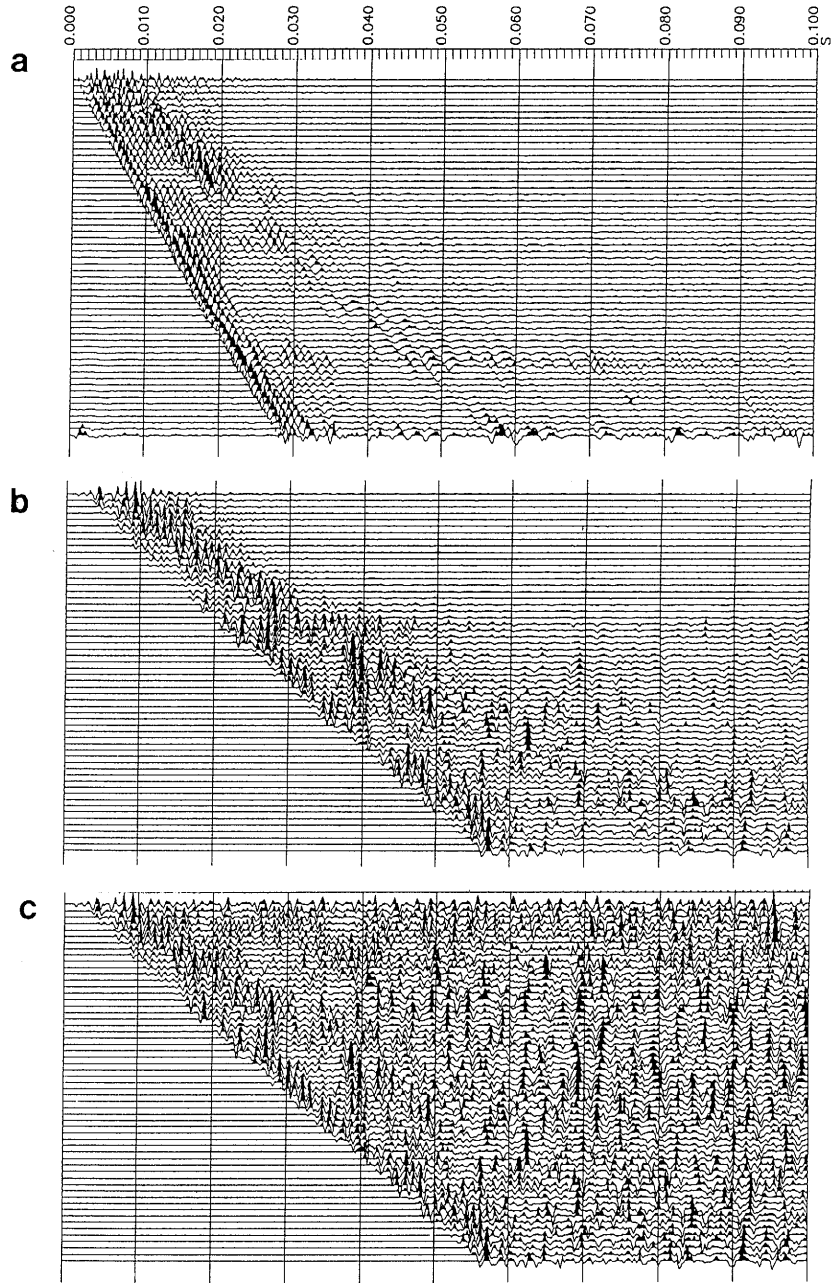

Figure 4.7 Seismic profile HSP 1-5 from GTS (stacked section). The same stages are depicted as in Figure 4.6. Results obtained by Schlumberger.

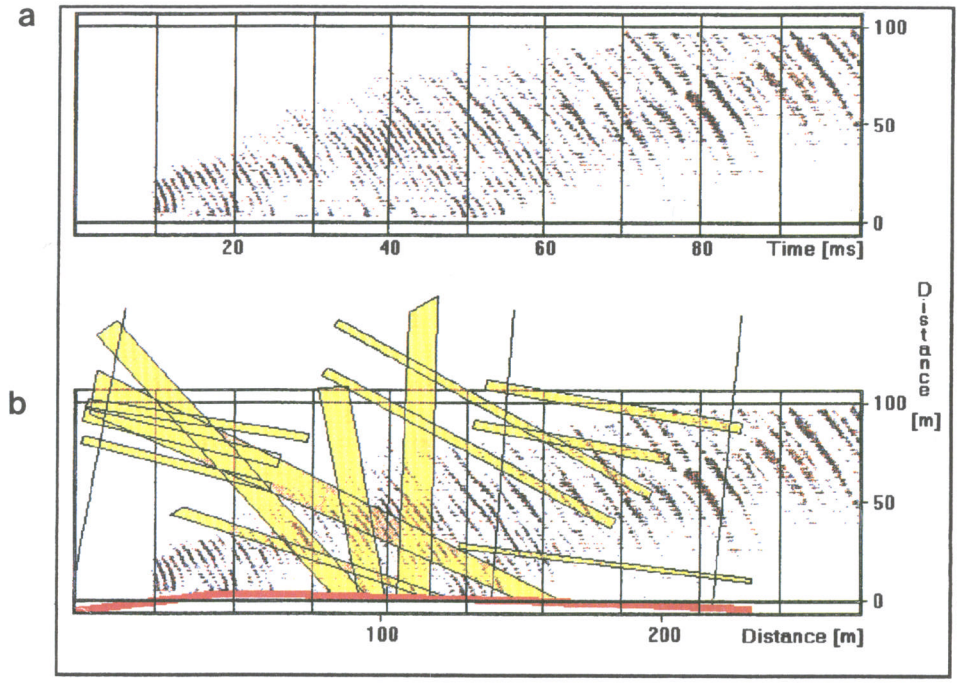

Figure 4.8 Profile HSP 1-4. Result of migration procedure

a) migrated section
b) the same section overlaid with structural model taken from the tomographic experiment (yellow bars indicate known fractured zones or lamprophyre dykes)

4.4 Processing by Vibrometric

The profiles were treated as normal VSP profiles, so that the shot points along the tunnel had to be represented as detector stations in a hypothetical borehole. Likewise, the real detector stations represented the source locations on a hypothetical surface. Two-dimensional filtering techniques were applied to the VSP-type profiles in order to separate the direct and the reflected waves. The point of interest for this processing procedure was the use of the τ-P filter routines with varying slowness limits.

The routines developed by Vibrometric for two-dimensional filtering are intended primarily for a VSP geometry. It is assumed that the detector stations are equally spaced along a straight line. With real VSP surveys, the bending of the hole does not introduce significant artifacts as long as the actual position of the borehole is known at all the detector depths.

In the present case the measuring stations were projected along the tunnel on a straight line, which amounted to a certain loss of accuracy. The condition of equal detector spacing was reached by choosing a subset of data which could comply with this requirement. The sources can be placed anywhere in relation to the detector array. The switching of the sources and detectors in order to achieve a down-the-hole VSP geometry bears no effect on the processing, when body waves (P and S) are concerned. However, a significant change occurs in the behavior of contact waves (surface and interface waves). With real down-the-hole VSP, the contact waves which have to be filtered out are tube waves, with much lower velocity than either P or S waves. With reversed HSP in a tunnel, one has to filter out surface and tunnel waves which are difficult to separate from S-waves and interfere strongly also with P-waves. The source positions were stacked (Figure 4.9) prior to processing in order to minimize the effect. The respective offsets were 5.0, 7.5 and 10.0 meters. This brought a certain improvement to the data.

Due to the source offset and different orientations of reflectors in crystalline rock, the reflected events are distributed in the HSP profiles on hyperbolic paths rather than on straight lines. It is therefore expected that two-dimensional filtering techniques based on apparent velocity would create a somehow distorted output. The approach followed in this work uses real wave velocities calculated from the geometry of the survey.

4.4.1 Processing Sequence

Band Pass Filtering - Normalization

The three profiles chosen were band pass filtered from 200 Hz to 1 kHz and an amplitude equalization operator was run along all traces ($t^{1.3}$). The trace length was reduced to 500 points to cut down the noise and spikes appearing at the end of the traces.

Stacking

The individual profiles were normalized according to the total energy per trace and then stacked with zero delay. Due to the transverse position of the array of sources, the events corresponding to reflectors are enhanced while the tunnel waves are delayed from profile to profile with appr. 1/3 of the dominant period and therefore attenuated.

Preliminary τ-P Filtering (apparent velocity)

The stacked profile of Figure 4.9 a was passed through a preliminary two-dimensional filtering procedure aiming at the enhancement of the events coherent over several traces (Figure 4.9 b). This was a standard τ-p transform with fixed slowness limits. Geometry dependent velocity limits were not used in this stage, this being only a pre-processing prior to deconvolution. The allowed apparent velocities ranged from -4500 m/s to +10000 m/s. In a layered structure a narrow velocity aperture around -4500 m/s would have been sufficient. We have considered that parts of the hyperbolic pattern of dipping reflectors may have positive apparent velocities, thus behaving as "down going" events.

Band-Pass Filtering

The τ-P filter may in some cases cause high frequency reconstruction noise. The profile was therefore re-filtered in the same band (200 Hz - 1 kHz). The filter used was causal in preparation for deconvolution, which is also a causal operation. This is a standard precaution to take but it did not change this profile in any noticeable way.

Deconvolution

A time-domain, data adaptive operator was used. It uses for self tuning the autocorrelation function. Its effect is the spiking of the trailing wavelets. The data adaptive procedure worked better than deterministic filters because the characteristics of the ringing vary from trace to trace and sometimes several ringing modes overlap in the same record each starting at a different time.

τ-P Filtering (real velocity)

The τ-P filtering is done considering the real wave velocities explained in chapter 3. The procedure can also be used as a velocity filter in the proper sense (by setting narrow slowness limits in the inverse transform). However, its role here was one of coherency enhancement rather than velocity filtering (Figure 4.9 c).

4.4.2 Results

The processing sequence outlined above has been applied on a trial basis only to one profile. The results were considered very good, especially regarding the capacity of the approach to enhance curved reflection events.

The events put in evidence after processing agree well with known rock features. The resolution power of the method could not be best proved by the relatively sparse measuring array. The resolution can be improved by taking a few precautions when interpreting the processed data. When estimating the position of the intersection of a reflector with the array one should take into account that the data is zero phase band pass filtered. Therefore, the intersection is to be found by following roughly the middle of the first cycle, not the beginning. A more accurate pick of the intersection can be also obtained by using the direct arrivals from unprocessed sections. The first arrivals are less accurately represented in the processed sections due to the filtering out of corresponding velocities.

Other observations are that most of the ringing could be removed and that the processing sequence taken as a whole is less sensitive to spatial aliasing than frequency domain methods.

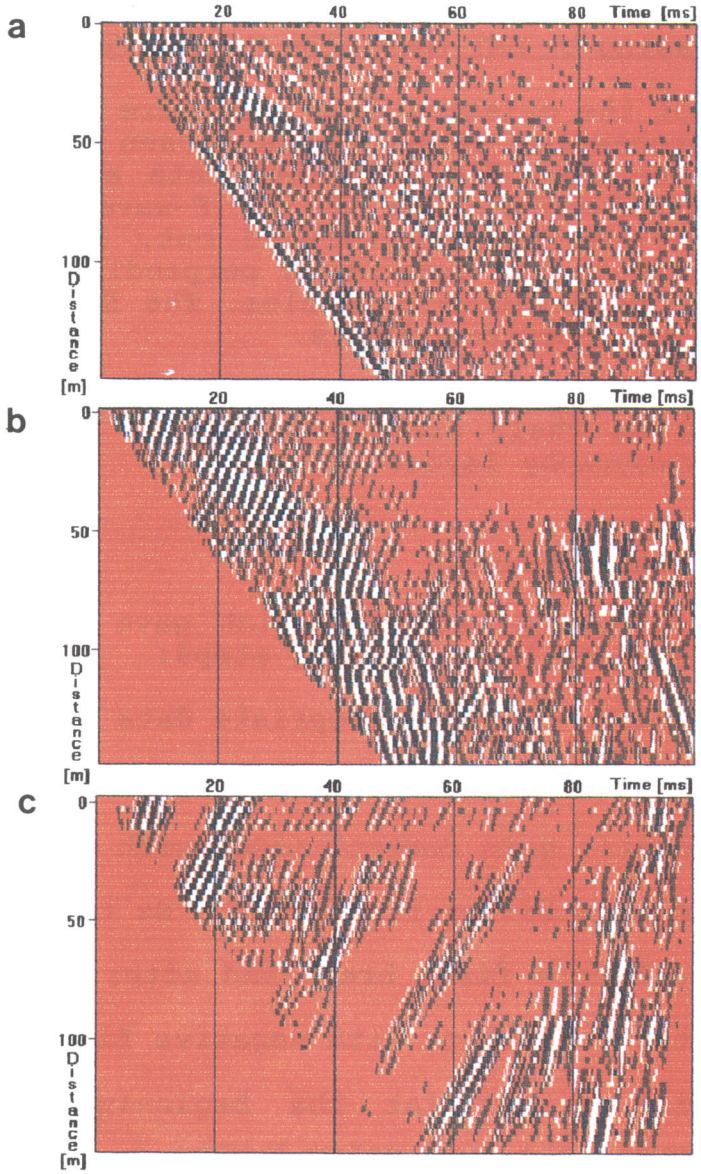

Figure 4.9 Stacked HSP profile 1-4 obtained from 3 shots at 5.0, 7.5 and 10.0 m depth in the source borehole.

a) Raw data. The section has a relatively noisy appearance even after stacking. P- and S-arrivals are the only traceable events.

b) Conventional τ-P filtering with apparent velocity limits (-10000 m/s - +5500 m/s) set to include both downgoing and upgoing events but still filter out the direct P- arrival. The τ-P filter has been applied after amplitude equalization.

c) The same HSP profile after τ-P filtering with variable velocity limits. The procedure permits to select in both the direct and inverse transform only the slownesses (P) associated to a subclass of P-wave reflectors , e.g reflectors cutting the tunnel ahead.

4.5 Processing by DMT (Deutsche Montan Technologie)

Most of the existing data sets were processed by DMT. The processing sequence was chosen for one data set and then used for all other data sets. Additionally to an interpretation of the P-wave reflections, an S-wave analysis was carried out. P-wave processing was done on the components perpendicular to the axis of the observation boreholes. The S-waves processing used the other components.

The profiles HSP 1-6 and 1-8 were not examined in detail as their profile length is 70 m only due to the tomography layout.

4.5.1. Processing Sequence

The processing sequence which gave the best results consisted of the following steps:

- Selection of the appropriate data set
- Sorting of data as common recording station profile
- Automatic gain control (AGC) with 20 ms window
- Band pass filter from 100/200 Hz to 700-1400 Hz
- Mute before first break and after 100 ms (tapered)
- Static correction with negative first break time
- Median filter (at the beginning FK-filter) to suppress the down going P-wave
- Additional static correction with negative first break time (at the US site at Grimsel Vp = 2 Vs)
- Median filter (at the beginning FK-filter) to suppress the down going S-wave
- Static correction with twice the positive first break time for P-wave reflection processing and 4 times the positive first break time for S-wave reflection processing
- Runmix to enhance P- and S- reflections resp.
- Migration of the data using a constant velocity model (5250 m/s resp. 2625 m/s)

4.5.2 P-wave Processing and Interpretation

All details like minor changes in processing parameters for certain profiles and all the results are documented in an internal report. The examples shown here are representative for these results.

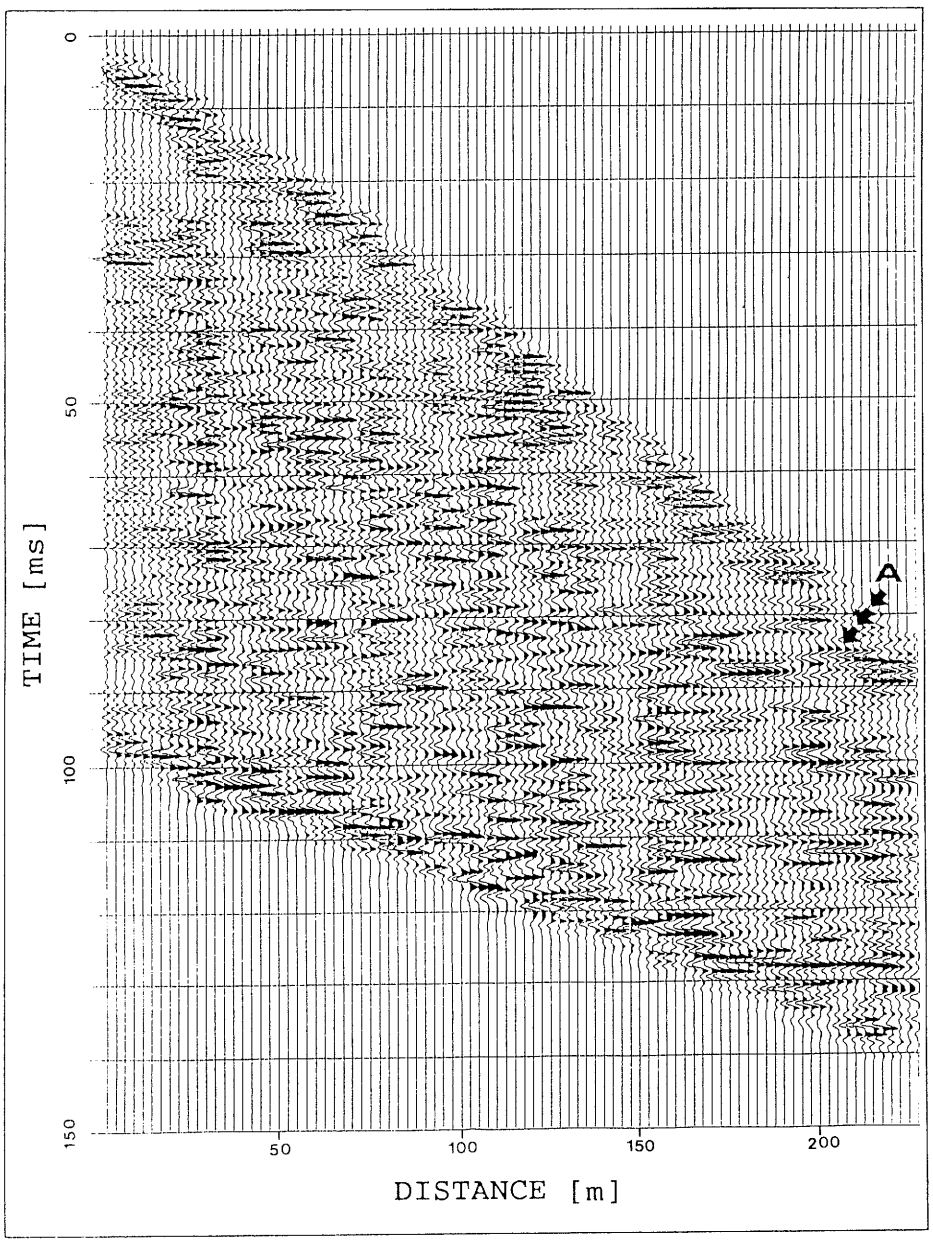

Figure 4.10 HSP profile after suppression of direct P- and S-waves and moveout correction.

The first data set presented is the result of the stacked section (HSP 1-5) when a P-wave processing was applied. The processed data before migration are displayed in Figure 4.10. It can be seen that the direct P- and S-wave energy are suppressed and that some reflections can hardly be seen. Some coherent energy seems to be present at the end of the array (A) but it is nearly impossible to give a good correlation for reflection events. The situation changes after the migration of the data (Figure 4.11 a). Now it is possible to identify different reflectors crossing the tunnel nearly perpendicular and in addition there are indications of reflectors with other strike close to the tunnel.

Although the best results were expected with the stacked data section, a much clearer picture was obtained from single shots. There are two possible reasons for that: first there is a chance that a non coherent interference was produced as no time correction for the different positions was taken into account; secondly one bad profile can disturb the whole stack and smear the weak reflections. For the migrated section of profile HSP 1-1 (Figure 4.11 b) the first breaks were muted before migration and therefore the direct wave was completely taken out.

It can be observed that this procedure leads to very pronounced reflectors along the array but only slightly improved results away from the array. An additional improvement in this area was reached by building envelopes on the migrated section. The results in Figure 4.12 display the real position of the well known S1/S2 shear zone and the lamprophyre dykes at the US site of GTS. Due to parameters chosen for the calculation of the envelopes, the reflected energy along the tunnel cannot be seen any more with the exception of the reflection from the lamprophyre about 100 m away from the shot.

The results that were obtained from the receiver positions in borehole BOUS 85.001 are less promising than the results from BOUS 85.003. The reason for this circumstance is the predominant direction of the reflectors and the position of the receivers. The reflection of the shear zone can be seen on profile HSP 1-9 (Figure. 4.13) at the intersection with the tunnel but there is no information about the direction of the zone. Some indications are given at the end of the array (L). Here the reflections could be interpreted as results from the lamprophyre dykes that cross the heat test tunnel. The indication for these dykes are very weak as the distance to the receivers is quite large.

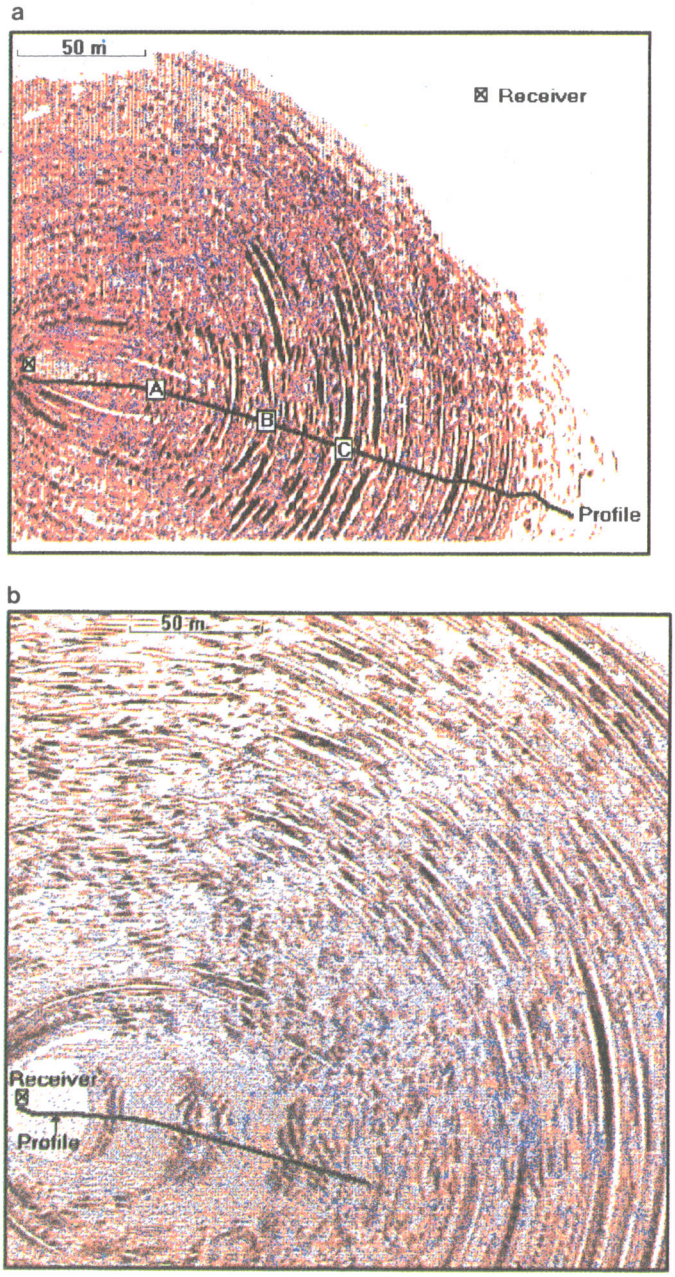

Figure 4.11

a) Result of migration applied to the HSP profile from Figure 4.10. A shows a reflection at the end of the array. A, B and C are positions of known discontinuities.

b) Result of migration of profile HSP 1-1. The direct arrivals were muted before processing.

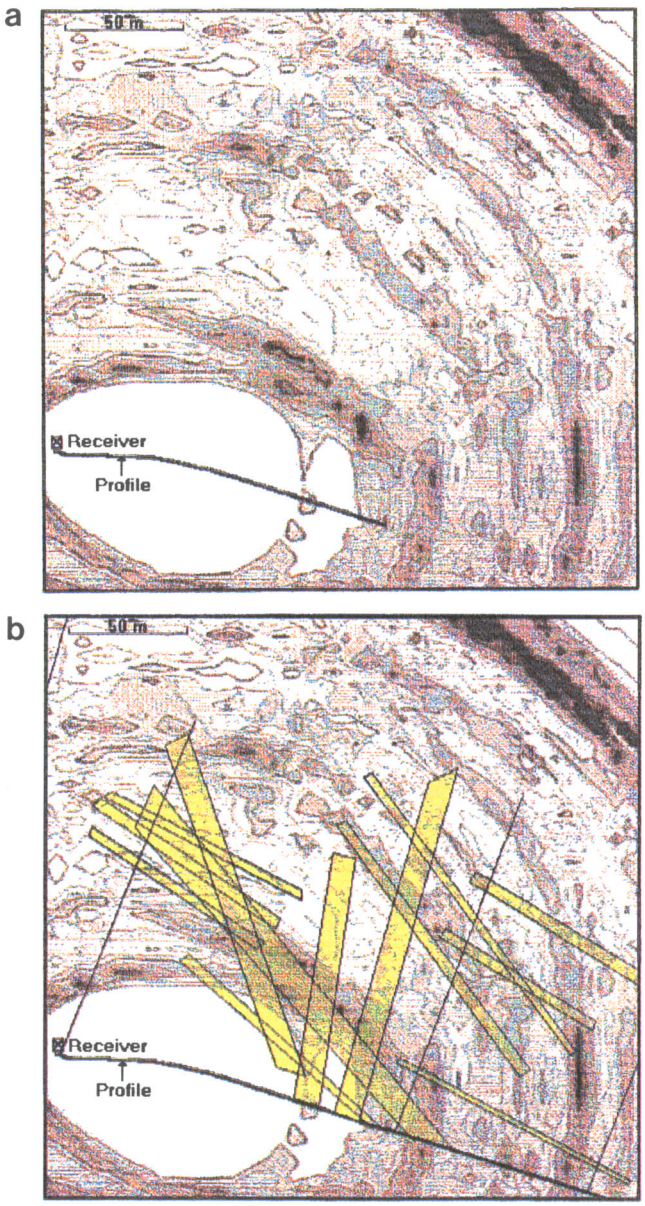

Figure 4.12
a) Envelope of migrated section from Fig. 4.11b
b) The S1/S2 shear system and lamprophyre dykes superposed for comparison.

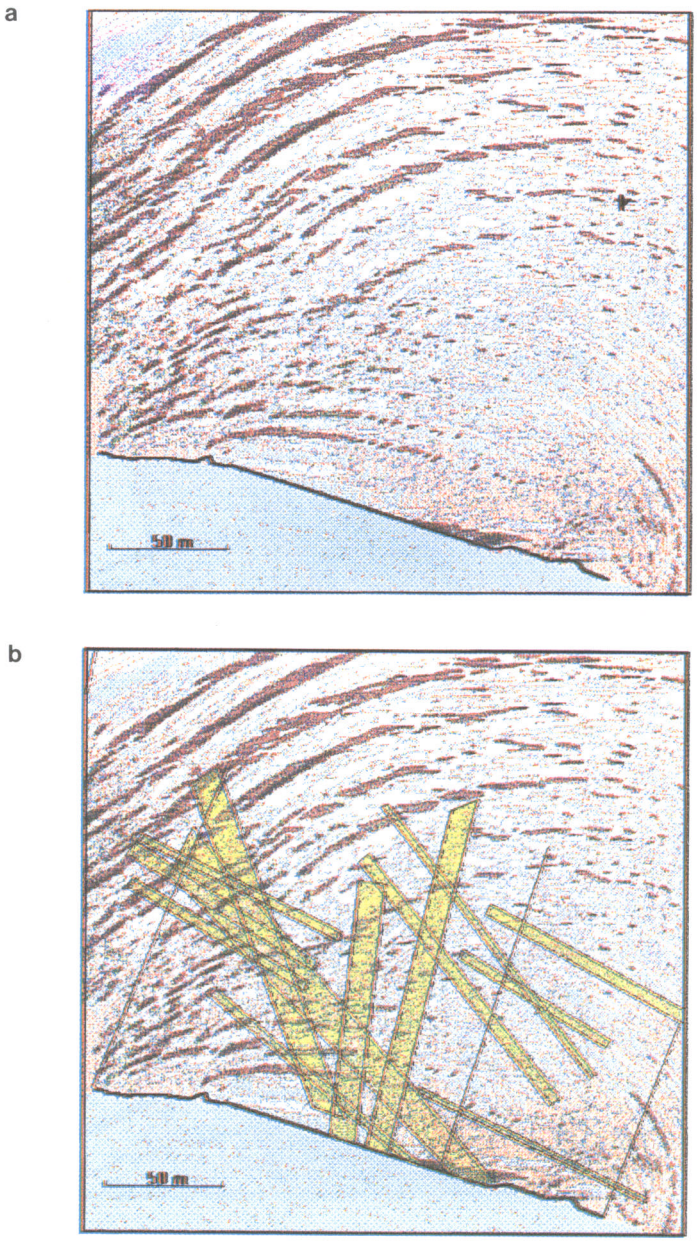

Figure 4.13
a) HSP profile 1-4 after migration and enveloping.
b) Known shear zones and lamprophyre dykes superposed.
For this profile the receiver was placed in borehole 85.001 and the source positions were along the laboratory tunnel.

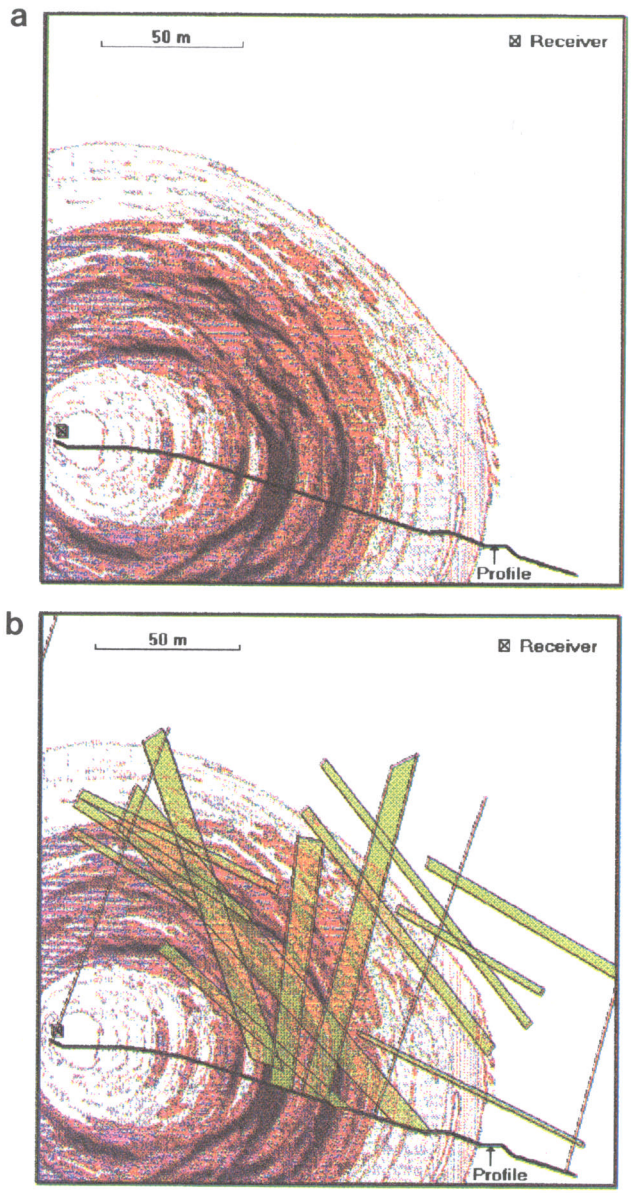

Figure 4.14
a) Migration procedure applied to S-waves.
b) Known zones and dykes superposed.

Receiver in borehole 85.003 and source along the tunnel.

4.5.3 S-wave Processing and Interpretation

The S-wave processing resulted in very promising migrated sections. Figure 4.14 shows the results from profile HSP 1-5. All possible reflectors along the array are clearly detected and there are additionally indications of reflectors in the vicinity which can be identified as S1/S2 zones and lamprophyre dykes. One problem in the S-wave processing is caused by the tunnel wave. It is shown in chapter 2 of this report that the same velocity is expected for tunnel and shear waves. Therefore it cannot been ruled out that the pronounced reflections in Figure 4.14 are caused by the tunnel wave which cannot be used for a real prediction measurement.

4.6 General Results and Conclusions from the Seismic Test

As shown in the previous chapters the data analysis of a subset of the seismic data taken from the tomography project displayed a number of reflections within and close to the array. Predictions for regions at larger distances from the array were not possible as the energy of the sledge hammer was not strong enough. It was shown that the reflection coefficients even for minor fracture zones was sufficient to allow the detection of the reflector.

Therefore we concluded that a field test, specially designed for the prediction, was going to be very promising. The following parameters need to be changed compared to the tomography data:

- higher energy

- denser station spacing

Additionally we learned the following from the results of the preliminary test:

Although the three companies used similar processing routines for the enhancement of the reflected energy the results are quite different. The best comparison of the various methods is given by looking at the results before the migration. The HSP 1-5 results directly show that we obtained the best signals using the Vibrometric approach. Therefore it was decided that Vibrometric should continue to process the following data for the subsequent tests.

5 RADAR PREDICTION USING THE TOMOGRAPHY DATA SET

Additionally to the seismic tomography at GTS, a similar radar tomography project had been carried out. The main difference between the seismic and radar layout was the station density in the tunnel. The spacing in the tunnel for the radar measurements was 5 m compared to 2.5 m in seismic. Only one profile was measured with a 2.5 m spacing as a test for the prediction measurements.

5.1 Field Geometry

The geometry of the profile is similar to the profile HSP 1-2 and is shown in Figure 5.1. The receiver is in borehole BOUS 85.003 at a distance of 6.5 m (point T2). The transmitter antenna was moved along the tunnel in steps of 2.5 m. In the mid part of the profile there is a data gap due to the intersection of the laboratory tunnel and the cavern of the fracture flow experiment. No measurements could be carried out in this area due to bad coupling of the antennas. As a comparison between tunnel and borehole measurements, a second profile was studied with the transmitter at T1 and receivers in borehole BOUS 85.002.

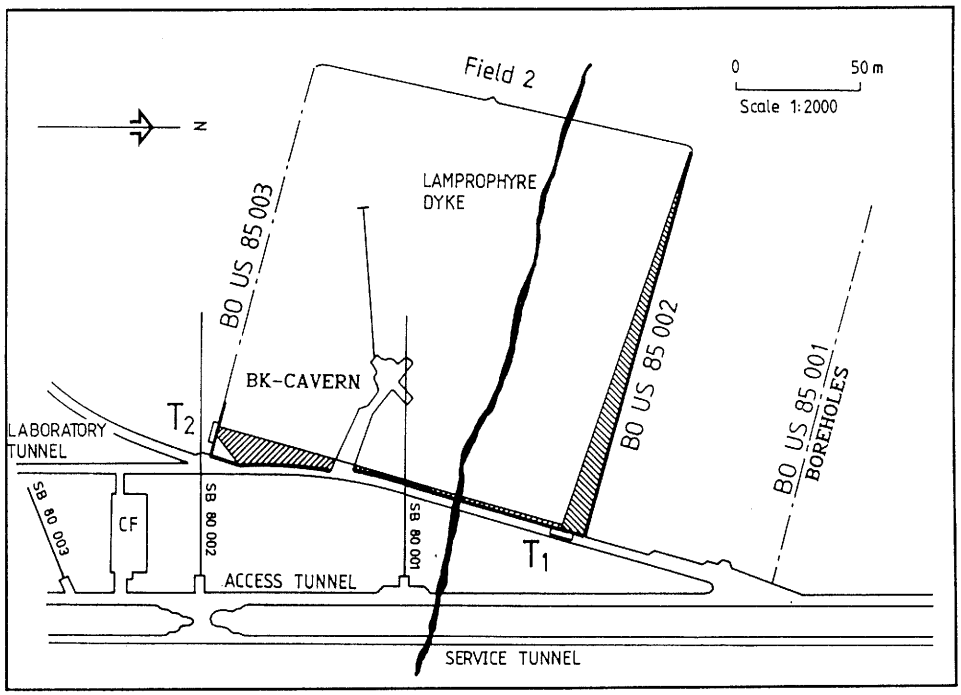

Figure 5.1 Layout and data subset used to the radar experiment at GTS. The shaded area represents the direct wave illumination of receivers.
T_1 = transmitter in tunnel
T_2 = receiver in borehole 85.003,

5.2 Data Processing and Interpretation

The raw data (Figure 5.2 a) show direct (A) and reflected (B-D) energy without any processing. Even multiple reflections between lamprophyre dyke and cavern can be observed. Although the raw data already showed the reflections, some data processing was carried out to enhance the results and probably detect hidden, low amplitude reflections.

The processing sequence consisted of a deconvolution to avoid ringing and an F-K filter to enhance the reflected energy. The result of this processing is shown in Figure 5.2 b and gives only minor improvements compared to the raw data. In principle the reflection (B) from the lamprophyre dyke (Figure 5.1) can be seen as well as the reflections from both side walls of the BK cavern (C + D).

5.3 General Results and Conclusions from the Radar Test

The radar reflections are so pronounced that an additional enhancement of the reflected energy only provides minor improvement. The software developed for the seismic processing can be used for radar data as well. A parallel development for radar is not necessary.

The main improvement for the radar prediction has to be made on the hardware. Especially the antennas need to be modified. In view of the projects of NAGRA in near future - measurements in sedimentary rather than in crystalline rock - the hardware development was not recommended as the penetration depth in sediments and especially in clays and marls is very limited for electromagnetic waves.

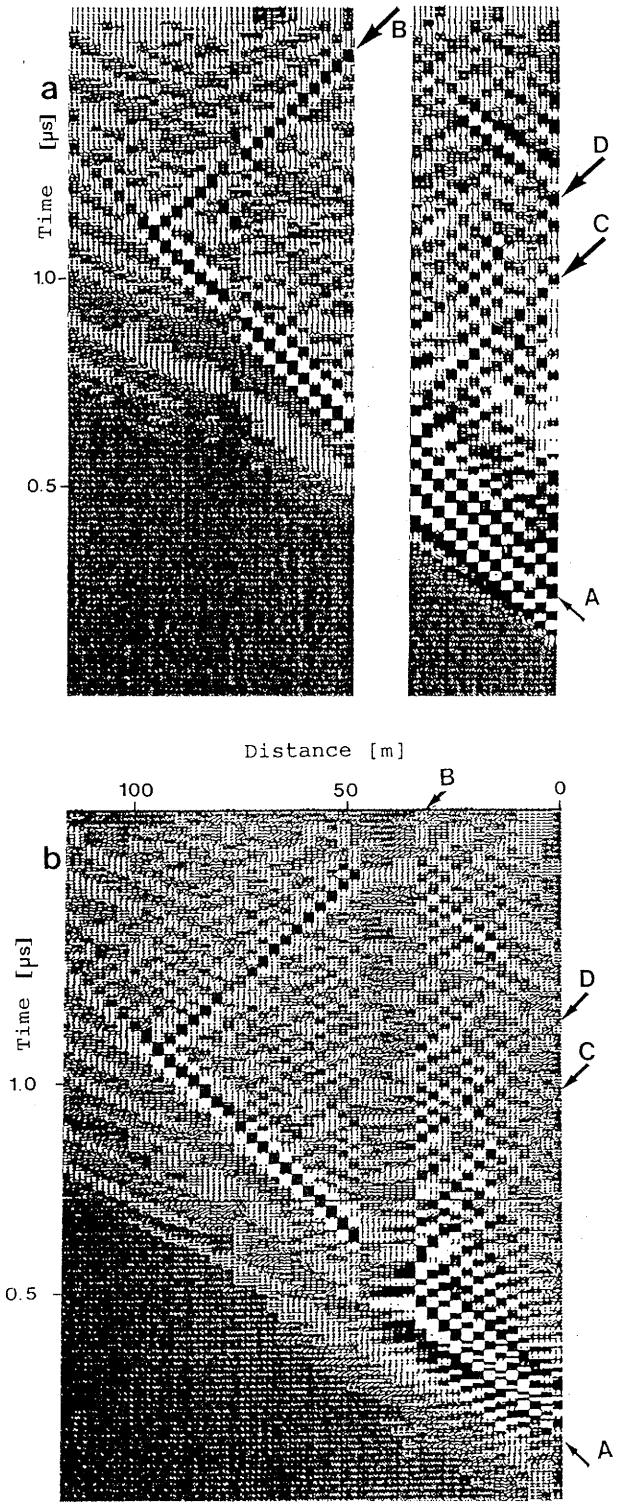

Figure 5.2 Radar profile (HRP) from profile measured at T_2, transmitters in the tunnel at 2-5 m spacing. A = direct wave. B, C, D = reflected waves.

a) Unprocessed profile with gap from Bk cavern.

b) The same profile after processing.

6 DATA ACQUISITION AND PROCESSING OF THE NEW SEISMIC DATA FROM THE GRIMSEL TEST SITE

The seismic field measurements were conducted from July to August 1988 at the Grimsel Test Site. Data acquisition and on-site interpretation was carried out by Fa. P. Frey, Zug. Quality control of the data was done by DMT, Bochum.

In the beginning it was decided that the heat test tunnel at GTS be used for the field measurements for the following reasons:

- the heat test tunnel has the right size (100 m) to allow for a reasonably long profile
- within the tunnel there are several discontinuities to investigate the problems due to the reflections of the tunnel wave at the tunnel face and/or discontinuities
- only minor interferences with other projects at GTS
- there are a number of potential reflectors nearby, known from other tunnels or boreholes, which can be used as targets for the prediction

It was intended that these measurements be conducted under circumstances as close as possible to realistic measurements in a tunnel under construction.

6.1 Equipment

The equipment for the field measurements was basically the same as in the tomography experiments. The data acquisition was carried out with a Seamex recording station (Figure 6.1). To account for the high frequency range which is necessary to achieve the high resolution we preferred accelerometers as seismic detectors. For borehole application these accelerometers (Endevco) were built in a receiver chain which allowed a good coupling of the receivers to the borehole wall. Accelerometers in the tunnel (PCB) were mounted on a metal spike which was clamped in small size boreholes (6 mm).

The data were recorded on magnetic tape in SEG-Y format. Immediately after the measurements the tapes were transferred to a Micromax processing system for quality checks and on site interpretation. Explosives and a sledge hammer were used as sources for the measurements.

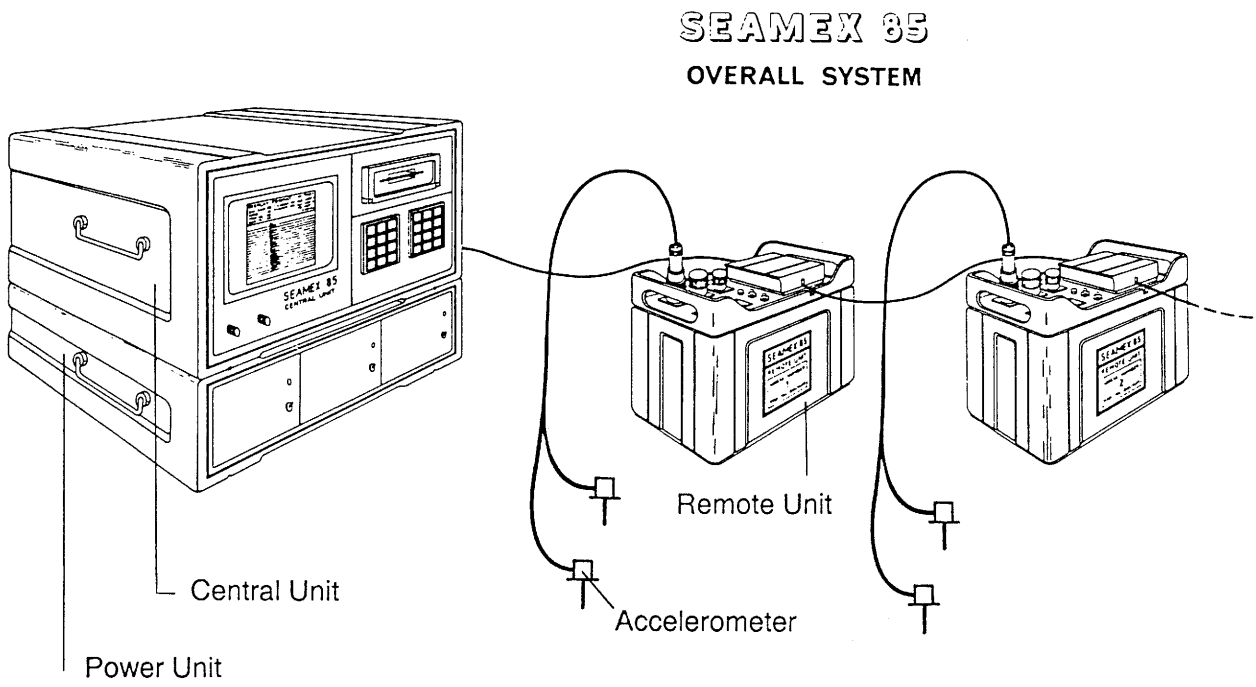

Figure 6.1 Seamex recording system

6.2 Layout of Field Measurements

This research program was designed to show the applicability of the VSP method for tunnel predictions in general. Additionally the measurements allowed to evaluate different acquisition techniques and a comparison with other measurements (standard reflection measurement).

The following techniques were tested:

- offset VSP measurements (Figure 6.2 a): shot in boreholes drilled in radial direction from the tunnel, seismic detectors in the tunnel
- offset reverse VSP measurements (Figure 6.2 b): receiver chain in the borehole and shots along the tunnel (source: explosives or sledge hammer)
- standard reflection measurements (Figure 6.2 c): shot and receivers along the tunnel; shot position between receiver position (source: explosives or sledge hammer)

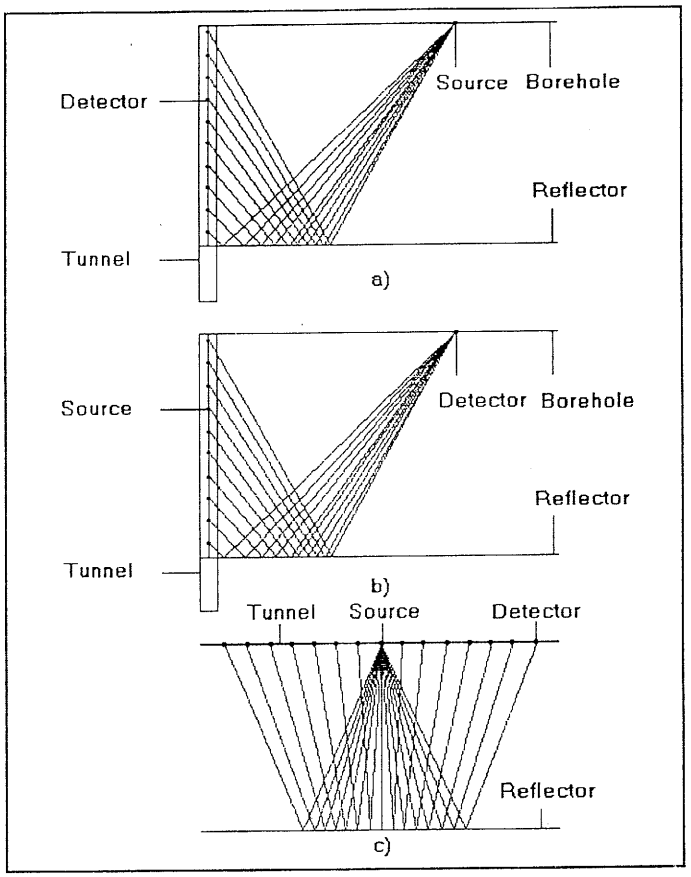

Figure 6.2 Experimental layouts used in reflection seismics

a) VSP (Vertical Seismic Profiling)
b) Reverse VSP
c) Standard reflection

The design of the seismic measurements was based on the results of the theoretical calculation (chapter 2). It was shown in the calculations that for an ideal case, source and receiver should be placed at about one tunnel diameter away from the tunnel wall. Realistically this procedure would be very time consuming and expensive because of the large number of receiver stations (or shot points for a reverse VSP) needed to avoid spatial aliasing. Therefore it was decided that only the source be positioned for the normal VSP and the receiver for the reverse VSP away from the tunnel wall.

Both configurations - normal and reverse VSP - were tested for two reasons: first the results for the different techniques are identical for body waves but can be different in the case of contact or surface waves and secondly the operational aspects concerning time and equipment are very different for these two options.

Additionally to the aspects mentioned above, it was considered that a layout be used allowing to locate the reflectors three-dimensionally and to overcome the non-uniqueness caused by the symmetry of a VSP survey. Therefore, we drilled at two locations in the tunnel radial boreholes up to 10 m away from the tunnel wall. The technical details of these boreholes which were percussion drilled with a diameter of 57 mm are given in Table 6.1.

Table 6.1

Identification	Location	Inclination	Azimuth	Length
SVP 88-01	W.000	-30°	120°	10.0 m
SVP 88-02	W.000	-30°	300°	7.2 m
SVP 88-03	W.000	+90°	--	2.5 m
SVP 88-04	W.070	-30°	120°	7.2 m
SVP 88-05	W.070	-30°	300°	6.6 m
SVP 88-06	W.140	-10°	210°	16.8 m

6.3 Processing of VSP data by Vibrometric

The primary purpose of this work - the processing of VSP data from the Grimsel Test Site - was to improve the reliability of interpretation, i.e. to increase the confidence level in distinguishing between real reflections and accidental coherency in the noise. For that reason more emphasis was placed on the $\rho\zeta$-processing. It has turned out to be an efficient tool in the interpretive processing of VSP data. The preliminary processing steps are explained only briefly.

Two different profiles are treated here, called 4B (shot hole 88-04) and 1B (shot hole 88-01). The detector positions in the test tunnel were the same for both profiles but the source points were separated by 70 meters. The source points as well as the detector positions are marked in Figure 6.3.

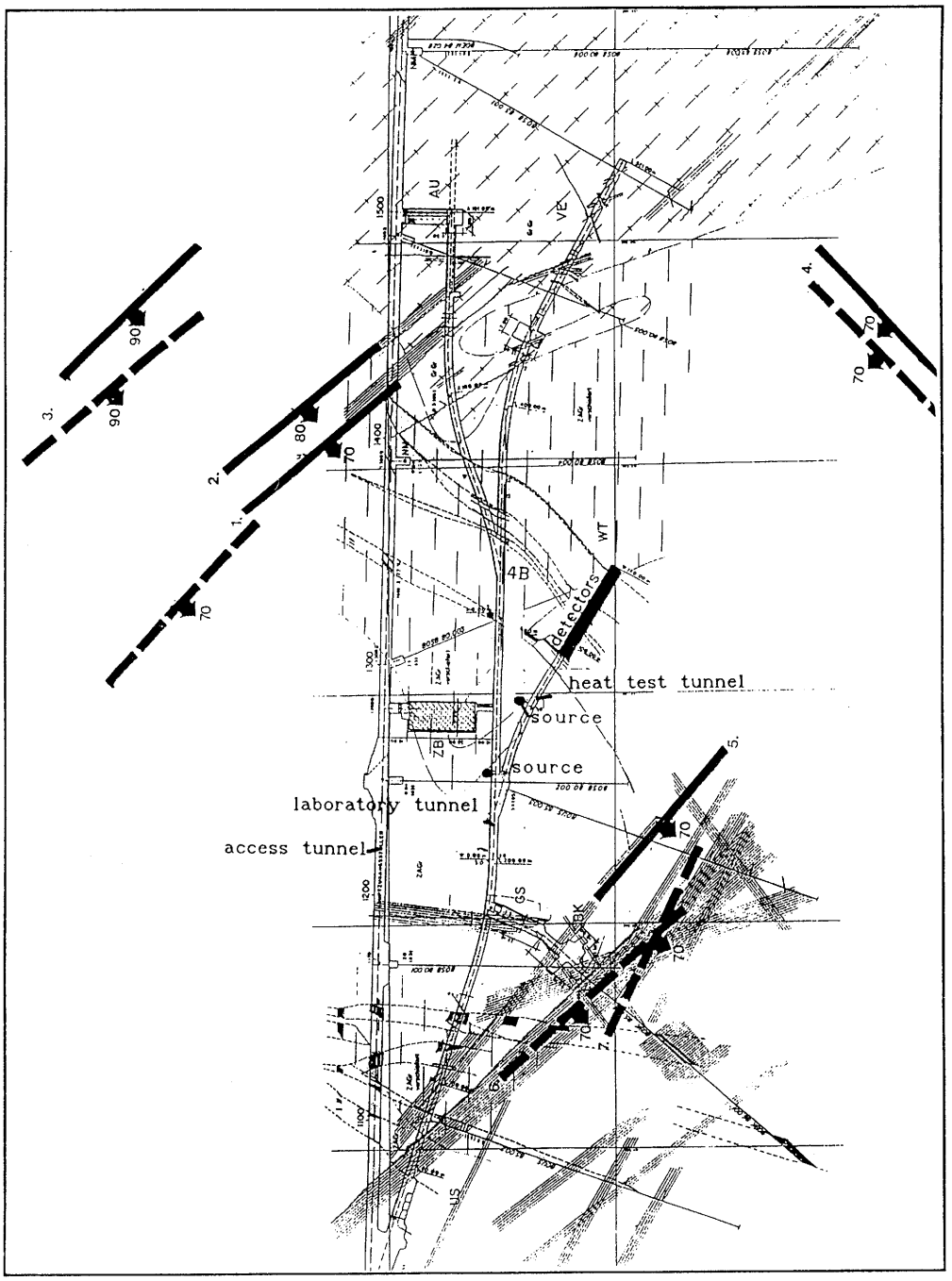

Figure 6.3 View of the GTS site with the location of the experimental layout and interpretation of seismic results. Dashed lines are reflectors found independently in profile 4B. The dip is marked on each line.

For the profiles 4B and 1B the detectors were along the tunnel and the sources were dynamite shots in the transversal boreholes drilled from the test tunnel (Figure 6.3). In the source point 1B there were six shots and from 4B four shots were recorded. The individual shots from the same source point were not exactly in the same location: the spacing between shots along the source hole was about 1 m.

From both source points several individual shots were recorded and five different data sets were processed: the stacked sections from 4B and 1B (individual shot records summed), one single shot section from the same profiles (shot number 4 in both cases) and a pseudo-synthetic noise section. As an example, the intermediate processing results of the stacked section from 4B are discussed. The other stacked section - from 1B - was processed exactly in the same manner.

The amplitude decrease with time - caused by wave front spreading and non-elastic attenuation - was compensated in each single shot section by applying a time dependent operator $t^{1.45}$. An example of a single shot section (from profile 4B) after amplitude compensation is shown in Figure 6.4. The data were frequency filtered using a band pass filter 200-700 Hz. In some traces there is reverberating noise, which has a very narrow spectrum. The frequency of the noise varies from trace to trace. To eliminate reverberation, a data adaptive notch filter was used and as it can be seen in Figure 6.4 b, it removed most of the ringing noise. After notch filtering the single shot sections were stacked (Figure 6.4 c).

The direct P- and S-waves were removed using a median filtering technique and then a two-dimensional AGC operator was applied to eliminate strong amplitude variations in the beginning of traces. The effect of this processing step is seen in Figure 6.5 a.

To enhance coherent energy a three-trace median filter was applied. This processing step does not bring much improvement in the amplitude ratio of the reflected events vs. noise (Figure 6.5 b) but it gives more stable and consistent reflection strength maps after $\rho\zeta$ processing than the sections before median filtering. This can be seen by comparing Figures 6.6 a and b where ζ is the projection of the image point on the tunnel axis (origin at source level) and ρ is the distance from origin to the position of the image point (see chapter 3.2.5). The blank areas at the left have $\zeta > \rho$, which is of course impossible. Black spots represent concentrations of reflection strength and they are better defined in Figure 6.6 b. For that reason, the median filtered sections were chosen as input for later processing.

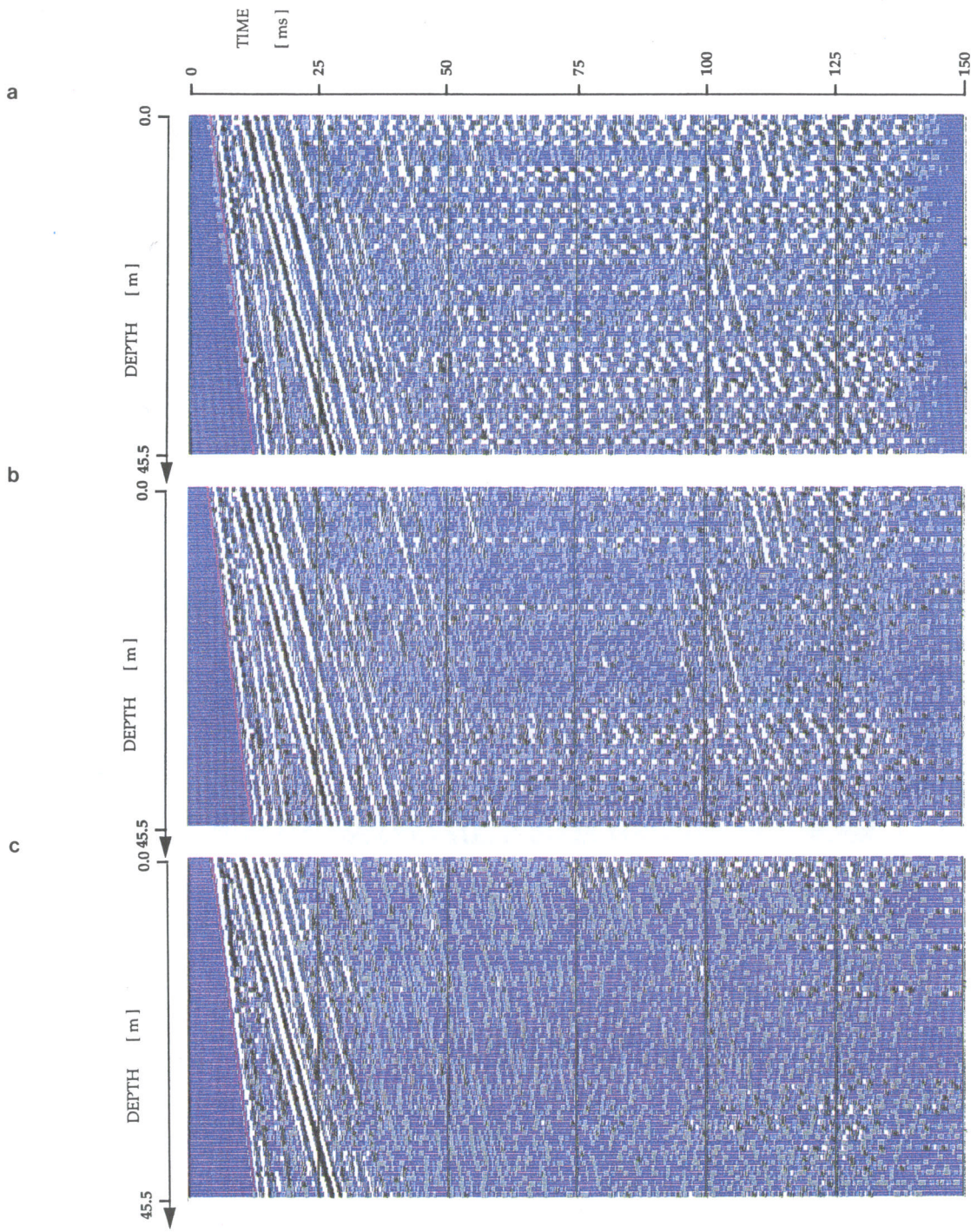

Figure 6.4
a) Raw single shotpoint data from profile 4B (see Fig. 6.3).
b) The profile in 6.4 a after data adaptive notch filtering for removing of ringing.
c) Stacked section (4 shots) from profile 4B.

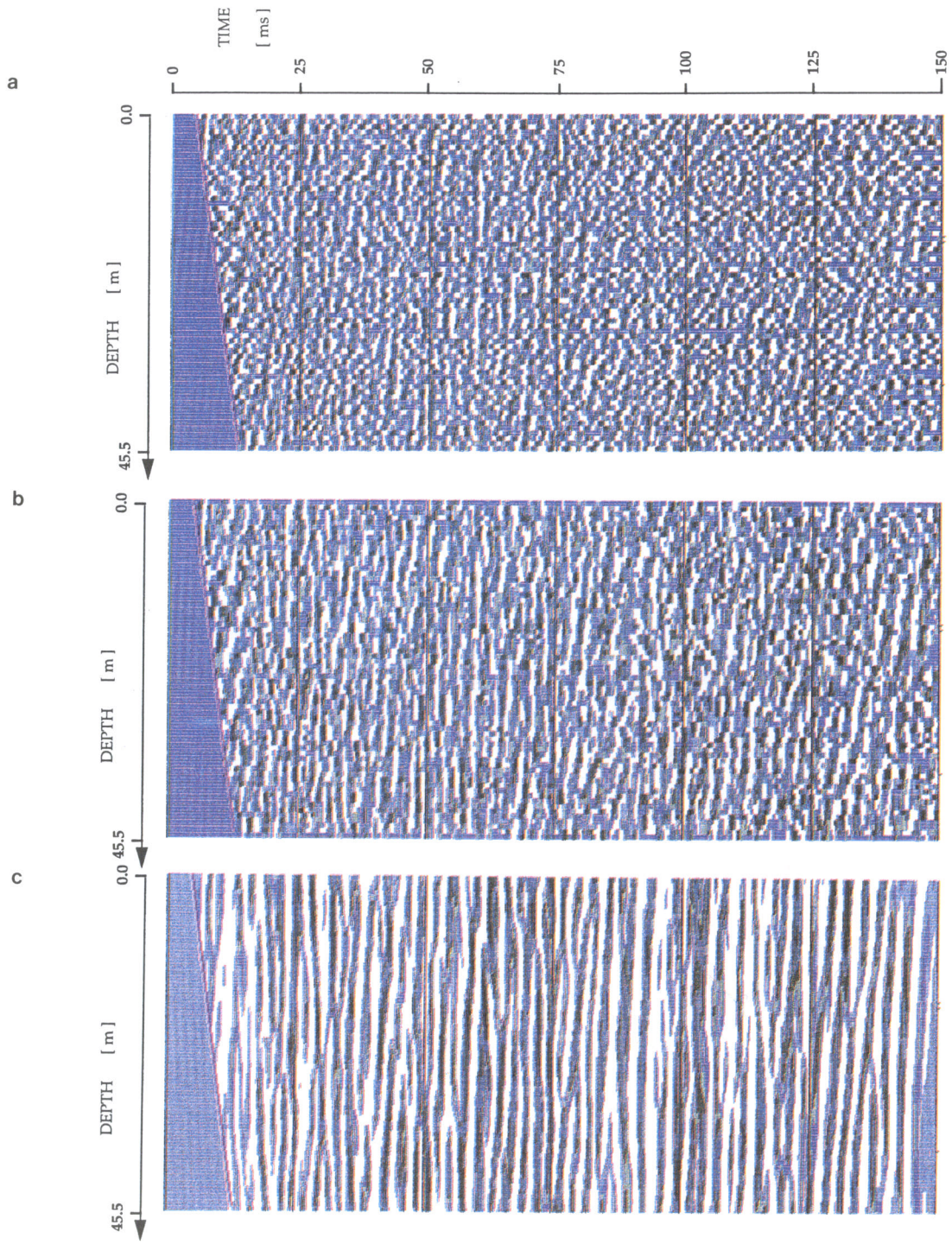

Figure 6.5
a) Result of the pre-processing sequence applied to Figure 6.4c.
b) Figure 6.5a after three-trace median mix.
c) Inverse transformed section from Figure 6.6b.

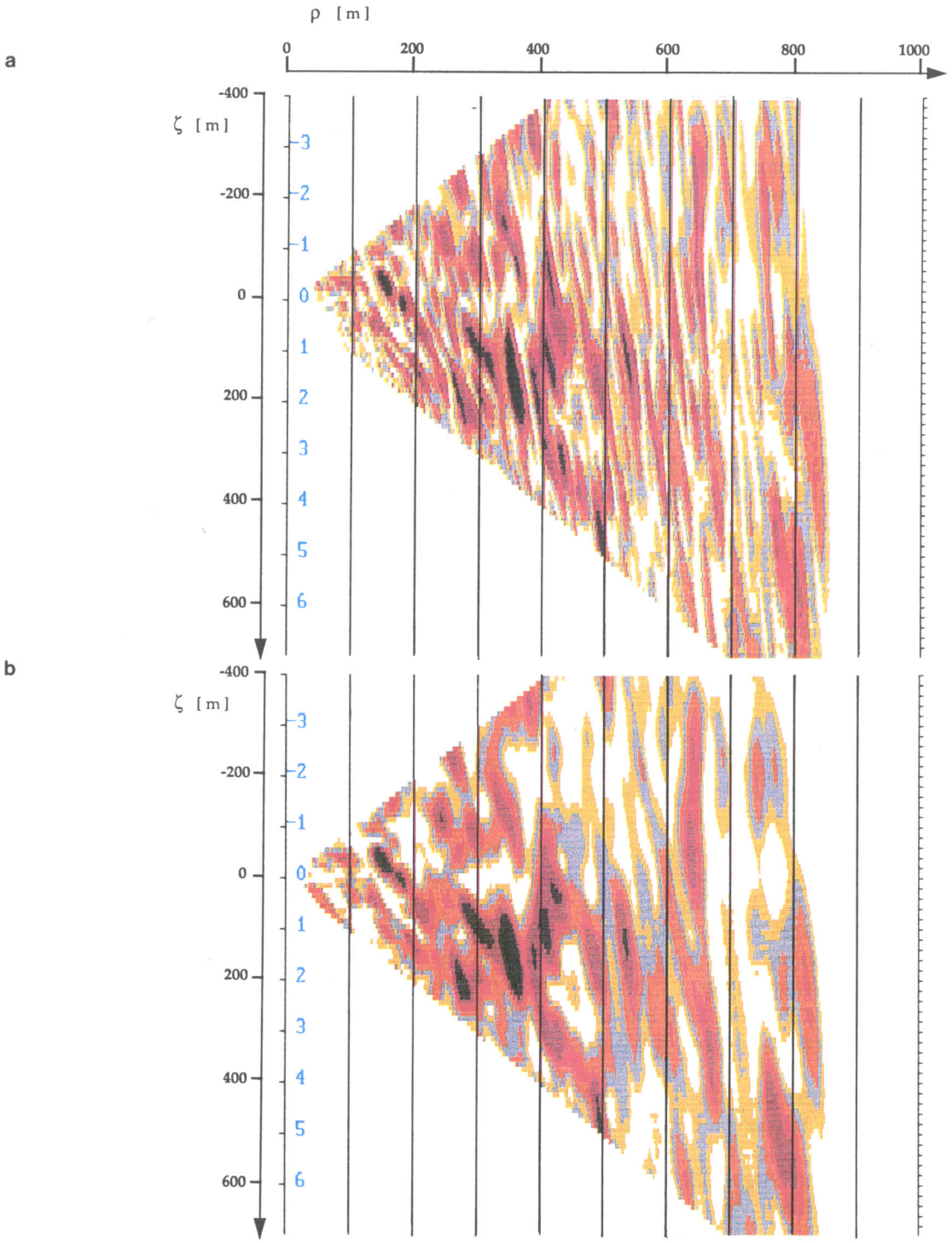

Figure 6.6
a) Image Space representation of the section in Figure 6.5a (stacked section).
b) Image Space representation of the section in Figure 6.5b (with median mix).

In Image Space reflectors are seen as isolated spots of color (the back spots are strong events). The transform performed after median mix (b) displays less noise.

In order to discriminate between probable reflection events and accidentally coherent noise, a pseudo-synthetic noise section was created from the real data in the following way: all traces from Figure 6.5 b were put together in one long seismogram into the memory of the computer. The pseudo-synthetic noise traces were constructed by taking random sequences of that seismogram, i.e. the starting point of each trace was chosen using a random number generator. This procedure gives the same spectrum and amplitude distribution for the real data and the noise. The resulting noise section is shown in Figure 6.7 a. The three-trace median filter was then also applied to the noise section (Figure 6.7 b).

The median filtered sections for both real data and synthetic noise were first transformed into the $\rho\zeta$-space. Those parts of the sections which were either in the unphysical region of the $\rho\zeta$-space or images of events seen only in few traces on the top or at the bottom of the profile were not included. The reflection strength maps (Figure 6.6 a for real data and Figure 6.8 for noise) were then calculated from the $\rho\zeta$-sections.

The inverse $\rho\zeta$-transform was performed with the same parameters for the real data sections (Figure 6.5 c) and noise (Figure 6.7 c). There is very little visual difference between these figures. On the other hand, the reflection strength maps of the real data (Figure 6.6 b) and noise (Figure 6.8) are clearly different; the amplitude level of the real data is higher than that of the noise and, what is most important, the increase of amplitude is due to a few localized spots representing coherent reflection events. This difference in amplitude distribution can be used to emphasize the reflection events.

The parts of the reflection strength map of the real data where the amplitude was less than the maximum noise level were set to zero and the areas with higher amplitude were set to one. The mask was then smoothed to avoid sharp corners The corresponding $\rho\zeta$-section (i.e. the section from which the reflection strength map was calculated by taking the envelope) was then multiplied with this function. The noise reduced versions of the $\rho\zeta$-sections were used in the later processing instead of the original ones.

As was mentioned earlier (chapter 3), the data can be further reduced by Image Space filters which can reject or accept reflectors depending on the angle θ between the measuring array and the reflector. When the inverse transform is performed after the reflector angles have been limited by filtering, the section will contain only few strong events which can quite reliably be interpreted as true reflections.

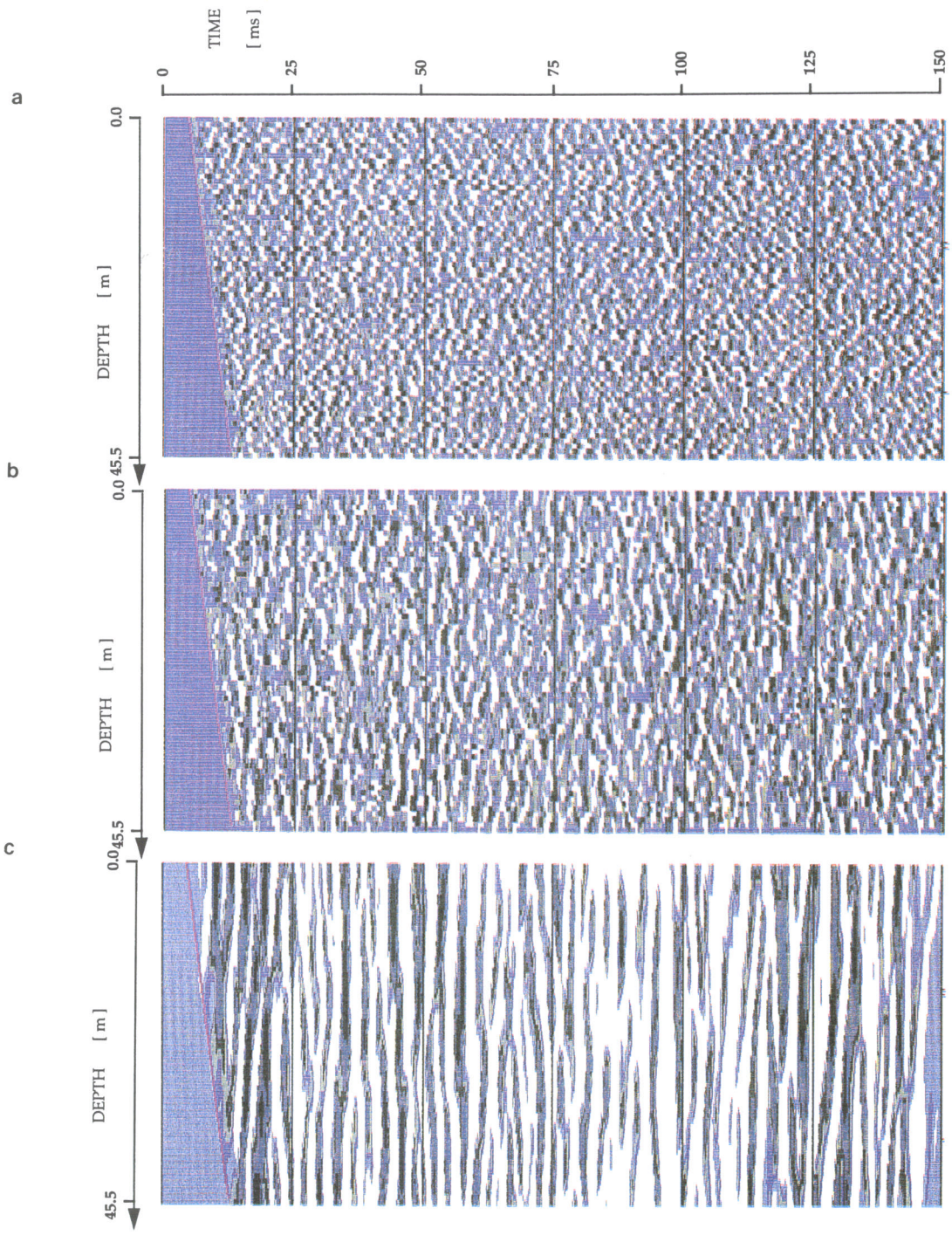

Figure 6.7
a) Pseudo-synthetic noise section used for noise filtering.
b) Three-trace median mix applied to the noise section from Figure 6.7a.
c) Back-transformed noise section from Figure 6.8.

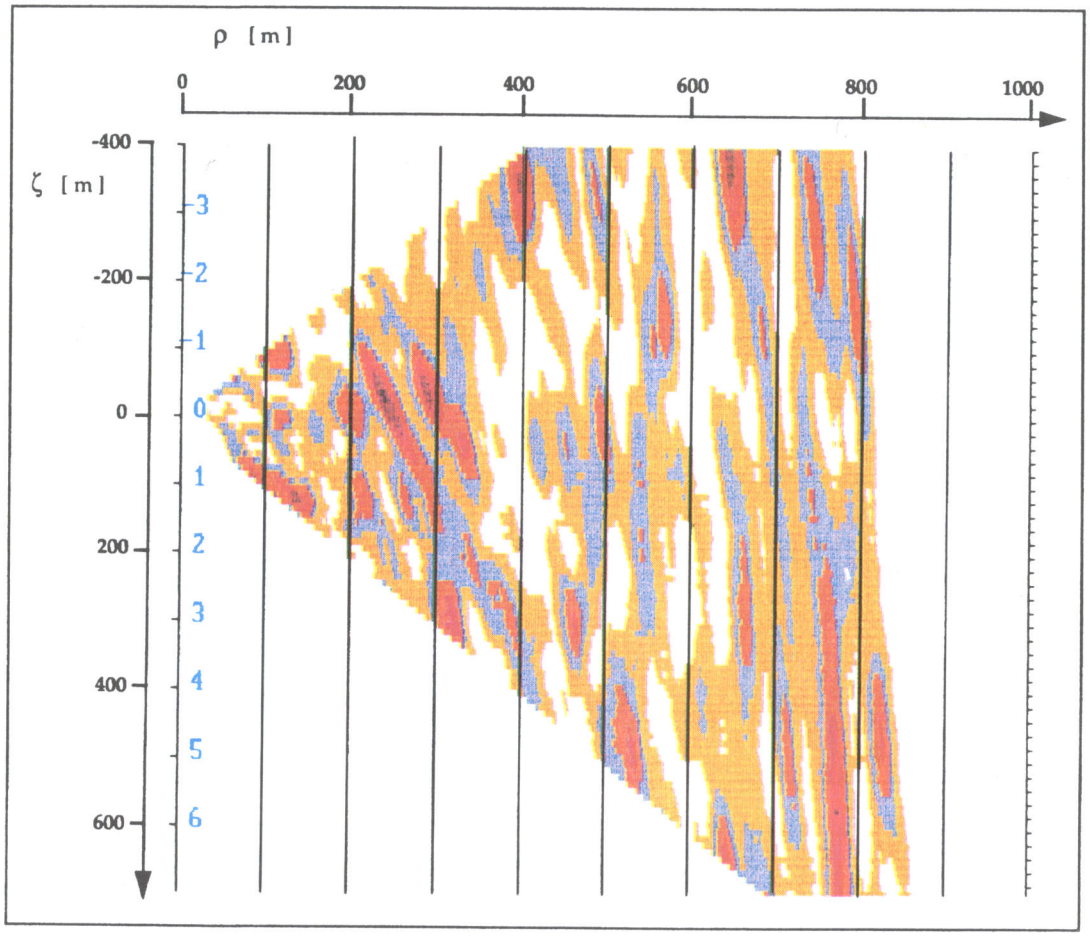

Figure 6.8 Image Space representation of the noise section in Figure 6.7b.

The $\rho\zeta$-filters were applied using three different pass bands for the angle θ: events coming from the side of the profile (angle between the array and the reflector ranging from -30° to $+30^\circ$), close to perpendicular to the tunnel (θ between $+60^\circ$ and $+90^\circ$) and oblique cutting the tunnel ahead (θ between $+30^\circ$ and $+60^\circ$). The last is given as an example in Figure 6.9 a (the Image Space representation) and Figure 6.9 b (the back transformed section).

6.4 Interpretation of the VSP data set

The interpretation of the VSP data was based on the reflection events picked from the $\rho\zeta$-filtered sections with the angle θ limited to the three bands mentioned in chapter 6.3. The procedure was carried out independently for the two profiles (4B and 1B). Generally, when data recorded from more shotpoints are available, it is normal to perform a combined interpretation in three dimensions. This requires that the experimental layout is also truly three-dimensional, i.e. that the detector array and the shotpoints are not co-planar. In a tunnel it is difficult to fulfill this condition. Although shotholes were drilled to decrease the amplitude of the tunnel waves, as explained in chapter 2, the offset of the shotpoints was too small compared to the length of the detector array to form an offset VSP configuration. Therefore, it was preferable to treat each profile separately and to use the similitudes of the models inferred as an additional confidence check.

With a zero offset configuration the point where the reflector will cut the tunnel can be determined as well as the angle between the reflector and the profile. It is not possible to determine independently both the dip and the strike of a reflector from only one shot point; for one reflection hyperbola in the VSP section, which corresponds to one point in Image Space, a multitude of dip-strike combinations can be found. In tunneling works it is of primary importance to know the position of intersection along the tunnel (or its future extension) and the relative angle of a possible fractured zone. Nevertheless, the 3D-positions of the reflectors can be determined to a certain extent if some additional geological or geophysical information is available.

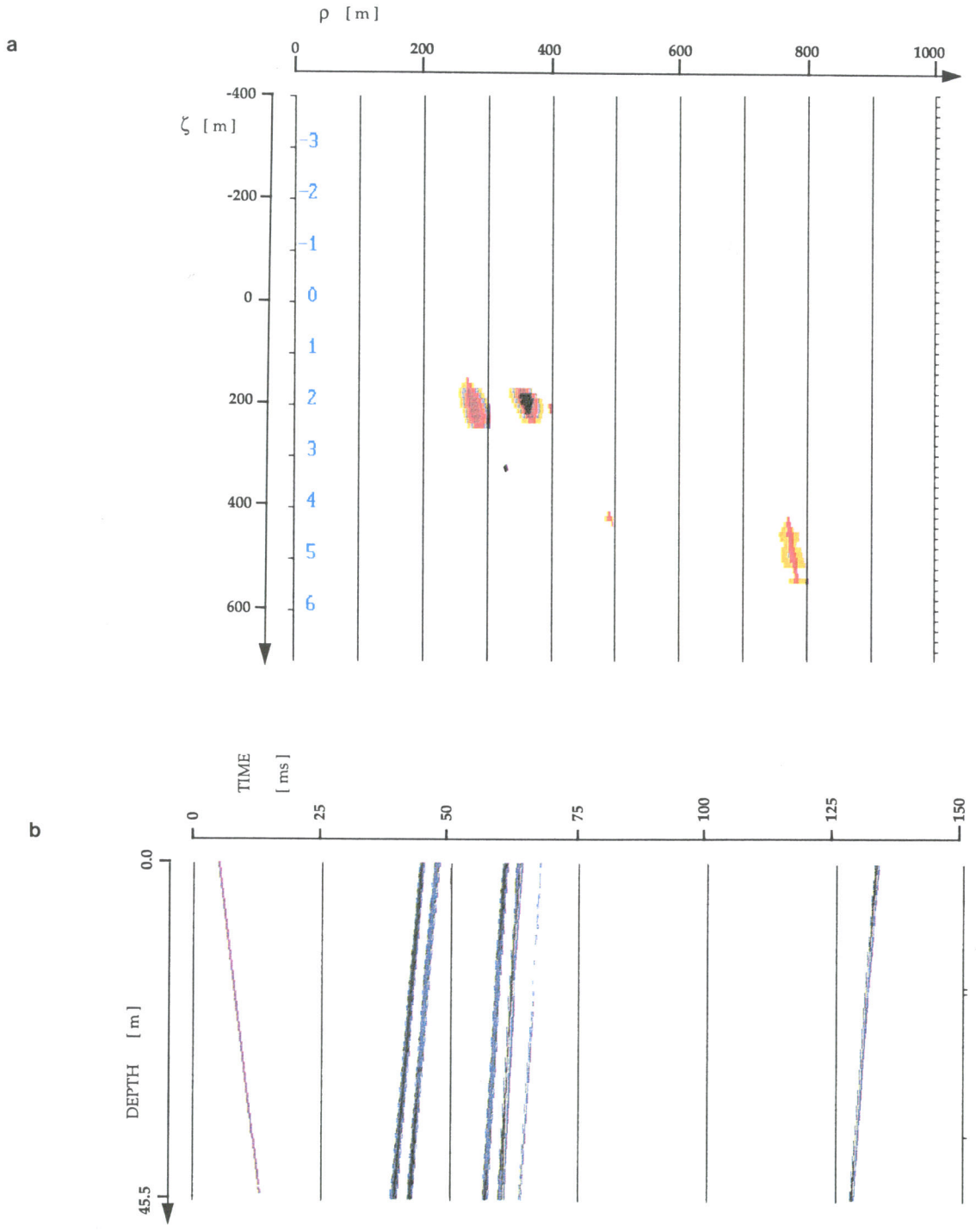

Figure 6.9

a) Image Space representation of the section in Figure 6.5a after noise filtering and limitation of the angle between the reflectors and the tunnel (angle slice).

b) Back-transformed section from Figure 6.9a (with filtering in Image Space).

We have tried here to match our findings with the predominant strike indications from the geological map, as seen in Figure 6.3. Only stacked sections were used because all reflectors seen in the individual sections can be found also in the stacked versions. The reflectors from 4B are marked by solid lines and the reflectors from 1B by hatched lines. The estimated dip of the reflector is given in the map. Reflector number 4 is marked although there is no evidence in the map for it. Its predicted position falls in a region less covered by drillings and other tests so that its existence can neither be proved nor disproved by previous investigations. Moreover, the event is strong in both sections and, being almost perpendicular on the measuring array, its position can be determined quite reliably.

6.5 Conclusions of the VSP Data Set Interpretation

The overall amplitude levels in the reflection strength maps of the stacked sections are higher than in the corresponding single shot ones, indicating a higher signal-to-noise ratio. Because the individual shots were fired in a transversal borehole, the shot separation might somewhat decrease amplitudes in the stacked sections for those rays which propagate perpendicularly to the tunnel. However, when the noise threshold is applied in the $\rho\zeta$-space, the single shot sections contain less events than the stacked sections and all reflectors of the individual sections are visible also in the corresponding stacked section. It happens sometimes that differences occur between the amplitude ratios of the reflectors in the stacked section and the corresponding single shot section. This happens when the amplitude level in the single shot section is very close to that of the noise section, due to the low signal-to-noise ratio.

Due to the cylindrically symmetric experimental layout (zero offset), it is not possible to determine the position of a reflector uniquely in three dimensions. However, we can determine the point where the reflector will cut the tunnel as well as the angle between the tunnel and the reflector. However, for reflectors nearly perpendicular to the tunnel the determination of the position is practically unique because it does not change much when one tries to rotate the reflector around the tunnel axis. For features making a sharp angle with the tunnel additional information is needed for a non-ambiguous three-dimensional fix.

In the $\rho\zeta$-filtered sections back-transformed to Data Space, there is a surprisingly small difference between the general appearance of the noise and the real data and even between their average amplitude levels. This is due to the mixing of several interfering reflections, which is a typical difficulty when interpreting data from VSP surveys in crystalline rock. Estimating the reliability of the reflection pick as well as locating the reflectors is a difficult task if only the Data Space representation is used. On the other hand, the reflection strength maps (represented in Image Space) of the real data and the noise are clearly different. The noise map is more diffuse and the maximum amplitude level for the real data is clearly higher than for the noise. As has been seen, this amplitude difference can be used in interpretation, when one estimate the importance of the individual reflections.

The interfering reflections can be unscrambled and presented in separate plots in Data Space after the two-way transform if $\rho\zeta$-filters are used. It is also possible to do this kind of separation with other methods, using multichannel velocity filters, for example. However, compared with the $\rho\zeta$-filters they have the disadvantage that the reflections are rejected or passed according to the apparent velocity of the event, which can be different in different parts of the section. Thus it is possible for the velocity filter to pass only part of the reflected event.

The basic assumption behind the $\rho\zeta$-processing is that the reflectors are nearly planar. If the back scattered signals are mainly diffractions, like in karst areas, it is obvious that the events will not stack properly in $\rho\zeta$-transformation. Their images will be blurred in $\rho\zeta$-space and, consequently, their amplitudes will be lower than for a planar reflection. However, the algorithms can be easily changed to take into account diffractions, in which case the $\rho\zeta$-transform will become equivalent to the Kirchhoff migration.

6.6 Processing of Reflection Data by DMT

Additionally to the VSP-processing of the data a seismic reflection processing was carried out using part of the data. The data available for such a processing were recorded in the heat test tunnel. The source was a hand hammer and the receivers were PCB accelerometers. Station and shot separation was 0.7 m. The shots were placed in between the shots. Due to the weak hand hammer source a lower signal to noise ratio and a more limited penetration depth compared to the VSP results can be expected.

The length of the recording array was 54.6 m and the shotline was 70 m. The measurements were made using a fixed array and a moving source. At every shot point 8 shots were stacked to improve signal to noise ratio. Although a time window of 500 ms was recorded it was decided to process only the first 100 ms (Figure 6.10).

The following processing steps were carried out to receive the best results:

- bandpass filter ranging from 200/400 Hz up to 1500/2000 Hz to suppress the low frequency ringing close to the shot while keeping all information in the high frequencies
- mute of the CDP offset seismograms from zero time to the arrival of the direct tunnel wave to suppress the p-wave
- predictive deconvolution to cancel the monofrequent tunnel resonance
- constant velocity analysis to get optimum stacking velocities for p- and s-reflections (5200 m/s and 2600 m/s resp.)
- static corrections
- editing of seismograms close to the source
- stacking

The result of this processing sequence is shown in Figure 6.11. One can observe a number of reflected tunnel waves which can be associated with the intersections of lamprophyre dykes and the heat test tunnel. Additionally a strong refection is seen from the intersection of the heat test and laboratory tunnel (A). As the tunnel wave does not penetrate very deep into the formation, the tunnel waves had to be canceled out to receive far distance information from body waves (p- and s-wave). This was achieved using a median filter routine. The resultant section

after applying an additional mute allowed to detect weak reflections from possible discontinuities which intersect the tunnel axis in front of the tunnel face. These reflectors can be predicted at distances of 11 to 66 m from the tunnel face. There is no direct observation of such discontinuities by independent observations (e.g. boreholes) but due to their direction it can be assumed that they represent additional lamprophyre dykes.

The processed data using a normal move out correction (NMO) of 3000 m/s before CDP stacking showed a very pronounced reflection (L) from the laboratory tunnel (Fig. 6.12) in the s-wave section. After the suppression of this reflection with a coherency filter and a migration of the data one can observe reflectors running nearly parallel to the tunnel. A decay of the reflection amplitude and offsets of the reflectors are observed at the intersection of these reflectors with known lamprophyre dykes (Fig. 6.13).

The p-wave sections again showed good reflections from nearby tunnels and additionally one could identify a reflector at a distance of about 90 m corresponding to the known S1/S2 shear zone in the US area of the Grimsel Test Site (Fig. 4.1).

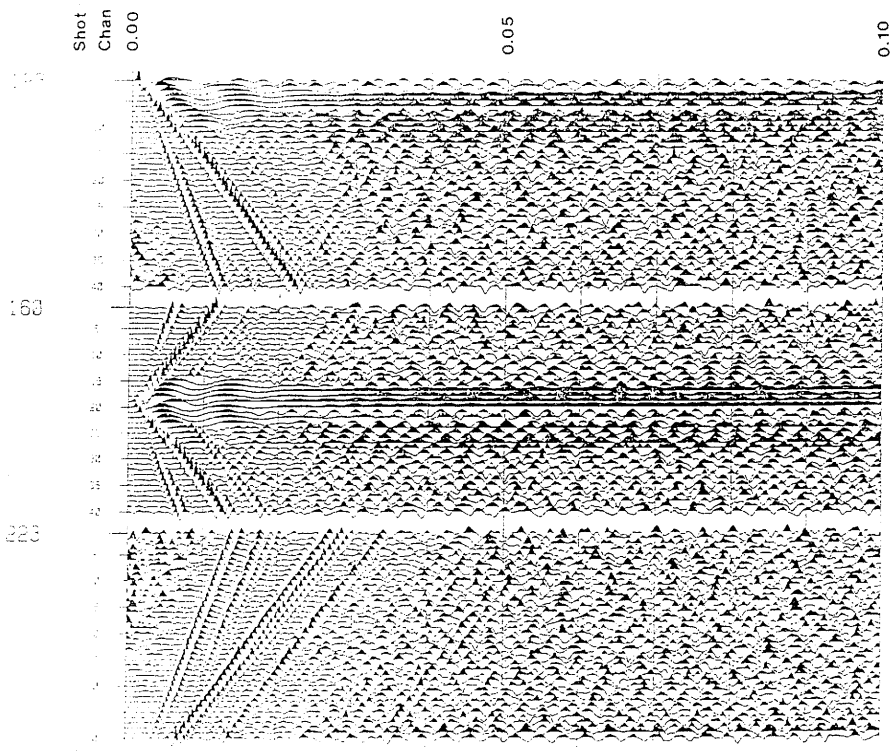

Figure 6.10 Examples of raw data which were used for the reflection processing. Station spacing is 0.7 m.

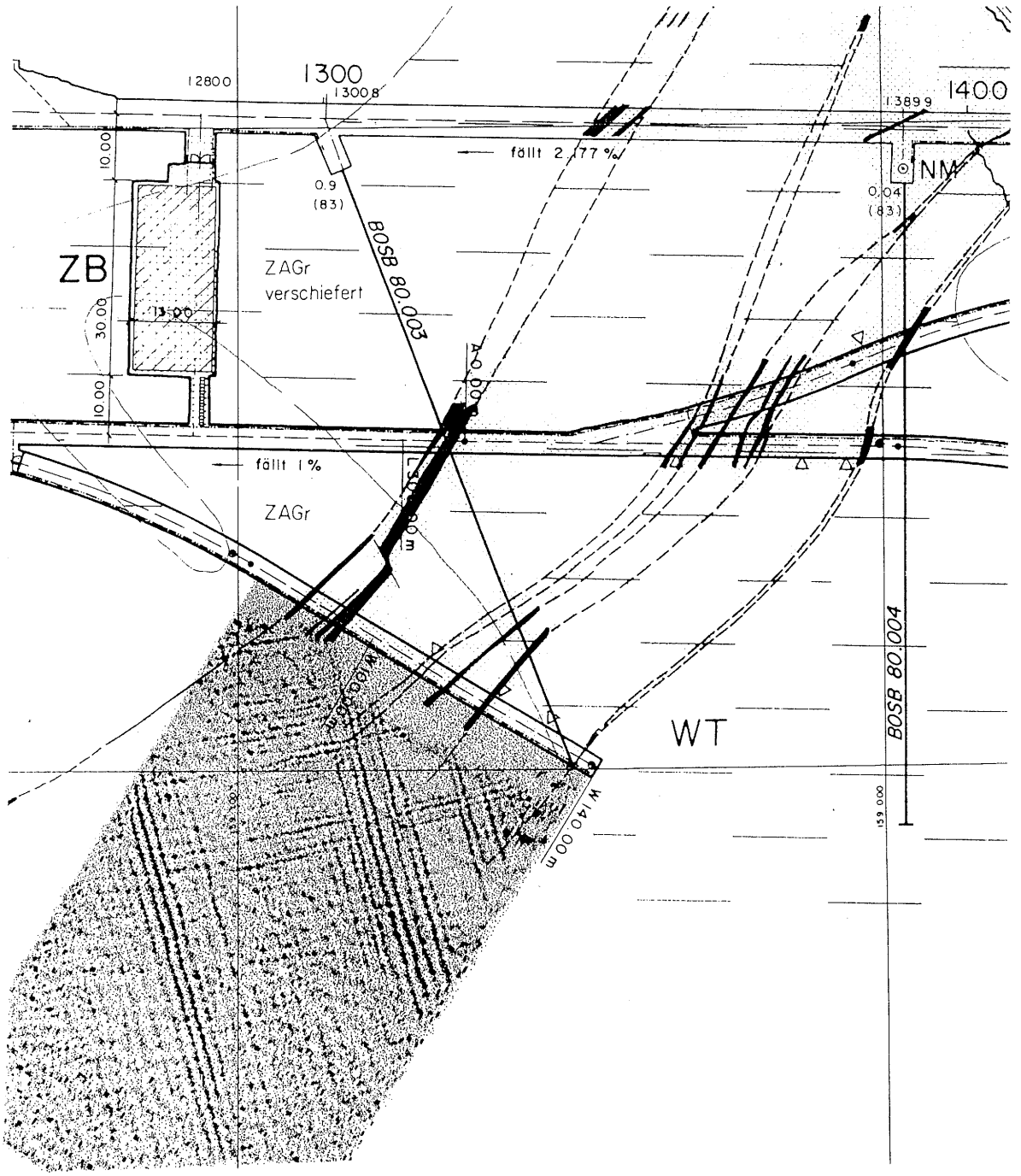

Figure 6.11 Processed reflection section (for processing sequence see text) showing reflections of the tunnel waves cause by lamprophyre dykes which intersect the tunnel. The positions of these dykes is displayed in the geologic cross section (explanations see fig 4.1)

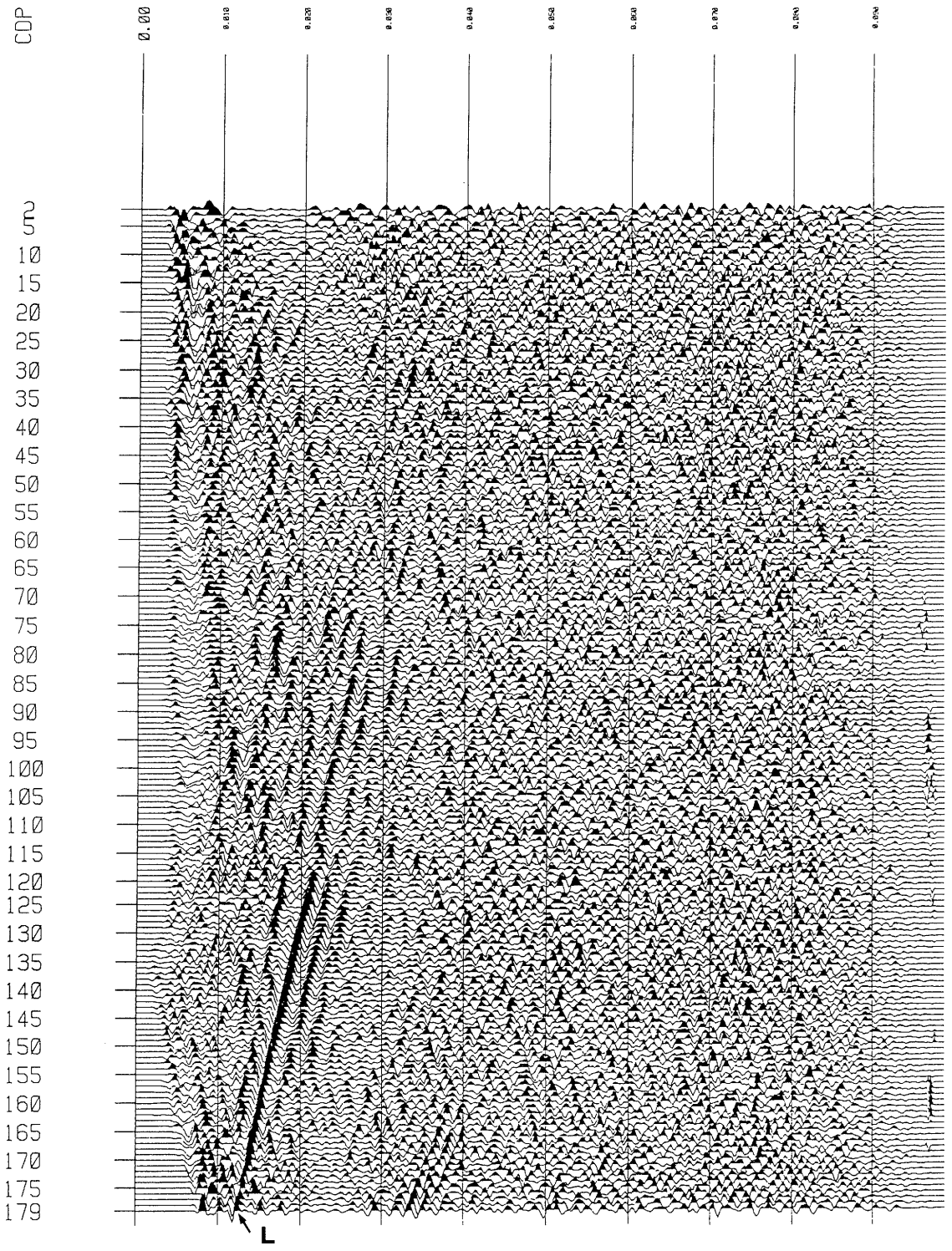

Figure 6.12 Stacked data (normal move out correction with 3000m/s) which show a pronounced reflection from the laboratory tunnel (L)

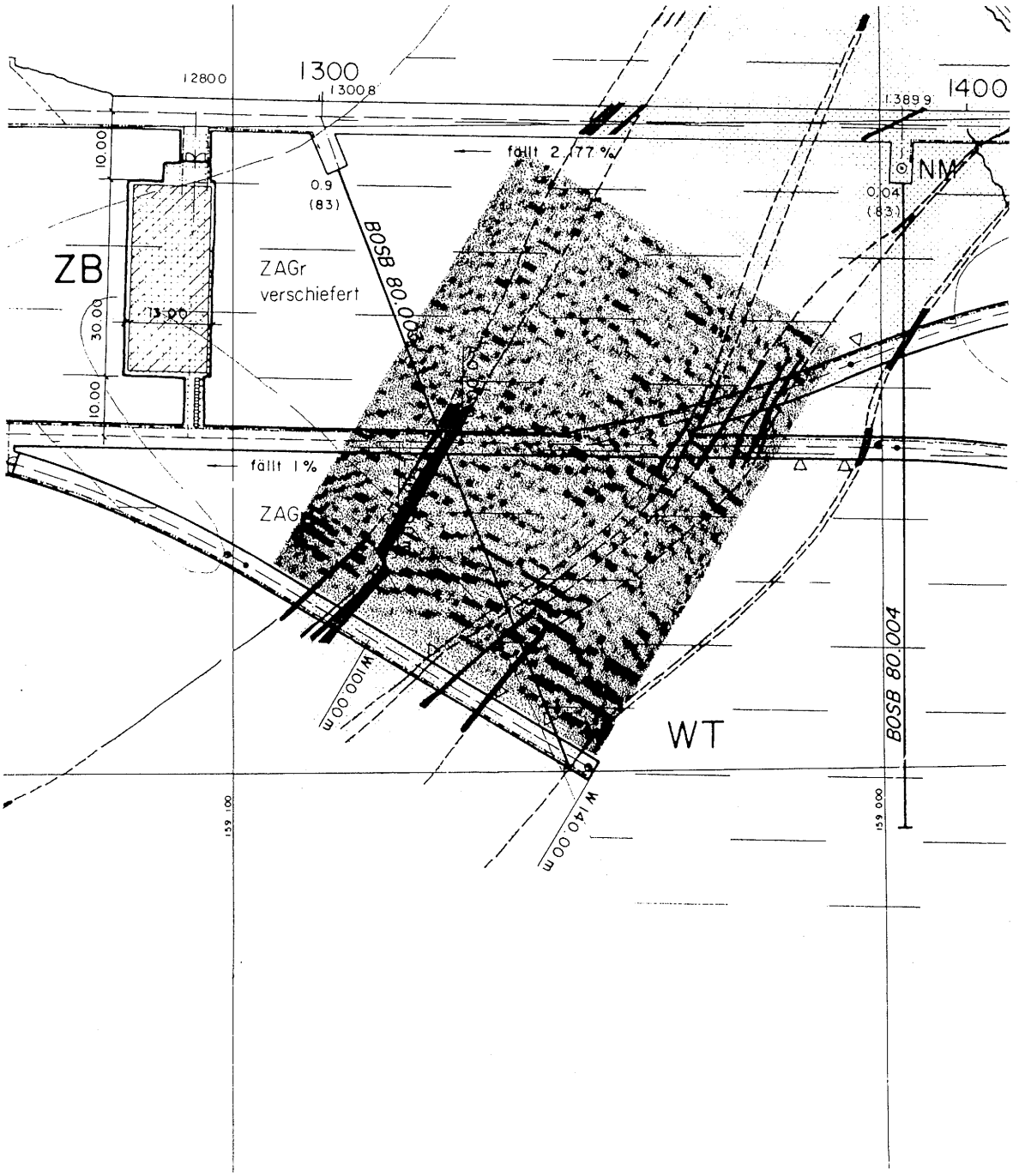

Figure 6.13 Migrated seismic section (normal move out correction 2600 m/s) overlaid with the geological cross section (explanations see fig. 4.1). A decay of the reflection amplitude and offsets of the reflectors are observed at the intersection of these reflectors with known lamprophyre dykes.

7 Seismic VSP Measurements in the Leissigen Tunnel

The methods developed during this project were subject to a trial in real life conditions in the Leissigen tunnel (Figure 7.1), which was under construction at the time of the test. The tunnel of Leissigen is a road tunnel close to the cities of Interlaken and Thun. The geology is characterized by marl sediments and sandstone.

The VSP-type reflection measurements were conducted in August 1990 using small explosives as sources and three component accelerometers as receivers along the tunnel. A piezoelectric borehole source developed by Vibrometric during the Stripa Project was also tried, but the poor rock quality demanded very much energy and a relatively low frequency, which could not be delivered by this device designed for competent crystalline rock. Finally dynamite was chosen as a means of producing seismic signals. Three different data sets are treated here, one for each component.

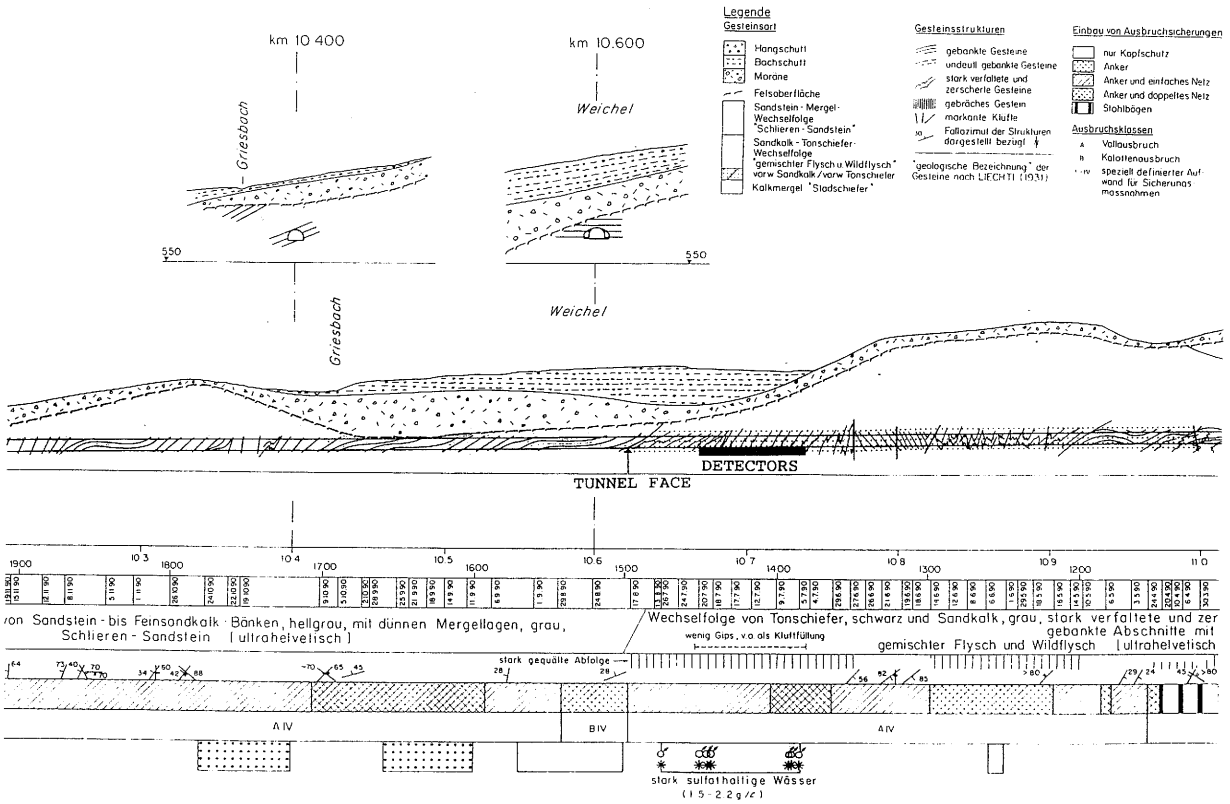

Figure 7.1 Test layout in the Leissigen Tunnel (geological cross section from H. R. Keusen, Geotest)

7.1 Test Site and Data Acquisition

Figure 7.2 depicts a vertical profile through the tunnel showing how the sources and detectors were placed in lateral short boreholes. The detectors used were three component accelerometers constructed by Vibrometric, clamped in boreholes drilled horizontally in the tunnel wall. The X component was directed along the tunnel, the Y component pointed upwards and the Z component was normal to the tunnel axis, as in Figure 7.2. There where 40 detector positions with 1 m spacing. The total length of the profile was thus 39 m. The distance from the shot point to the first detector was 31.3 m and to the last 69.9 m. The shots (about 10 g) were fired in a hole drilled perpendicularly to the tunnel and dipping slightly downwards, to hold the water for acoustic coupling of the explosions to the rockmass (Figure 7.2). There were four shot points in the hole at the depths of 4, 5, 6 and 7 meters. The data consisted of 12 sections: three components for each of the four shot points.

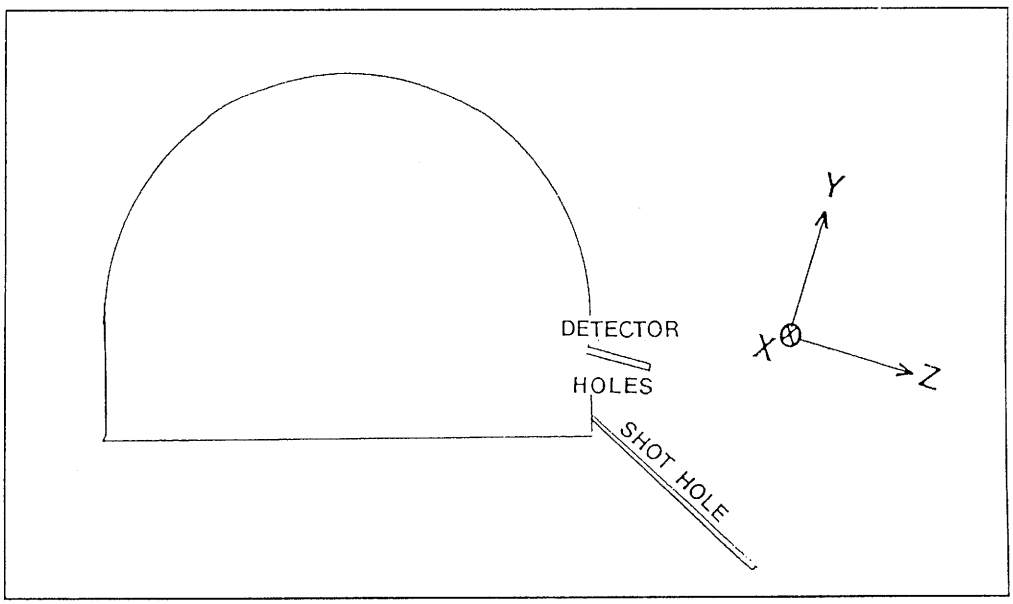

Figure 7.2 Position of shothole and triaxial receivers in the Leissigen experiment (transversal section through the tunnel.

7.2 Data Processing

As the first processing step, the amplitude decay caused by geometrical spreading and non-elastic losses was compensated in each recorded profile (single shot section) by applying a compensating gain function $G_{ain} = t^{1.5}$. The data were filtered using a band-pass window of 250 Hz - 750 Hz and the average amplitudes of the traces were equalized to eliminate the amplitude variations between the traces caused by different detector coupling at different positions along the measuring array. Subsequently, the 12 recorded profiles (4 shots x 3 components) were stacked resulting in three sections (one section for each component) shown in Figures 7.3 a - c. The later processing steps were applied on the stacked sections only.

The direct P- waves were removed using a median filtering technique and then a two-dimensional AGC operator was applied to eliminate strong amplitude variations in the beginning of traces. The P-wave velocity used, 4400 m/s, was picked from the raw data X component section. The result is displayed for the X-component in Figure 7.3 d.

Afterwards, all sections were transformed into the corresponding $\rho\zeta$-space sections. The reflection strength maps (Figure 7.4 a for the X-component) were then calculated from the $\rho\zeta$-sections by taking the envelope.

For estimating the confidence level of the prediction, a synthetic noise section was created and treated in the same way as explained in chapter 6. Image Space processing was performed for the noise section with the same parameters as for the real data sections. Also for this survey the reflection strength maps of the noise and the real data were clearly different (Figures 7.4 a and b) while the Data Space representations were much less interpretable. Therefore, the same approach was followed for enhancing reflection events than at GTS.

The amplitude criterion was used to outline the most probable and marked reflectors. The discrimination threshold was set to 90 % of the maximum noise amplitude. The noise filtered versions of the $\rho\zeta$-sections were then used for the inverse transform (Figure 7.6 a for the X-component, Figure 7.6 b for the Y-component and Figure 7.6 c for the Z-component). Figure 7.5 shows the noise filtered Image Space section, i.e. those parts of the reflection strength map of Figure 7.4 a which are above the amplitude threshold.

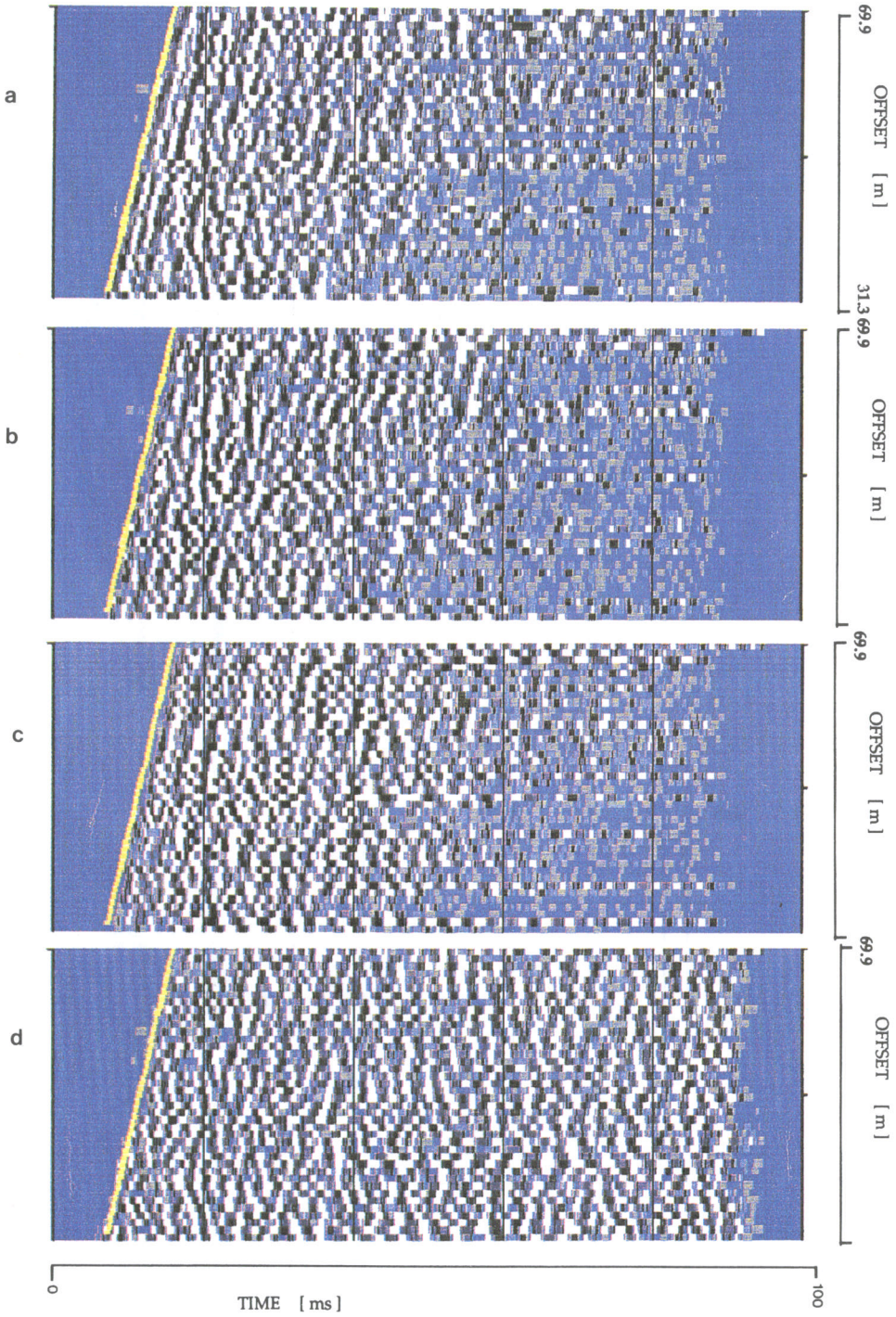

Figure 7.3
a) X-component (along the tunnel) seismograms recorded at Leissigen.
b) Y-component (Figure 7.2) seismograms recorded at Leissigen.
c) Z-component (Figure 7.2) seismograms recorded at Leissigen.
d) X-component section (Figure 7.3a) after preprocessing.

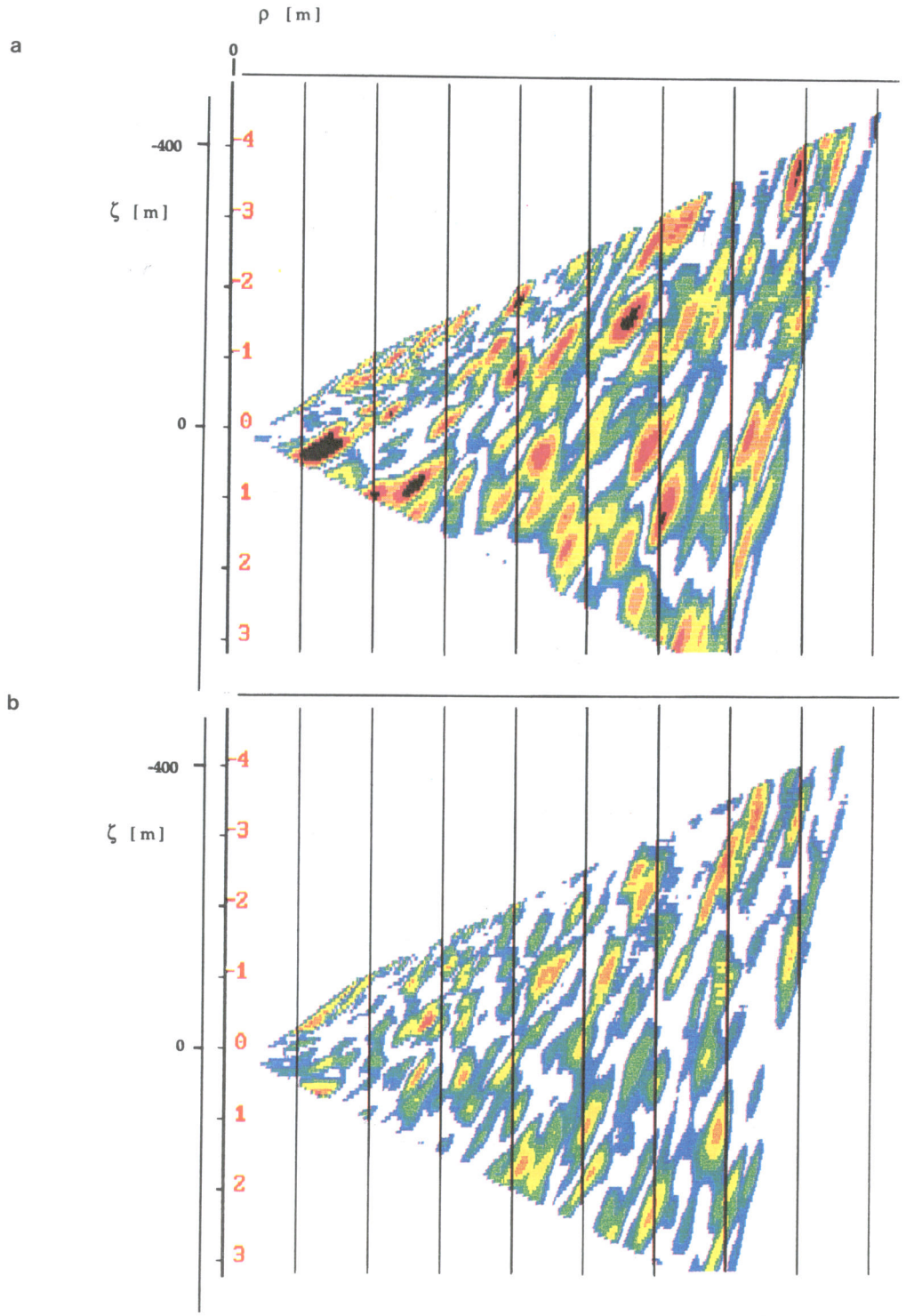

Figure 7.4
a) Image Space representation of the section in Figure 7.3d.
b) Image Space representation of the pseudosyntetic noise section.

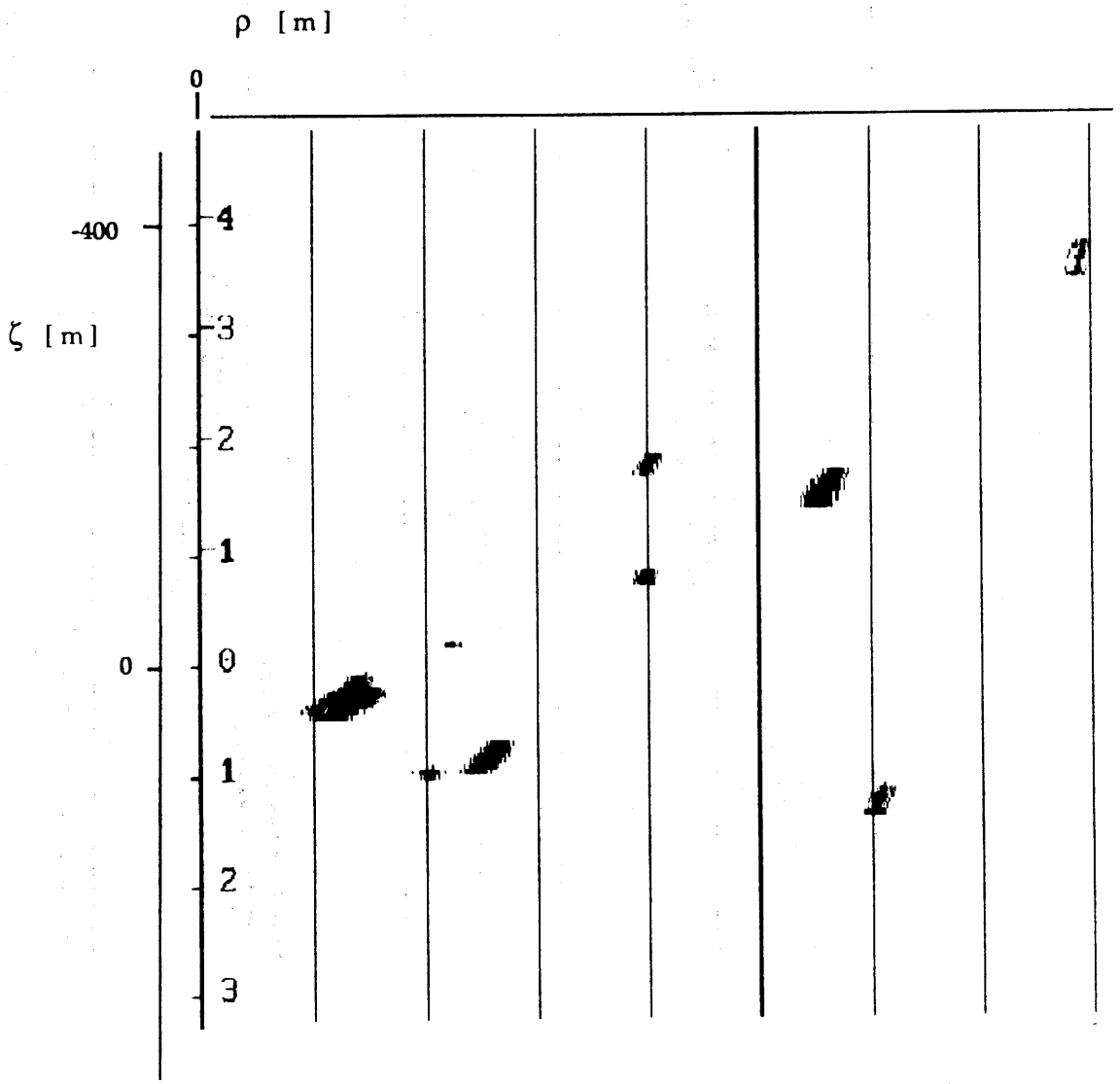

Figure 7.5 The Image Space section from Figure 7.4a after noise filtering.

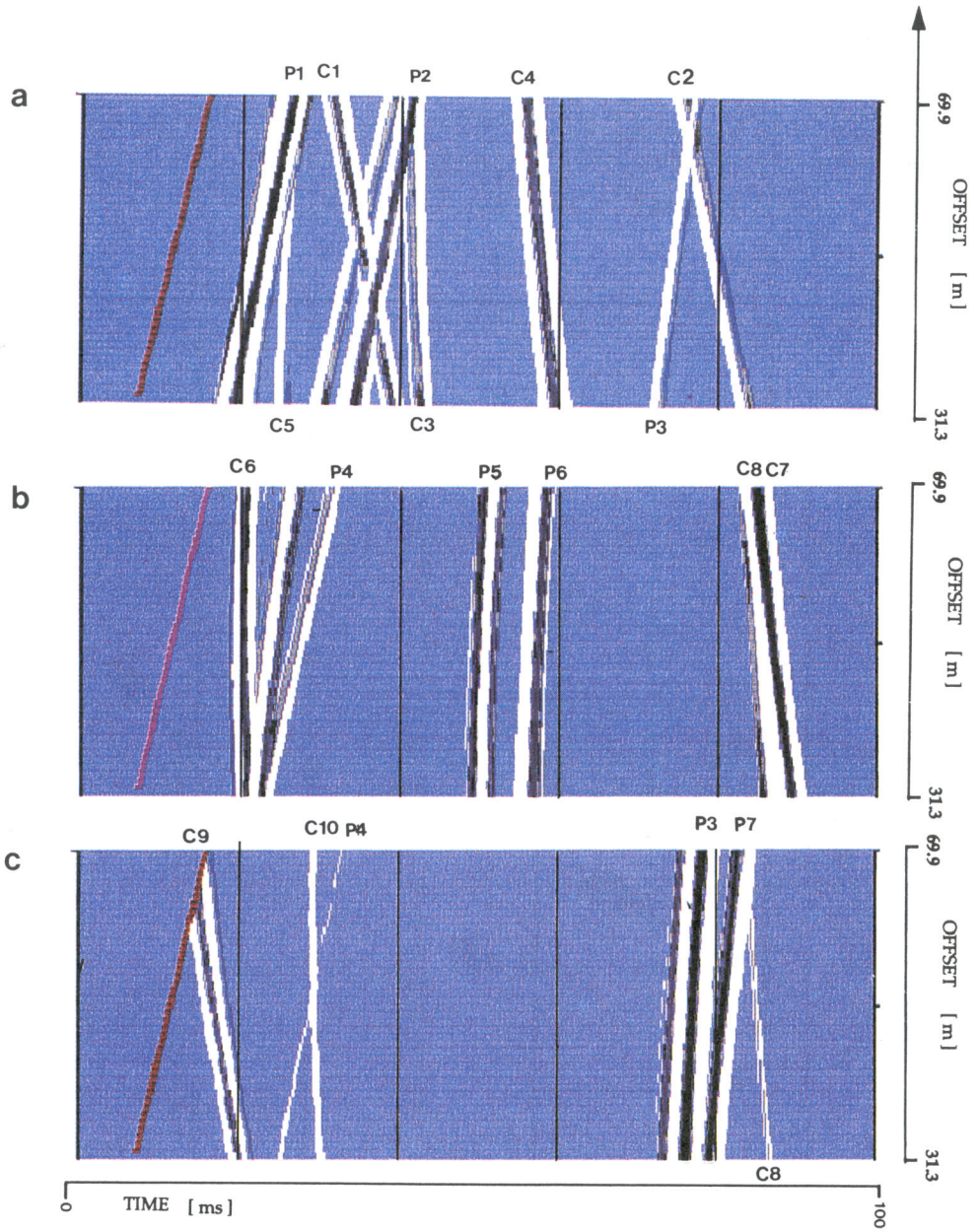

Figure 7.6

a) X-component section from the Leissigen test after Image Space filtering and retransformation back to Data Space. The events identified as reflectors are marked in the figure.

b) Y-component section from the Leissigen test after Image Space filtering and retransformation back to Data Space. The events identified as reflectors are marked in the figure.

c) Z-component section from the Leissigen test after Image Space filtering and retransformation back to Data Space. The events identified as reflectors are marked in the figure.

As in chapter 6, the interpretation was refined in the final stage by the use of Image Space filters, which can reject reflectors depending on the angle θ (defined in chapter 3) between the measuring array, i.e. the tunnel, and the reflector.

7.3 Interpretation of the Leissigen data

The reflectors seen in the amplitude limited sections of Figures 7.6 a - c were included in the interpretation. The reflectors identified are also marked in these figures but, for a more precise location, their positions are also given in Tables 7.1 and 7.2.

Table 7.1 lists the reflectors intersecting the tunnel line. The convention of naming the reflectors is the same as in the figures. The 'Depth' parameter is somehow improperly used in this context. With a true VSP survey, this is the depth measured along the hole at which the reflector cuts either the borehole or its extension. In the present case, the 'Depth' represents the distance calculated along the tunnel from the shot point. The third column in the table contains the angles between the reflectors and the tunnel. The apparent strength of a reflector in each component is indicated by Roman numerals (I: strong, II: intermediate, III: observed, -: not observed). The apparent strength is estimated from the angle limited sections. The classification is not more detailed because the relation between the reflection strength as determined by this procedure and the engineering significance of the corresponding fractured or contact zone is not strictly quantitative. The four level hierarchy provides information comparable with the true geology. A finer discretization would lead to a loss of reliability of the prediction.

These reflectors, or to be more precise parts of them, are marked in Figures 7.7 - 7.9 for the X, Y and Z components, respectively. Here, instead of applying the inverse transform back to the data space, a migration-like procedure was used. The $\rho\zeta$ migration, like the whole analysis based on the Image Point technique, emphasizes only planar reflectors. Figures 7.7 a, 7.8 a and 7.9 a display the whole transformed field. Figures 7.7 b, 7.8 b and 7.9 b show the transformed Image Point sections after filtering.

There are also strong events, which do not cut the tunnel and can be seen in all three components. They are listed separately in TABLE 7.2. These events probably represent reflections from the ground surface and near surface features.

TABLE 7.1 : REFLECTORS CUTTING THE TUNNEL

Reflector	Depth	Angle	Apparent Strength		
			X	Y	Z
C1	111	64	I	-	-
C2	216	66	I	III	II
C3	245	24	II	-	-
C4	244	35	I	II	III
C5	331	10	II	I	III
C6	114	26	II	I	III
C7	376	33	II	I	II
C8	455	25	III	I	I
C9	66	60	II	II	I
C10	150	29	III	-	II

TABLE 7.2 : REFLECTORS NOT CUTTING THE TUNNEL

Reflector	Distance from Shot Point	Component		
		X	Y	Z
P1	25	I	I	II
P2	80	I	I	II
P3	120	I	II	II
P4	150	I	I	I

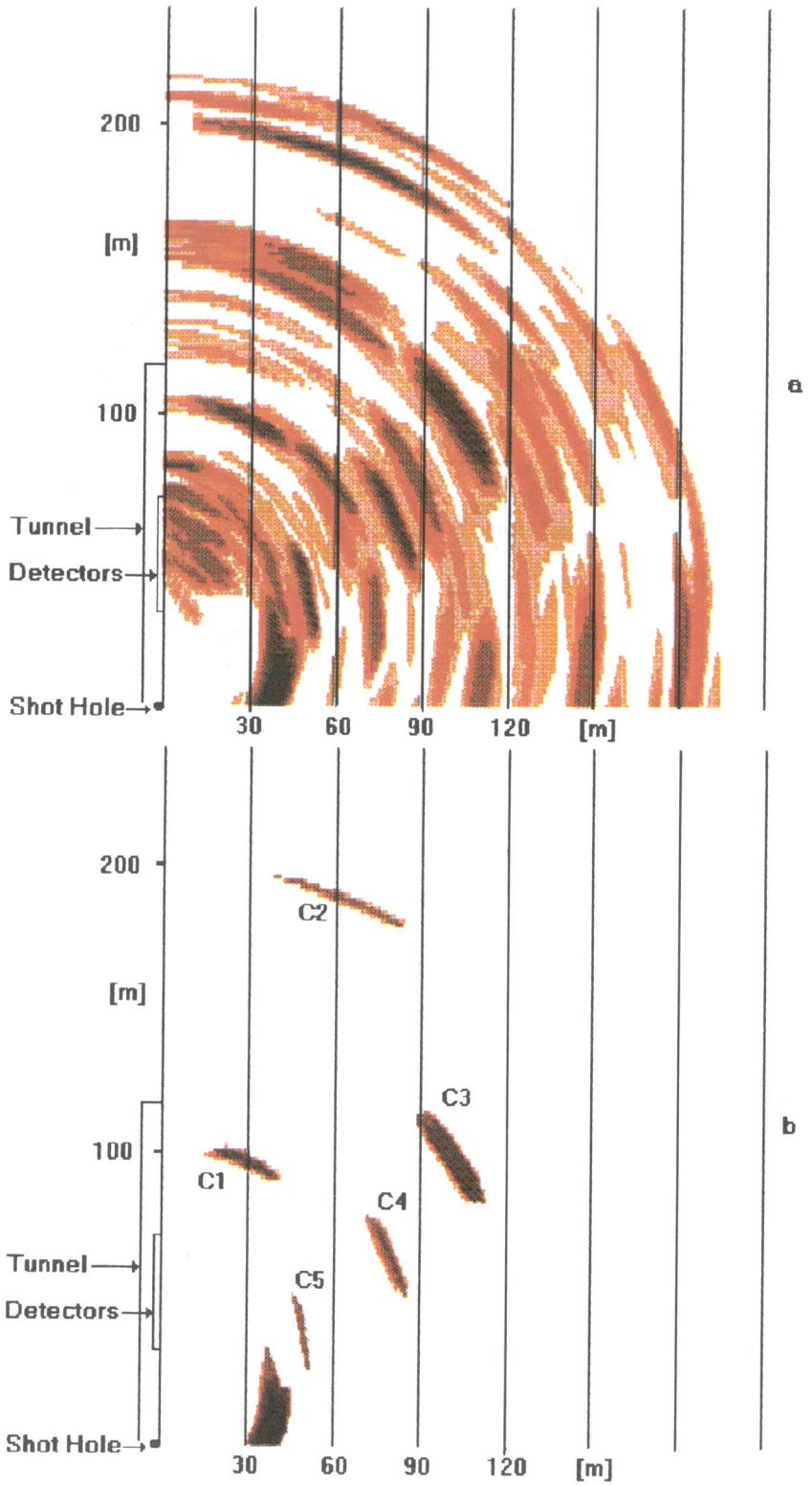

Figure 7.7 Positions of the seismic reflectors in the X-component section from Leissigen.
a) Without filtering
b) After filtering in Image Space

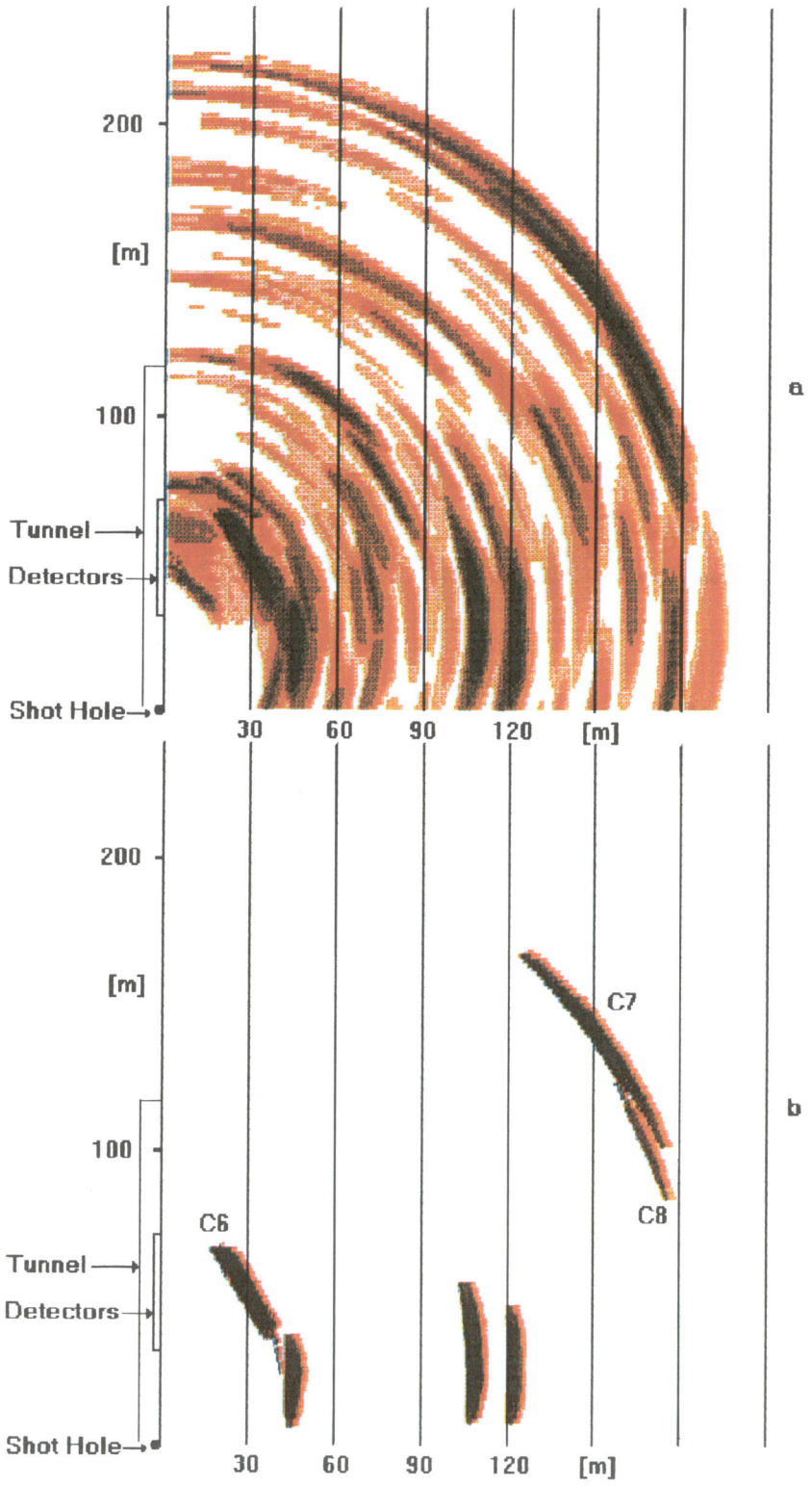

Figure 7.8 Positions of the seismic reflectors in the Y-component section from Leissigen.
a) Without filtering
b) After filtering in Image Space

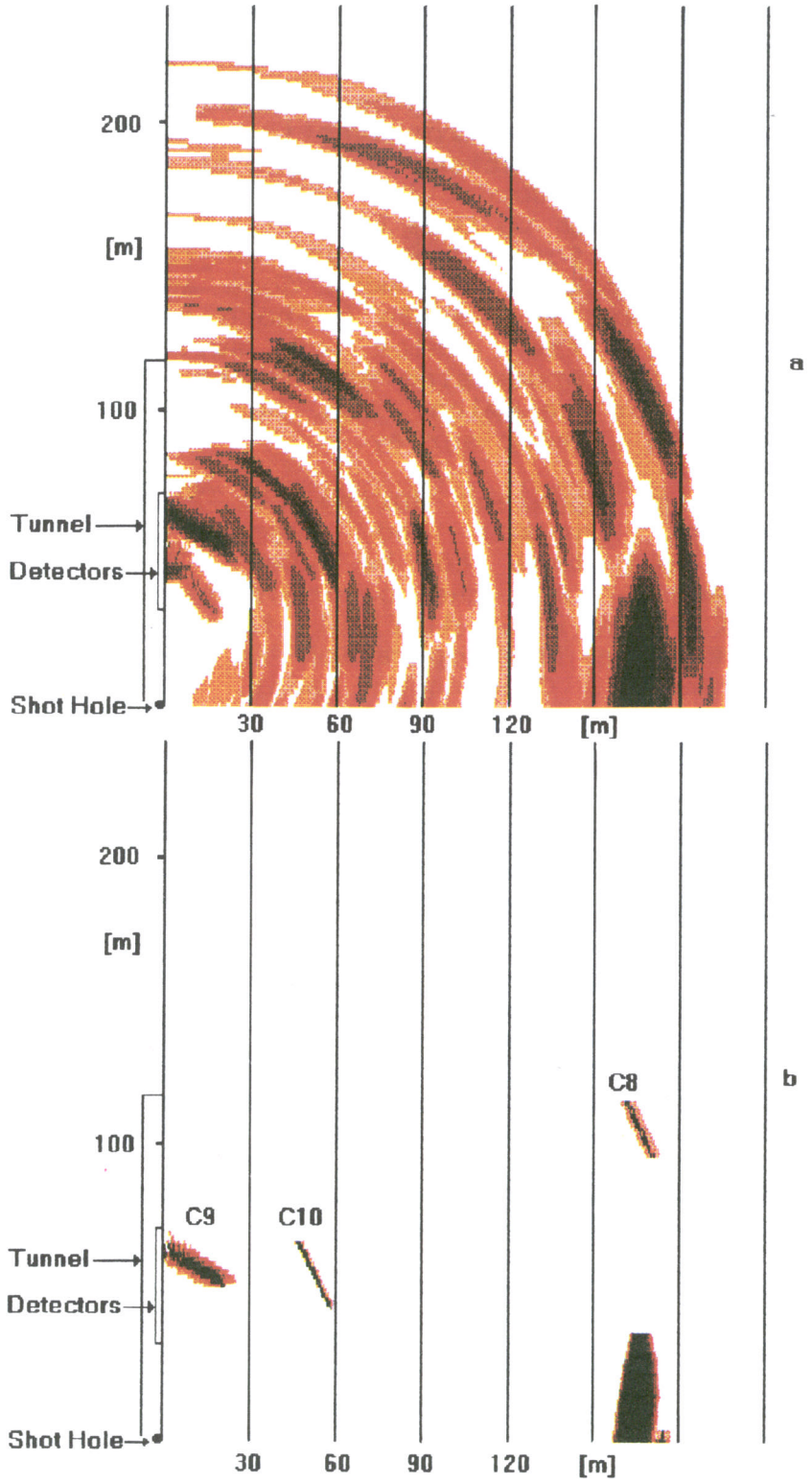

Figure 7.9 Position of the seismic reflectors in the Z-component section from Leissigen.
a) Without filtering
b) After filtering in Image Space

8 CONCLUDING REMARKS

The present study has been based on seismic methods rather than electro-magnetic (radar) due to the shallow penetration depth of the latter in electrically conductive sediments. Nagra focused their interest to this kind of formations (e.g. clays and marls) for future site characterization work. However, most of the work done and the conclusions obtained are applicable to both seismics and radar. Especially the choice of suitable experimental layouts and processing procedures, described in this report for seismics, can be of great help when designing a radar survey.

It became apparent during the Leissigen test that straight forward and rugged data acquisition techniques have to be used. With sophisticated equipment, like the coherent piezoelectric source tried there, it is difficult to ensure the conditions for trouble free operation in a construction site environment. Concerning radar, additional problems may appear due to drilling rods, electric cables and large metal objects normally found at a construction site.

The reflection seismic experiment carried out in a tunnel environment has shown that seismics can provide the following type of information:

- Disturbances nearly perpendicular to the tunnel can be located and their position determined in relation to the tunnel. Of special importance is the prediction of disturbances (e.g. fractured zones) laying ahead of the tunnel and possibly cutting the extension of the tunnel.

- Cavities around the investigated segment of tunnel can be clearly imaged.

- Fractured zones and other quasi planar rock interfaces running parallel to the tunnel can be detected and their orientation determined.

A few comments must be made on the reliability of the prediction. The segments seen in Figures 7.7 b - 7.9 b are the parts of the reflectors from which the reflected signals were actually received. The length of the segment depends on the relative position of the reflector with respect to the detector array. For the reflectors cutting the tunnel at steep angles, e.g. C1 and C2 (Figure 7.7 b), the segments are short, which means that the orientation of such reflectors is less accurately calculated than of the

reflectors cutting the tunnel at sharp angles (C3, C4 and C5). On the other hand, the extrapolation to the intersection with the tunnel is shorter for C1 and C2, which leads to a better localization of the intersection with the tunnel. The model gains in accuracy if longer detector arrays are used. This can be achieved in a simple way by repeating the measurements at certain intervals while the tunneling works are progressing.

A special measuring geometry must be selected to avoid the non-uniqueness in the position of the reflectors around the tunnel. This can be achieved for example by placing a detector array in a borehole perpendicular to the tunnel. In principle, also polarization analysis of the multi-component data can give direction information. Geological information concerning the main directions of the structural features at a given site may help in solving the non-uniqueness problem in an easy manner and with an accuracy sufficient in most cases.

We have not tried to estimate the true three-dimensional positions of the reflectors, because it is impossible to determine both the dip and the strike of a reflector from only one shot point or even from several shot points if they are collinear with the detector array. The information concerning the predominant strike of the rock features was used for the GTS site, where it was available. A three-dimensional model could be thus obtained, which displayed a remarkable agreement with the known geology.

At Leissigen, although the data recording had been triaxial, the low level of the reflected signals did not encourage efforts towards the use of polarization analysis. From the geological map which we were able to consult after presenting the results, we could have inferred some information on the general orientation of the main site features. This information has not been used in drafting the prediction maps, being external to the seismic test itself. The tables of results contain only the results derivable directly from our project. As stated above, our goal has been to determine the point where the reflector will cut the tunnel as well as the angle of the reflector with the tunnel axis.

Some of the strong events which do not cut the tunnel and can be seen in all components are reflections from the surface and near surface layers. The detection of these events is particularly important for tunnels under rivers and straights. With inland tunnels, reflections from surface are used to check and calibrate the prediction.

As the individual shots were fired in a transversal borehole, it is possible in principle, that the shot separation decreases the amplitudes in the stacked sections for the events nearly parallel with the tunnel. However, the results from processing the VSP data from Grimsel showed that the stacked sections were clearly better for these events too.

With the field arrangements described here, it is possible to conduct a VSP survey during breaks in excavation; a few hours are enough for setting up the detector chain and the required shots. If only the area close to the tunnel head is concerned (e.g. 50 meters ahead), the processing can also be done in a few hours so that the results will be ready for the next day. If measurements are repeated often enough (e.g. every 50 meters) their results can be correlated easily and we can construct a reliable picture of the reflector. This can be seen in Figure 6.3, where all major reflecting zones can be found in both profiles measured.

The processing and interpretation of data from VSP surveys in tunnels has been performed in parallel with various methods. Generally, the standard techniques of the oil prospecting industry are not suitable without important modifications. The Image Space method proved to be a good tool for interpretation, both for estimating the relevance of the reflection events and for locating the reflectors reliably. Migration techniques seem so far to be less appropriate for surveying tunnels. Their efficiency is reduced by the low reflectivity and the complex geometry of the rock features.

One can observe that, during the project, the power of the methods used and the reliability of the interpretation have increased from phase to phase. This is due to the fact that knowledge, both theoretical and practical, related to tunnel surveying has accumulated gradually. The study of the wavefield in the vicinity of the tunnel has to be noted as a very useful phase of the project. It brought into light specific phenomena which are not generally encountered in standard surface seismic surveys.

REFERENCES

Cosma, C., Heikkinen, P. and Pekonen, S., 1991. Improvement of High Resolution Borehole Seismics. Technical report 91-13, Stripa project. SKB, Stockholm.

Gelbke, C., 1988. Seismische Durchscallungs-tomographie. Technischer bericht 88-06, Felslabor Grimsel. Nagra Schweiz.

Griffiths,L.J.,Smolka, F.R. and Trembly, L.D., 1977. Adaptive Deconvolution: a New Technique for Processing Time-varying Seismic Data. Geophysics, 42, 742-759.

Hardage, B. A., 1983. Vertical Seismic Profiling. Part A: Principles . Geophysical Press, London.

Lee, M.W. and Balch, A., 1983 . Computer Processing of Vertical Seismic Profile Data. Geophysics, 48, 272-287.

Miller, D., Oristaglio, M. and Beylkin, G., 1987. A New Slant on Seismic Imaging: Migration and Integral Geometry. Geophysics, 52, 943-964.

Niva, B., Olsson, O.,Blümling, P., 1988. Radar Crosshole Tomography with Application to Migration of Saline Tracer Through Fracture Zones. Technical report 88-31, Grimsel Test Site. Nagra, Switzerland.

Sheriff, R.E., 1973. Encyclopedic Dictionary of Exploration Geophysics. Society of Exploration Geophysicists, Tulsa, 266 pages.

Tatham,R.H.,1989. Tau-p Filtering . In:Paul M. Stoffa (editor) , Tau-p: a Plane Wave Approach to the Analysis of Seismic Data .Kluwer Academic Publishers , Dordrecht/Boston/London, pp. 35-70.

Winkler, G. R. and Cassell, B.R., 1989. Deep VSP Study in a Complex Alpine Overthrust Area. First Break, 7, 111-123.

Acknowledgement

This project was carried out as a research and development program by Nagra under the terms of the German/Swiss cooperation agreements between Nagra (National Cooperative for the Disposal of Radioactive Waste), BGR (Federal Institute for Geoscience and Natural Resources) and GSF (Research Centre for Environmental Science).

The authors gratefully acknowledge the efforts of a large number of individuals who provided extensive support during the planning, prepration and execution of the field measurements as well as during the data processing and interpretaion. The field work was carried out by the companies P. Frey, Zug; Deutsche Montan Technologie (DMT), Bochum; Vibrometric, Helsinki and Swedish Geological AB, Uppsala. The technical staff at GTS, T. Baer and H. Aplanalp, provided helpful assistance during the field work at GTS. The measurements in the road tunnel at Leissigen were made possible by the dedicated efforts of C. Amstad (ETH), Mr. Pfäffli (on site representative of the tunnel owner) and Mr. Jenk (Tiefbauamt des Kantons Bern).

In addition, we would like to thank H. Emmerich, G. Müller (both at the University of Frankfurt), E. Reimers, B. Lehmann (both at DMT, Bochum), P. Heikkinen, J. Keskinen (both at Vibrometric, Helsinki), E. Sandberg and O. Olsson (formerly both at Swedish Geological AB) for their invaluable help during theoretical studies and data processing.

Finally we would like to acknowledge the support by C. Sprecher (Nagra) and G. Sattel (now at Amberg Ingenieurbüro) during the whole program.